Met Office
Hadley Centre

Hadley Centre Technical Note 95

Revised vertical mixing parameters for the UK community standard configuration of the global NEMO ocean model

23rd October 2013

Daley Calvert and John Siddorn

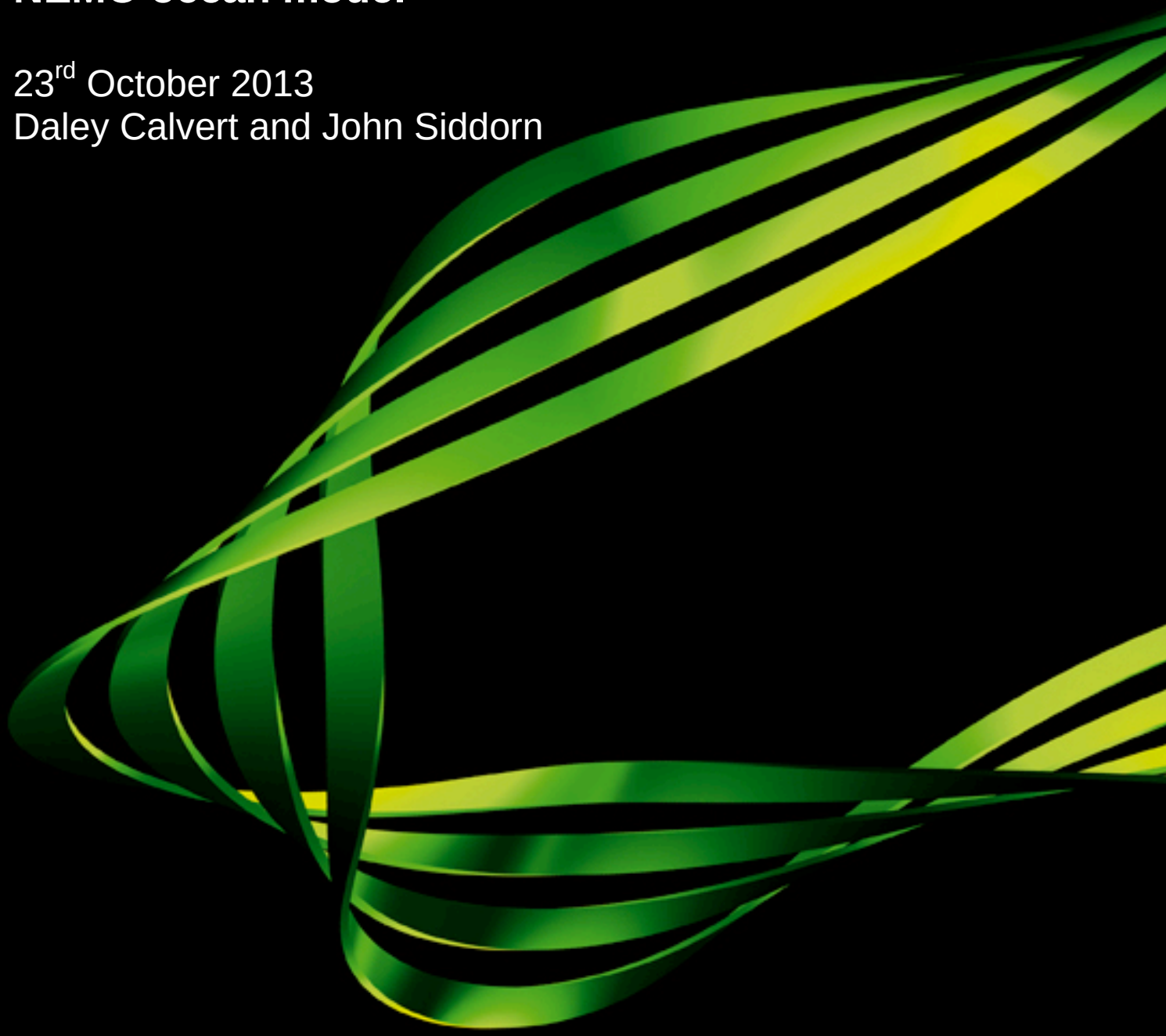

Abstract

A set of revised parameter settings for a modified version of the Gaspar et al. (1990) turbulent closure scheme are presented as part of the definition of the latest standard configuration (GO5.0) of the NEMO ocean model, defined jointly by the Met Office and National Oceanography Centre. These revisions are supported by a series of sensitivity experiments using a 75 vertical level, ORCA1 configuration of NEMO coupled to the CICE ice model, which have been used to indicate where possible alleviation of a global shortfall in vertical mixing is possible within theoretically-limited parameter adjustments. Relative to a set of vertical mixing parameter settings based on an N96-ORCA1 configuration of HadGEM3, these revised settings are seen to improve vertical mixing-related biases (warm SSTs and shallow mixed layer depths) in the summer hemispheres. Most notably, the introduction of a parameterization for Langmuir turbulence and near-inertial wave breaking individually reduce large summer SST and MLD biases in the Southern Ocean by ~25%. Several ideas for future work are suggested. Firstly, the Langmuir turbulence and near-inertial wave breaking parameterizations have important shortcomings that undermine confidence in their performance; future work should concentrate on addressing these shortcomings. Secondly, several parameters relating to the Gaspar et al. (1990) turbulent closure remain poorly-defined and simplified relative to several well-studied second-order closures; a systematic comparison of these schemes with the present vertical mixing scheme is warranted. Finally, a combined test of the revised parameter settings in a coupled configuration is highlighted as a necessary extension to the ocean-only modelling underpinning the presented revisions.

Contents

1. Introduction 3

2. Overview of the NEMO TKE scheme 7

2.1. The 'TKE scheme' turbulence closure 8

2.2. Implementation in the NEMO OGCM 11

3. Model details 17

3.1. Settings and model configuration of the control experiment 17

3.2. Sensitivity experiments 18

4. Results 20

4.1. Impact and sensitivity of the turbulence surface boundary condition 20

4.2. Impact and sensitivity of the near-inertial wave breaking parameterization 29

4.3. Impact of the Langmuir turbulence parameterization 43

4.4. Sensitivity of the turbulence closure stability functions 49

4.5. Impact and sensitivity of the minimum TKE and length scale thresholds 54

5. Summary and recommendations 61

6. References 64

1. Introduction

Accurate representation of vertical mixing in Ocean Global Circulation Models (OGCMs) has been a long-standing issue and as such continues to be an active area of research. However despite improvements in both empirical (Large et al., 1994) and statistical (Umlauf and Burchard, 2005) approaches to turbulence modelling, OGCMs continue to exhibit biases to varying degrees that reflect an inadequate representation of vertical mixing.

A common issue is that of insufficient vertical mixing in the stratified summertime mixed layer (Martin, 1985; Ezer, 2000), which manifests as an anomalously warm SST and cold subsurface temperature bias accompanied by a shallow summer mixed layer depth (MLD) bias. Shallow biases in the MLD are a particularly persistent problem in the Southern Ocean for various atmosphere-coupled and forced models (Huang et al. 2012) but have also been observed to be a wintertime issue (Weijer et al., 2012).

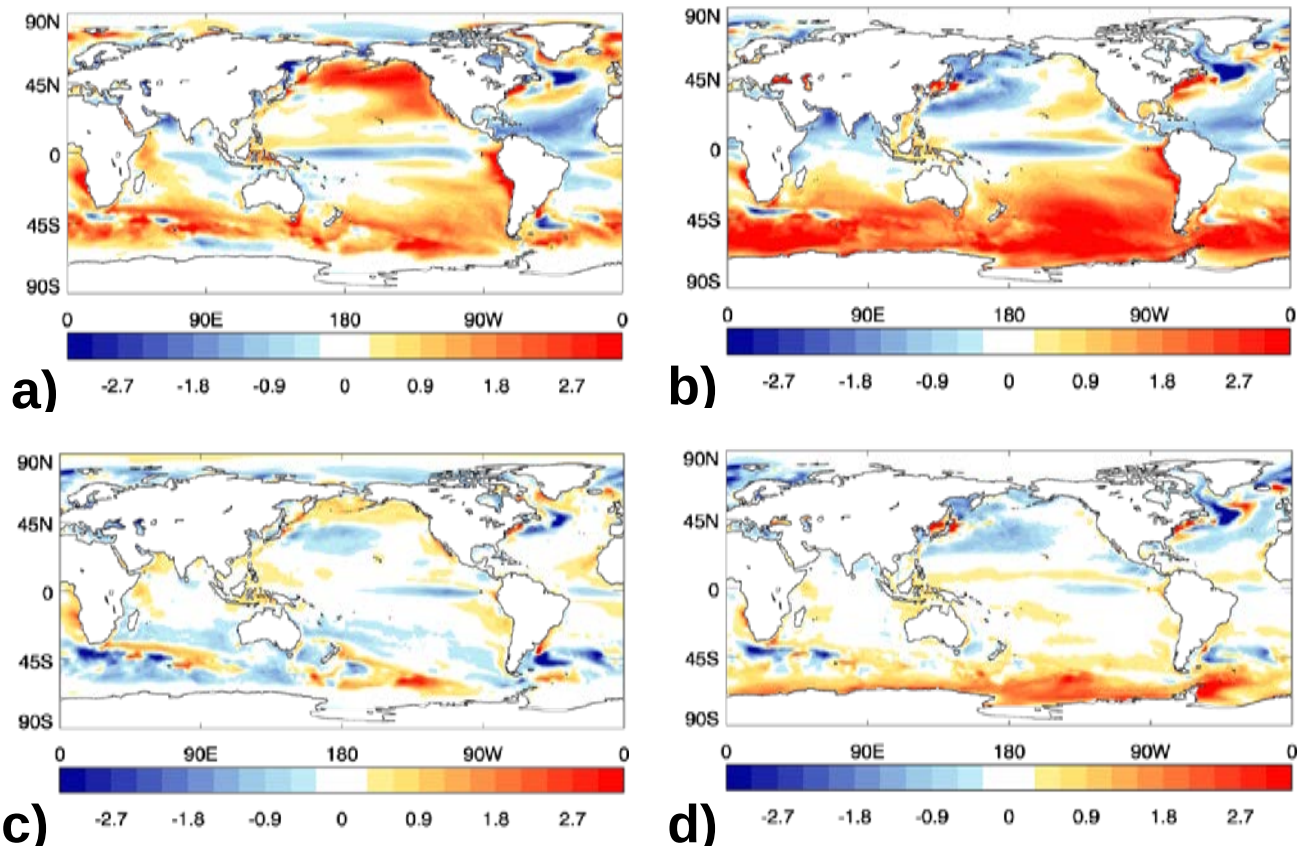

Figure 1.1: JJA (a,c) and DJF (b,d) SST biases relative to the Reynolds SST climatology for HadGEM3 (top) and NEMO-CICE (bottom), averaged over model years 11-30.

This report concerns such biases in the NEMO OGCM and in the Met Office models in which NEMO is a component, including the HadGEM3 (Hewitt et al., 2011), FOAM (Storkey et al., 2010) and GloSea (Arribas et al., 2011) systems. Figure 1.1 illustrates the June-August (JJA) and December-February (DJF) average SST biases and figure 1.2 illustrates the mean annual minimum and maximum MLD biases (representing the hemispheric summer and winter biases respectively) in an N96-ORCA1 configuration of HadGEM3 and in an equivalent forced configuration of NEMO coupled to the CICE ice model (henceforth referred to as the NEMO-CICE model).

These diagrams illustrate that summer biases suggestive of insufficient vertical mixing are not only present in both configurations but are generally more severe in the coupled configuration. Shallow summer MLD biases are found over much of the globe and are most severe in the Southern Ocean (figures 1.2a,c), constituting up to a 50% error relative to their climatological values and are also present to a lesser degree in the North Pacific and North Atlantic. Warm SST biases accompany these shallow MLD biases and are much more severe and widespread in the coupled configuration. Biases in the winter mixed layer are evident in both configurations to varying degrees: whilst comparable in

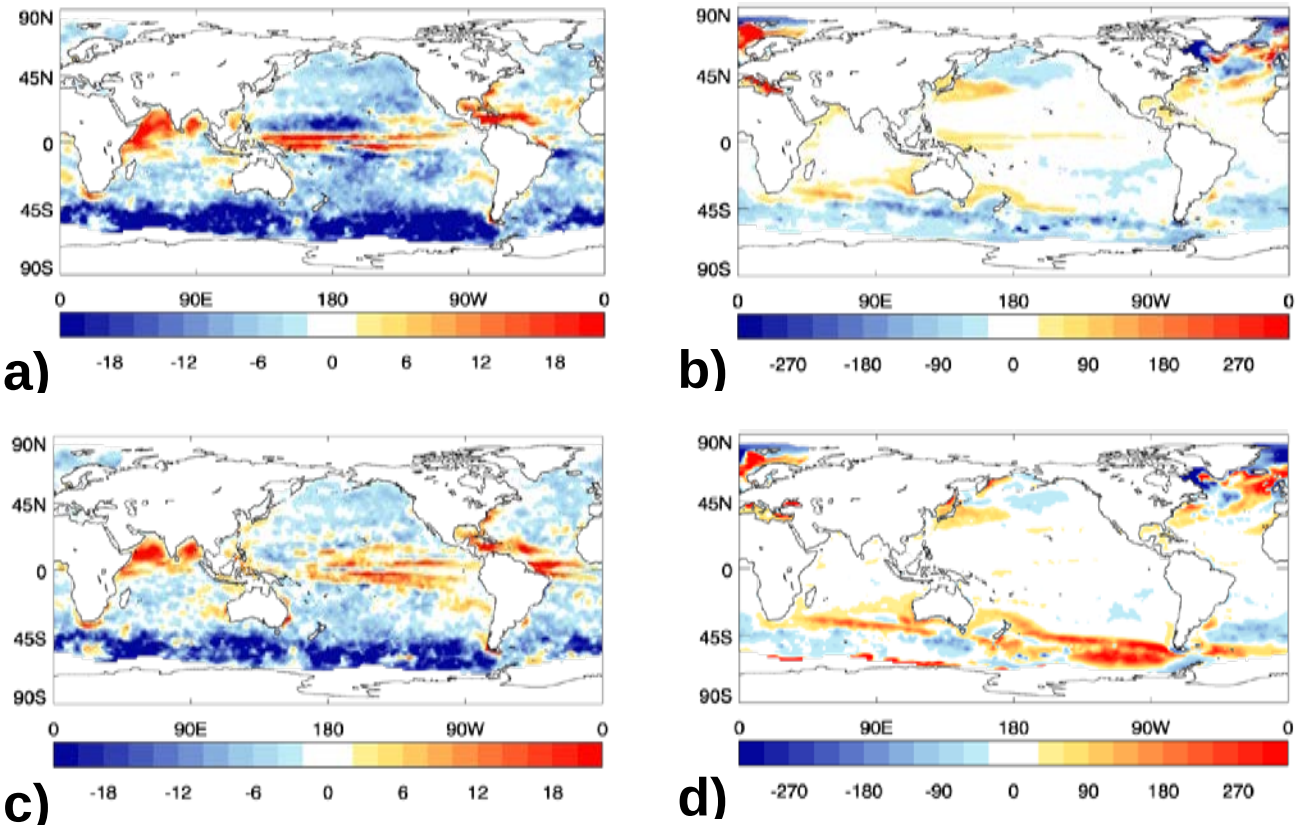

Figure 1.2: Mean annual minimum (a,c) and maximum (b,d) MLD biases relative to the de Boyer Montégut et al. (2004) climatology for HadGEM3 (top) and NEMO-CICE (bottom), averaged over model years 11-30.

other regions, the forced configuration exhibits deep winter MLD biases in regions of the Southern Ocean where Subantarctic Modal Water (SAMW) and Antarctic Intermediate Water (AAIW) is formed while biases in the coupled model are more generally shallow in this region. Biases in the winter SSTs are also generally larger in the coupled configuration; in the Southern Ocean in particular they are more widespread and consistently warmer than those in the forced configuration.

As vertical mixing in the winter hemispheres is predominantly driven by convection (which is crudely parameterized in many OGCMs), these wintertime biases are not the focus of the present work, although they are no doubt of importance to an accurate representation of water mass formation. While it is not a simple task to attribute model biases in temperature to specific processes, the presence of a widespread shallow summer MLD bias in both forced and coupled configurations of NEMO is a robust indicator of a shortfall in vertical mixing in these models. The focus of this report is on these persistent summertime vertical mixing biases, which are shown in figure 1.2 to be a fundamental problem for much of the global ocean in NEMO-CICE and HadGEM3.

The vertical mixing scheme used in NEMO is a statistical-type closure based on the Navier-Stokes equations, which explicitly calculates the ocean turbulence as a function of the large-scale mean ocean state via a prognostic equation for the TKE, and as such is informally known as the ‘TKE scheme’. Whilst directly traceable to fundamental physical laws (unlike empirical schemes like the KPP scheme which depend mainly on the accuracy of the observations on which they are based), the ability of these statistical schemes to resolve turbulent processes depends on the approximations made in their derivation. See Burchard et al. (2008) for a broad overview of both types of vertical mixing scheme.

For vertical mixing schemes of this type typically used in OGCMs, examples of unresolved processes include Langmuir circulations, internal wave breaking and turbulence due to breaking (Craig and Banner, 1994) and non-breaking (Huang et al., 2011) surface waves. Other processes may be partially resolved and require a compensating parameterization, such as convection and near-inertial wave breaking in the NEMO TKE scheme.

Persistent biases in vertical mixing schemes of this type are therefore likely to mostly be a consequence of poorly-represented or missing processes which must instead be

explicitly parameterized. Such parameterizations inherently give rise to uncertainty in the overall model via the introduction of tuneable parameters. Many of the above processes are represented in this manner in the NEMO TKE scheme, and so the accuracy of the scheme is strongly dependant on the use of appropriate settings for these parameters. Therefore while alleviation of most of the summer vertical mixing bias in NEMO is likely to require the development of new or improved process-based parameterizations, errors will also be introduced by poorly-tuned existing parameters in the vertical mixing scheme.

An effort has been made to better define these parameters for the latest standard global configuration of NEMO defined jointly by the Met Office and National Oceanography Centre (known as 'GO5.0'). A number of 10-year sensitivity experiments were performed on the parameters of the TKE scheme using a forced configuration of NEMO coupled to the CICE ice model, based on the parameter settings of the N96-ORCA1 configuration of HadGEM3. The results of these experiments have been used to indicate where improvements to the summer vertical mixing biases in NEMO (and subsequently to those in HadGEM3 and other Met Office models utilising NEMO) may be possible via reasonable adjustments to the parameters of the TKE scheme. The intention of this report is to outline a set of revised parameter settings and to describe the above work supporting these revisions. As such, this report is not an exhaustive description of all adjustments to the vertical mixing scheme that were made in defining the GO5.0 configuration. Additionally, this work provides a partial overview of the parameter sensitivity of the NEMO TKE scheme and therefore may be more widely relevant to the NEMO user community.

A description of the TKE scheme and its implementation in the NEMO OGCM is given in section 2. Details of the NEMO configuration used for the sensitivity experiments and of the experiments performed are outlined in section 3. The results of these experiments and their support of the recommendations of this report are given in section 4.
Section 5 outlines the findings of this report, presenting a set of revised parameter settings for the NEMO TKE scheme and suggested directions for future work with the aim of further improving the representation of vertical mixing in the NEMO model.

2. Overview of the NEMO TKE scheme

The 'TKE scheme' of NEMO is a turbulence closure scheme developed by Bougeault and Lacarrére (1989) (henceforth BL89) originally developed to model the atmospheric boundary layer. In the Mellor and Yamada (1974) hierarchy it is a 1.5-level closure and consists of a prognostic closure for the TKE and an algebraic formulation for the mixing length scale.

It is in this algebraic length scale that the merits of using such a scheme are evident over the higher order alternatives. Such 'k-models' offer a computationally efficient solution of the length scale while providing a reasonable approximation to the prognostic alternative (the so-called two-equation or 2^{nd}-order closures), though as Meier (2001) argues the use of a prognostic length scale is not a significant additional cost for modern parallelized computational resources.

The TKE scheme was first implemented in an oceanic configuration by Gaspar et al. (1990), who compared the results of a 1D configuration to OS PAPA and LOTUS data. Blanke and Delecluse (1993) (henceforth BD93) then implemented the scheme in a regional 3D configuration of the equatorial Atlantic using the predecessor of NEMO; the OPA model. It is this most recent implementation by BD93 that the current form of the TKE scheme in the NEMO OGCM is based on (Madec, 2008), and an overview of the turbulence closure is presented in section 2.1.

Enhancements to the TKE scheme have been made through subsequent development of the NEMO model, which involve the introduction of new parameterizations and some revisions to the TKE scheme boundary conditions. These and other details specific to the NEMO implementation of the TKE scheme are summarised in section 2.2.

2.1. The 'TKE scheme' turbulence closure

As with all turbulence closures the purpose of the TKE scheme is to calculate the unresolved subgridscale vertical turbulent fluxes, parameterized using the classical concept of eddy diffusivity:

$$\overline{-T'w'} = K_\rho \partial\overline{T}/\partial z \quad (2.1a)$$

$$\overline{-S'w'} = K_\rho \partial\overline{S}/\partial z \quad (2.1b)$$

$$\overline{-U_h'w'} = K_m \partial\overline{U_h}/\partial z \quad (2.1c)$$

where the temperature (T), salinity (S) and horizontal momentum ($\overline{U}_h = \sqrt{\overline{U}^2 + \overline{V}^2}$) fluxes respectively are written with Reynolds decomposition ($x = \overline{X} + x'$).

The eddy diffusivity and viscosity coefficients K_ρ and K_m are parameterized following the Prandtl-Kolmorogov hypothesis, as a product of a length scale and velocity scale:

$$K_m = c_k l_k \overline{e^{1/2}} \quad (2.2a)$$

$$K_\rho = K_m / P_{rt} \quad (2.2b)$$

where $\bar{e} = 0.5\left(u'^2 + v'^2 + w'^2\right)$ is the TKE, l_k is a mixing length scale and P_{rt} is the turbulent Prandtl number.

The parameter c_k is known as a stability function and is defined as a constant in the TKE scheme. However it is possible to arrive at more complex algebraic functions of this parameter via the derivation of Algebraic Stress Models (see for example Canuto et al., 2001), which are non-linear functions of shear, buoyancy, TKE and dissipation. These are designed to correct the above eddy diffusivities for the effects of stratification and shear (in addition to those explicitly included in the prognostic TKE equation), and are a further aspect in which the TKE scheme is simplified with respect to other turbulence closures.

The Prandtl number is given a dependence on the local Richardson number by BD93, such that:

$$\begin{aligned} P_{rt} &= 1 \quad \text{for} \quad Ri \le 0.2 \\ P_{rt} &= 5\,Ri \quad \text{for} \quad 0.2 < Ri \le 2 \\ P_{rt} &= 10 \quad \text{for} \quad 2 < Ri \end{aligned} \tag{2.3}$$

Assuming a one-dimensional balance and neglecting horizontal terms, the prognostic equation for the TKE is generally given as:

$$\frac{\partial \overline{e}}{\partial t} = -\overline{u_h' w'} \bullet \frac{\partial \overline{U_h}}{\partial z} + \overline{b'w'} - \frac{\partial}{\partial z}\left(\overline{ew'} + \rho_0^{-1}\overline{p'w'}\right) - \varepsilon \tag{2.4}$$

where $b = g\rho_0^{-1}\rho$ is the buoyancy, $\rho_0 = 10^3$ kgm^{-3} is a reference density, ρ is the density, p is the pressure and g is the acceleration due to gravity. z is here defined as being positive upwards.

This can be simplified via the eddy diffusivity approximation (2.1a,b) into:

$$\frac{\partial \overline{e}}{\partial t} = K_m\left(\frac{\partial \overline{U_h}}{\partial z}\right)^2 - K_\rho N^2 + \frac{\partial}{\partial z}\left(K_e \frac{\partial \overline{e}}{\partial z}\right) - \varepsilon \tag{2.5}$$

where N^2 is the Brunt-Väisälä frequency.

The individual terms on the right hand side of (2.5) are respectively: TKE production due to shear, TKE production/dissipation due to buoyancy, TKE vertical diffusion (which here is expressed as the sum of the turbulent and viscous transport terms) and dissipation. The third term on the RHS introduces a further eddy diffusivity coefficient for the TKE, which is usually set equal to K_m. BD93 find that $K_e = 30K_m$ is a good fit for their tropical configuration, noting that their coarse vertical resolution may inhibit the vertical diffusion in this type of turbulence closure. For the 75 vertical level configuration of NEMO used in this study however, this is likely to be less of an issue and so $K_e = K_m$ is used.

The dissipation term is given in the usual form of Kolmogorov (1942):

$$\varepsilon = c_\varepsilon \frac{\overline{e}^{3/2}}{l_\varepsilon} \tag{2.6}$$

where c_ε is a constant and l_ε is a dissipation length scale.

To close the scheme at this point, the forms of the algebraic length scales l_k and l_ε must be specified and the constants c_k and c_ε must be chosen appropriately for this formulation. It was shown by Therry and Lacarérre (1983) that $l_k \neq l_\varepsilon$, which led to the development of separate expressions for l_k and l_ε by BL89 for the TKE scheme:

$$l_k(z_0) = \min\left[l_d(z_0), l_u(z_0)\right] \tag{2.7a}$$

$$l_\varepsilon(z_0) = \left[l_d(z_0) \cdot l_u(z_0)\right]^{1/2} \tag{2.7b}$$

where the master length scales l_u and l_d are based on the length scale formulations of Bougeault and André (1986):

$$g\rho_0^{-1} \int_{z=z_0}^{z=z_0+l_u} \left[\rho(z_0) - \rho(z)\right] dz = \bar{e}(z_0) \tag{2.8a}$$

$$g\rho_0^{-1} \int_{z=z_0-l_d}^{z=z_0} \left[\rho(z) - \rho(z_0)\right] dz = \bar{e}(z_0) \tag{2.8b}$$

The physical interpretation of the previous two equations is intuitive; the master length scales l_u and l_d are respectively the upward and downward distances a fluid parcel is able to travel from $z=z_0$, converting its TKE into potential energy by doing work against the stratification. This allows the mixing length scale l_k to have the property that it is naturally limited by the distance to the sea surface and bottom, and to strongly stratified layers.

(2.8a) and (2.8b) were further simplified by Gaspar et al. (1990) for the specific case where the ocean is stably stratified with N^2 constant:

$$l_u = l_d = \frac{\sqrt{2\bar{e}}}{N} \tag{2.9}$$

However, this form no longer uses the stratification of the entire water column as for (2.8a) and (2.8b). Madec (2008) retains this simplified form but restores the directional interpretation of the length scales (so that $l_u \neq l_d$) by bounding l_u and l_d such that:

$$\frac{\partial(l_u, l_d)}{\partial z} \leq 1 \tag{2.10}$$

This in effect means that (2.9) is bounded by remote stratification as for (2.8a) and (2.8b), but avoids the iterative calculation for the vertical integral.

A major shortcoming of the simplified mixing length scale (2.9) is that while it is simple and computationally efficient, it also becomes unphysical for the case of unstable stratification. Where this occurs, BD93 locally set the master length scales l_u and l_d equal to their respective maximum values (the distance to either the sea surface or bottom).

For the above form of the algebraic length scale, Bougeault and Lacarrére (1989) were able to find that $c_\varepsilon = 0.7$ by fitting to observed profiles of turbulent dissipation in the atmospheric boundary layer. If we assume that the TKE equation (2.5) is both in a steady state $\left(\partial\bar{e}/\partial t = 0\right)$ and vertically homogeneous $\left(\partial\bar{e}/\partial z = 0\right)$ and that $P_{rt} = 1$ and $l_u = l_d = l_k = l_\varepsilon$, it can be shown using (2.2a), (2.2b), (2.5), (2.6) and (2.9) that:

$$Ri_{st} = \frac{N^2}{\left(\frac{\partial \overline{U_h}}{\partial z}\right)^2} = \frac{2}{2 + \frac{c_\varepsilon}{c_k}} \qquad (2.11)$$

where Ri_{st} is the stationary Richardson number.

For $c_\varepsilon = 0.7$ and using $Ri_{st} = 2/9$, we find from (2.11) that $c_k = 0.1$ in a similar manner of derivation as for Gaspar et al. (1990).

2.2. Implementation in the NEMO OGCM

While the general form of the TKE scheme discussed in the previous section is mostly identical to that implemented by BD93, some specifics of the NEMO implementation differ and will be discussed here for NEMO version 3.0.

One such specific is the treatment of the boundary conditions on the turbulent closure. Madec (2008) follows BD93 in imposing surface and bottom boundary conditions on the TKE of:

$$\bar{e}\big|_{z=0} = \max\left(\alpha \frac{|\tau|}{\rho_0}, e_{min0}\right) \qquad \bar{e}\big|_{z=bot} = e_{min} \qquad (2.12)$$

where $|\tau| = \sqrt{\tau_x^2 + \tau_y^2}$ is the surface wind stress, α is a constant and e_{min0} / e_{min} are minimum numerical thresholds on the surface and subsurface TKE respectively.

It is shown by Mellor and Blumberg (2004) (henceforth MB04) that the Craig and Banner (1994) surface boundary condition on the TKE due to surface wave breaking can be expressed in the same form as (2.12):

$$\bar{e}\big|_{z=0} = \frac{(15.8\alpha_{CB})^{2/3}}{2}\frac{|\tau|}{\rho_0} \tag{2.13}$$

where α_{CB} is the wind-wave energy coefficient of Craig and Banner (1994).

Furthermore Terray et al. (1996) show that α_{CB} is dependant on the surface wave age, which for the range of wave ages given by MB04 suggests that a value of $47 \leq \alpha \leq 87$ is required to represent the effects of surface wave breaking, while the value of $\alpha = 3.75$ used by BD93 for a state of no wave-breaking can be taken as an absolute lower bound. Following Craig and Banner (1994), Madec (2008) approximately uses an 'optimal' value of $\alpha_{CB} = 100$ ($\alpha = 67.83$) and sets $\alpha = 60$ in (2.12), which is representative of a fully-developed sea.

Madec (2008) additionally specifies boundary conditions for the mixing and dissipation length scales, which are set for the surface and bottom boundaries to minimum numerical thresholds on the surface and interior length scales respectively:

$$l_k\big|_{z=0} = l_\varepsilon\big|_{z=0} = l_{min0} \qquad l_k\big|_{z=bot} = l_\varepsilon\big|_{z=bot} = l_{min} \tag{2.14}$$

Alternatively, a Charnock-style boundary condition is used for the surface mixing and dissipation length scales:

$$l_k\big|_{z=0} = l_\varepsilon\big|_{z=0} = \kappa\beta\frac{|\tau|}{\rho_0 g} \tag{2.15}$$

where $\kappa = 0.41$ is the von Kármán constant and β is a wave age-dependant constant, set to $\beta = 2\text{x}10^5$ following Stacey (1999). The surface boundary conditions given by (2.14) and (2.15) are denoted here as l_{const} and $l_{Charnock}$ respectively.

Another specific of the TKE scheme in NEMO concerns the application of minimum numerical thresholds to the calculated TKE and mixing lengths. The general purpose of these thresholds is to ensure that their respective variables do not become too low in weakly-turbulent regions like the pycnocline. Furthermore, because the numerical integration of (2.5) does not guarantee a positive value, the use of a minimum threshold avoids unphysical negative values of TKE which can result otherwise.

The minimum thresholds on the surface and interior length scales (l_{min0} and l_{min}) are applied to (2.14), (2.15) and (2.9) such that $l_k\big|_{z=0} = l_\varepsilon\big|_{z=0} = \max\left(l_k\big|_{z=0}, l_{min0}\right)$ and $l_u = l_d = \max\left(\sqrt{2\bar{e}}/N, l_{min}\right)$. The values of l_{min0} and l_{min} here follow the logarithmic boundary layer approximation of $l_{min0} = l_{min} = \kappa z_0$, where z_0 is a surface roughness length taken to be 1 m. Values of $l_{min0} = l_{min} = 0.4$ m are therefore used in the present model configuration.

Similar thresholds are imposed on the surface and interior TKE (e_{min0} and e_{min}) and are applied to (2.12) and (2.5) respectively. Madec (2008) sets e_{min0} to 10^{-4} m^2s^{-2} to recover conditions for no surface wave breaking ($\alpha = 3.75$) and a minimum 10m wind speed of 3.85 ms^{-1} as for BD93. The value of e_{min} depends on the characteristics of mixing in weakly turbulent regions. Following Gaspar et al. (1990), Madec (2008) sets e_{min} to 10^{-6} m^2s^{-2} so that (2.9) agrees with the findings of Gargett (1984) in the thermocline and deep ocean where $K_\rho = 10^{-3}/N$, although BD93 instead find from their model of the tropical Atlantic that this latter value is too large for some cases in the thermocline and propose $e_{min} = 10^{-11}$ m^2s^{-2}.

The lack of a solution for the Gaspar et al. (1990) turbulent mixing length scale (2.9) for convective situations is addressed by Madec (2008) in a similar manner to BD93 (section 2.1). This highlights a weakness of the model in its ability to represent the turbulent mixing resulting from convection and so in the present model configuration convective mixing is parameterized by an enhancement to the eddy viscosity and diffusivity, where for $N^2 < 0$ K_m and K_ρ are locally set to the value of the parameter K_{conv} (typically 1-100 m^2s).

A further closure problem relating to vertical mixing schemes in general is that of parameterizing unresolved ‘background’ mixing processes, which typically include

breaking internal waves. Such parameterizations usually take the form of a prescribed background diffusivity, the simplest of which is constant in time and space. Beyond this, a range of time-constant profiles for the background diffusivity have been suggested with variation over depth and latitude (Jayne, 2008; Jochum, 2009), and other more complex schemes attempt to parameterize these processes with a dependence on the time-varying stratification (Gargett, 1984).

Madec (2008) implements two vertical profiles for the background diffusivity in NEMO: a simple vertically-constant profile and an observationally-based profile increasing linearly with depth after Kraus (1990), denoted here as $K_{\rho 0\_zconst}$ and $K_{\rho 0\_zKraus}$ respectively. This latter profile is roughly similar to the widely-used profile of Bryan and Lewis (1979), but is simpler in structure and does not asymptote to a vertically-constant value at abyssal depths. These vertical profiles are compared in figure 2.1.

The surface value of the background diffusivity profile is controlled by the parameter $K_{\rho 0}$. Madec (2008) here follows the tracer release experiment of Ledwell et al. (1993) where diffusivity in the pycnocline was measured to be $1.1 \pm 0.2 \times 10^{-5}$ m^2s^{-1} for a 5 month period, setting $K_{\rho 0}$ to 1.2×10^{-5} m^2s^{-1}. The background viscosity takes a vertically-constant profile as for $K_{\rho 0\_zconst}$ and is similarly controlled by a parameter for the surface value, K_{m0}. Given the choice for $K_{\rho 0}$ and assuming that $P_{rt} = 10$ in (2.2b), the value for K_{m0} is accordingly set to 1.2×10^{-4} m^2s^{-1}.

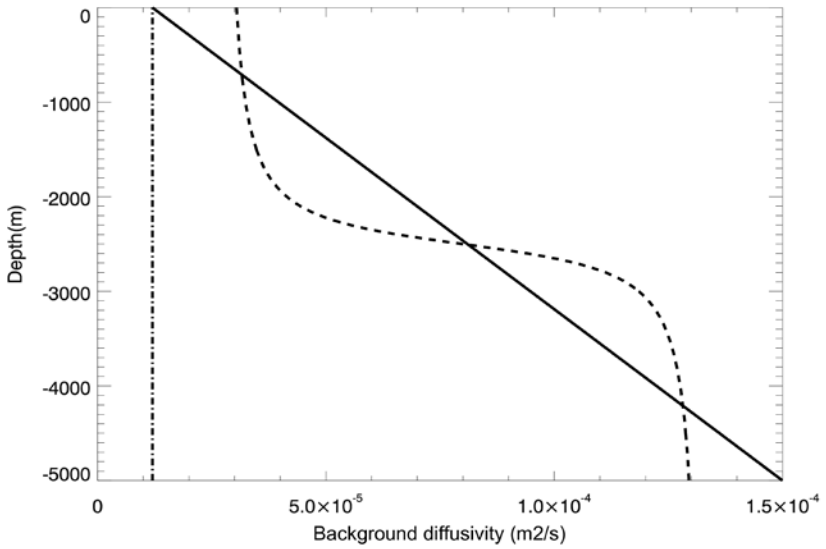

Figure 2.1: Background diffusivity profiles. The dash-dotted and solid lines represent the constant and linearly increasing profiles used in NEMO, with $K_{\rho 0}$ = 1.2e-5 m^2s^{-1}. The dashed line is the Bryan and Lewis (1979) profile for comparison.

Madec (2008) also implements a latitudinal profile of $K_{\rho 0}$ based on the observations of Gregg et al. (2003), where diapycnal mixing rates due to breaking internal waves were observed to be less than 10% at the equator compared to mid-latitude levels. For this profile a linear ramp-down is applied from 15° to 5° latitude, so that the equatorial background diffusivity between ±5° is a tenth of the 'global' value $K_{\rho 0}$ poleward of 15°. This profile and the alternate globally-constant horizontal profile of $K_{\rho 0}$ are denoted $K_{\rho 0\_yGregg}$ and $K_{\rho 0\_yconst}$ respectively.

A final modification made by Madec (2008) to the turbulent closure of BD93 introduces two parameterizations of physical processes unresolved by the scheme.

Firstly, a parameterization of Langmuir turbulence (Axell, 2002) is implemented as an additional production term in (2.4) and (2.5). By assuming that the dissipation term balances the Stokes drift production term in the TKE budget equation (as derived by Craik and Leibovich, 1976 from the wave-filtered Navier-Stokes equations), this term can be expressed as a velocity scale and a length scale:

$$\frac{d\overline{e_{LC}}}{dt} = -\overline{u'w'}\frac{dV_S}{dz} = \varepsilon \approx \frac{W^3}{L} \qquad (2.16)$$

where V_s is the Stokes drift, and W and L are characteristic velocity and length scales. W is taken to be the maximum downwelling velocity of the Langmuir cell, which is assumed to be directly related to the wind forcing. Following Leibovich (1983) $W = cV_{10}$, where V_{10} is the 10m wind magnitude and c is a constant, and following Li and Garrett (1993) $V_s\big|_{z=0} \approx 0.016V_{10}$ for a fully-developed sea. If we also assume that W takes a sinusoidal form based on the idealised structure of a Langmuir cell, this gives:

$$W = cV_{10} \approx c_{LC}V_S\big|_{z=0}\sin\left(-\frac{\pi \cdot z}{L}\right) \qquad \text{for } -z \le L \qquad (2.17)$$

$$W = 0 \qquad \text{for } -z > L$$

where c_{LC} is a constant ranging from 0.15 to 0.54 based on the observations of c by Leibovich (1983), but limited by Axell (2002) to between 0.15 and 0.2 based on comparisons of their model to LES simulations.

L is taken to be the vertical extent of the Langmuir cell, defined similarly to (2.8a,b) in being the distance that a fluid parcel at the surface of the cell can penetrate downwards, doing work against the stratification:

$$g\rho_0^{-1}\int_{z=-L}^{z=0}[\rho(z)-\rho_0].dz=\frac{1}{2}V_s^2 \qquad (2.18)$$

In addition to the above parameterization of Langmuir turbulence, an ad-hoc parameterization is included for mixing due to the breaking of near-inertial waves excited by high-frequency winds, a source of TKE henceforth referred to as $e_{inertial}$.

This is directly dependent on the TKE surface boundary condition in (2.12), and as a result the production term is an increase in the time-integrated TKE rather than a source term in the TKE budget equation:

$$\bar{e}(t+\Delta t,z)=\int_t^{t+\Delta t}\left(\frac{\delta\bar{e}}{\delta t}(z)\right)+\bar{e}_{inertial}(t,z) \qquad (2.19)$$

where:

$$\bar{e}_{inertial}(t,z)=\gamma.\bar{e}\big|_{z=0}\exp^{z/\lambda} \qquad (2.20)$$

where γ is the fraction of the TKE permeating down from the surface layer, λ is an e-decay length scale, and $\bar{e}_{inertial}$ is zero for the first model level.

Madec (2008) suggests the use of γ = 0.05 (but without a clear justification for doing so) and specifies several global profiles for the value of λ, which are denoted:

λ_{10m} : λ = 10m globally

$\lambda_{0.5-30m}$: λ = 0.5m at 0° latitude, increasing sinusoidally to 30m at 60° (2.21)

λ_{5-40m} : λ = 5m at 0° latitude, increasing sinusoidally to 40m at 60°

Based on work by the DRAKKAR consortium (Molines et al. 2006), Madec (2008) uses the $\lambda_{0.5\text{-}30m}$ length scale profile by default. The above settings for the $e_{inertial}$ parameterization (γ = 0.05 and $\lambda = \lambda_{0.5\text{-}30m}$) are henceforth referred to as the 'standard' settings for the present NEMO-CICE configuration.

3. Model details

This section describes the model configuration used in the sensitivity experiments discussed in the following results section. The details of this configuration and the definition of the control experiment settings are given in section 3.1, while a list of the sensitivity experiments for which results are presented is given in section 3.2.

3.1. Settings and model configuration of the control experiment

The sensitivity experiments discussed in this report use version 3.0 of the NEMO OGCM (Madec, 2008) coupled to version 4.0 of the CICE ice model (Hunke and Lipscomb, 2008). The model was run at a 1° horizontal resolution on the ORCA1 grid (Murray, 1996), using 75 vertical levels with a grid thickness of ~1 m at the surface and ~200 m at the lowest level.

The experiments were initialised from rest using the EN3 2004-2008 temperature and salinity climatology (Ingleby and Huddleston, 2007), and were forced using the DFS4.1 surface forcing dataset (Brodeau et al., 2009) and CORE bulk forcing algorithm (Large and Yaeger, 2004). The experiments were run from 1st January 1976 for 10 years, of which model years 7-10 (1982-1985) were analysed.

The configuration of the NEMO-CICE control experiment on which the sensitivity experiments were based (henceforth the ‘reference configuration’) was designed to mirror that of the N96-ORCA1 development configuration of HadGEM3. Here we limit discussion of the specifics of this experiment to the vertical mixing parameter settings, which are given in table 1 and will henceforth be referred to as the ‘control values’ of the TKE scheme parameters. This particular version of NEMO has two implementations of the NEMO TKE scheme, referred to as the ‘old’ and ‘new’ schemes. The main numerical difference between these two implementations is the use in the ‘new’ scheme of the Burchard (2002) discretization for the TKE production due to shear and buoyancy, which has little impact on the model results. The sensitivity experiments therefore use the ‘old’ implementation of the TKE scheme to be consistent with the N96-ORCA1 configuration of HadGEM3.

Parameter	NEMO parameter	Description	Reference
α	rn_ebb	Surface wave breaking coefficient	60
γ	rn_efr	Near-inertial wave breaking TKE scaling	-
λ	nn_htau	Near-inertial wave breaking length scale	-
$K_{\rho 0}$	rn_avt0	Surface value of background diffusivity	$1.2\text{x}10^{-5}$ m^2s
K_{m0}	rn_avm0	Surface value of background viscosity	$1.2\text{x}10^{-4}$ m^2s
$K_{\rho 0\_zKraus}$ or $K_{\rho 0\_zconst}$	nn_avb	Choice of vertical profile of $K_{\rho 0}$	$K_{\rho 0\_zKraus}$
$K_{\rho 0\_yGregg}$ or $K_{\rho 0\_yconst}$	nn_havtb	Choice of latitudinal profile of $K_{\rho 0}$	$K_{\rho 0\_yconst}$
l_{min}	rn_lmin	Minimum interior length scale threshold	0.4 m
l_{min0}	rn_lmin0	Minimum surface length scale threshold	0.4 m
e_{min}	rn_emin	Minimum interior TKE threshold	10^{-6} $m^s s^{-2}$
e_{min0}	rn_emin0	Minimum surface TKE threshold	10^{-4} $m^2 s^{-2}$
c_{LC}	rn_lc	Langmuir turbulence coefficient	-
K_{conv}	rn_avevd	Value of K_{m0} and $K_{\rho 0}$ used for convection	100 $m^2 s^{-2}$
c_k	rn_ediff	Stability function for TKE	0.1
c_ε	rn_ediff	Stability function for dissipation	0.7
$l_{Charnock}$ or l_{const}	ln_mxl0	Choice of surface length scale	$l_{Charnock}$

Table 1: Vertical mixing parameter settings in the reference configuration. Blank settings refer to parameterizations that were not used in the configuration.

3.2. Sensitivity experiments

Table 2 lists the parameter settings of the sensitivity experiments discussed in the following results sections. These settings mostly comprise single-parameter perturbations of the parameters given in table 1 from their control values. The exceptions to this are the experiments with the near-inertial wave breaking parameters γ and λ (for which all values of γ were run for each setting of λ), the experiments with the surface wave breaking parameter α (run with and without $e_{inertial}$) and the experiments where c_k and c_ε were run in constant proportion to each other (see section 4.4).

A series of initial sensitivity experiments using a coarser-resolution model (ORCA2 with 31 vertical levels and a 5m surface grid box thickness) were used to help define the range of parameter values used for the full set of parameter experiments, of which the experiments in table 2 are a subset. It should be noted however that the parameter c_{LC} had a hard-coded limit on its value of 0.15-0.2 in this version of NEMO, and as a result the full range of c_{LC} estimated by Leibovich (1983) was not tested.

Parameter	Reference	Parameter values											
α	60	20	33.3	46.7	73.3	86.7	100	200	300	400	500	600	700
α, $e_{inertial}$	-	20		33.3		46.7		60		73.3		86.7	100
γ	-	0.005		0.02		0.05		0.035		0.065		0.08	0.095
λ	-	λ_{10m}				$\lambda_{0.5\text{-}30m}$				$\lambda_{5\text{-}40m}$			
$l_{Charnock}$ or l_{const}	$l_{Charnock}$	l_{const}											
l_{min}	0.4	1.2											
l_{min0}	0.4	3.7		7		10.3		13.6		16.9		20.2	
e_{min}	10^{-6}	$9\text{x}10^{-6}$											
e_{min0}	10^{-4}	$14.15\text{x}10^{-4}$		$27.3\text{x}10^{-4}$		$40.45\text{x}10^{-4}$		$53.6\text{x}10^{-4}$		$66.75\text{x}10^{-4}$		$79.9\text{x}10^{-4}$	
c_{LC}	-	0.15						0.2					
c_k	0.1	0.04	0.06	0.08	0.12	0.14	0.16	0.18	0.2	0.22	0.24	0.26	0.28	0.3
c_ε	0.7	0.1		0.25		0.4		0.55		2		5	10
c_k , $c_\varepsilon = c_k$ x 7	0.1	0.2			0.3			0.4			0.5		0.6

Table 2: Sensitivity experiments presented in the results section.

The four parameters in table 1 related to background mixing are not included in the list of sensitivity experiments in table 2. While the specification of the background mixing is shown to have a short-term impact on the near-surface thermal structure of the model, multi-decadal model integrations are required to accurately quantify the impact on the deep ocean. It is therefore difficult to make confident revisions to the specification of the background mixing based on the present set of 10-year sensitivity experiments and cost-prohibitive to perform multi-decadal simulations with the present model configuration. Any revisions to the values of the background mixing parameters are therefore outside the scope of this report

4. Results

This section discusses the main results of the NEMO-CICE sensitivity experiments, which have been run for 10 years from 1976-1985. Analysis is presented for model years 7-10 (1982-1985), and where appropriate recommendations for changes are presented with respect to the control values of TKE scheme parameters outlined in section 3. These recommended changes are summarised in section 5.

4.1. Impact and sensitivity of the turbulence surface boundary condition

Here the sensitivity of the model to the parameters governing the TKE scheme surface boundary condition is discussed. In particular the impact of the choice of surface mixing length formulation and the surface wind-wave energy coefficient α are examined.

As discussed in section 1, it is evident that the model suffers from a lack of mixing in the summer hemispheres. Given that the control value of α neatly bisects the bracketing

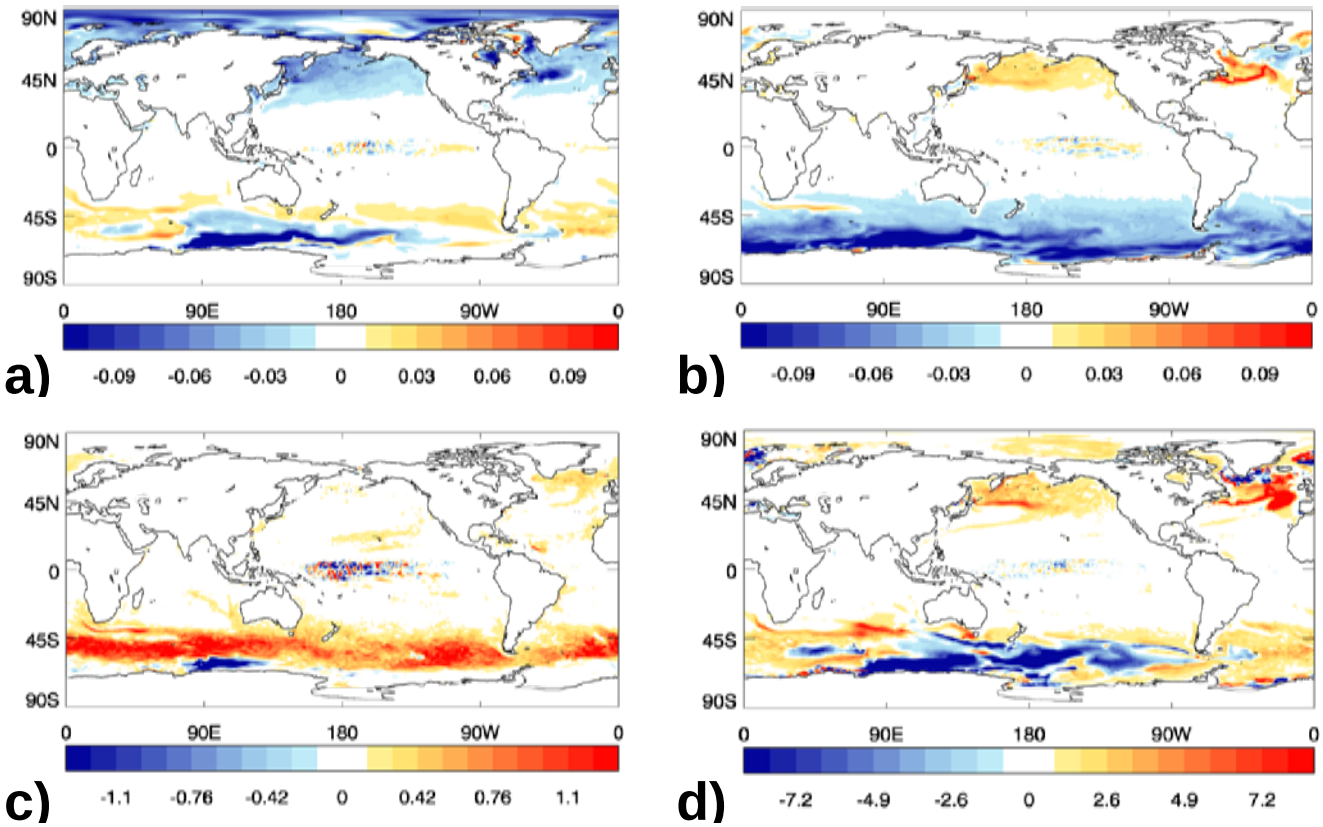

Figure 4.1: Difference in: (a) JJA SST, (b) DJF SST, (c) mean annual minimum MLD and (d) mean annual maximum MLD for the experiment with α = 86.7 minus the reference configuration with α = 60.

values of MB04 given in section 2, a logical test of parameter sensitivity here is to increase α to the upper bracketing value of 86.7 in order to understand the extent to which the near-surface vertical mixing can be increased by realistic adjustment of this parameter.

Figure 4.1 shows the impact of this increase in α on the model SST and MLD relative to the reference configuration. The most coherent impact is seen to be on the summer MLD (here represented by the mean annual minimum MLD) in the storm track region of the Southern Ocean. This is perhaps expected given the dependence of (2.12) on the surface wind stress; in theory the model will be most sensitive to α in regions of high wind stress.

Consequently there are also notable impacts on summer SSTs in the North Pacific storm

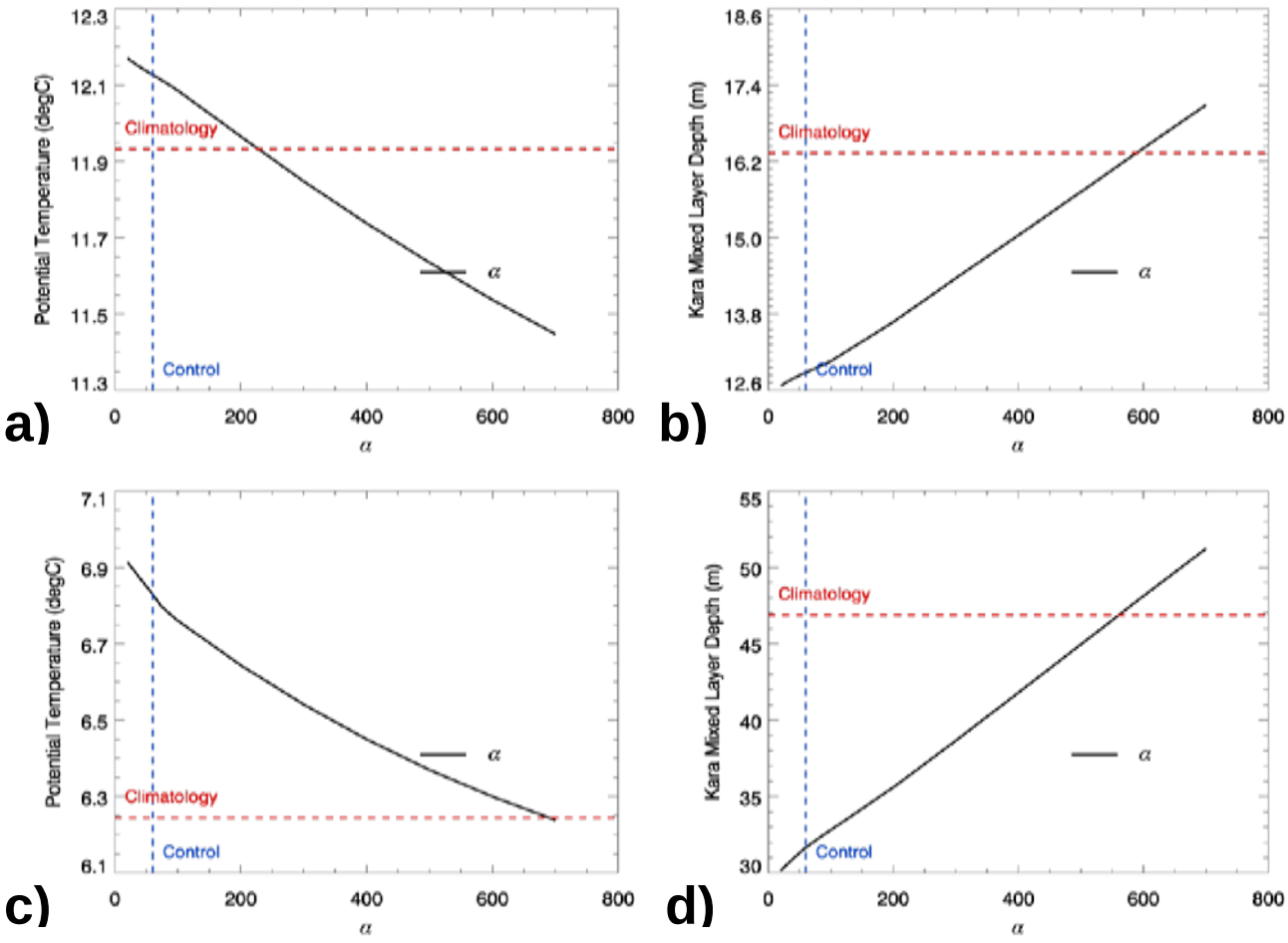

Figure 4.2: Mean (a) JJA SST and (b) annual minimum MLD averaged over the North Pacific (40-60N, 120-180W), and (c) DJF SST and (d) annual minimum MLD averaged over the Southern Ocean (45-60S) as a function of α. The blue dashed lines correspond to the reference configuration value of α, while the red dashed lines represent the climatological (a,c) Reynolds SST and (b,d) de Boyer Montégut MLD

track where there is a widespread cooling around the north of the basin, though the impact on the summer MLD is much less apparent here. There is also some impact on the winter MLD (here represented by the mean annual maximum MLD), including some shoaling around the Antarctic coastline associated with an increase in melt water and deepening throughout much of the North Atlantic, which is not enough to significantly impact major biases. The winter mixed layer itself warms in response to the increase in summer mixing, and while this acts to alleviate cold winter SST biases the impact is again only a small proportion of these biases.

Focussing on the summer biases, figure 4.2 illustrates the impact on the North Pacific and Southern Ocean MLD and SST over the full range of values of α used in the NEMO-CICE experiments.

In both locations an increase in α acts to alleviate the shallow summer MLD and warm SST biases. Upon closer examination however, the upper bracket value of $\alpha = 86.7$ constitutes only a minor impact on these biases with significant alleviation of MLD biases occurring only when α is increased to very large values. Tuning of the surface wave

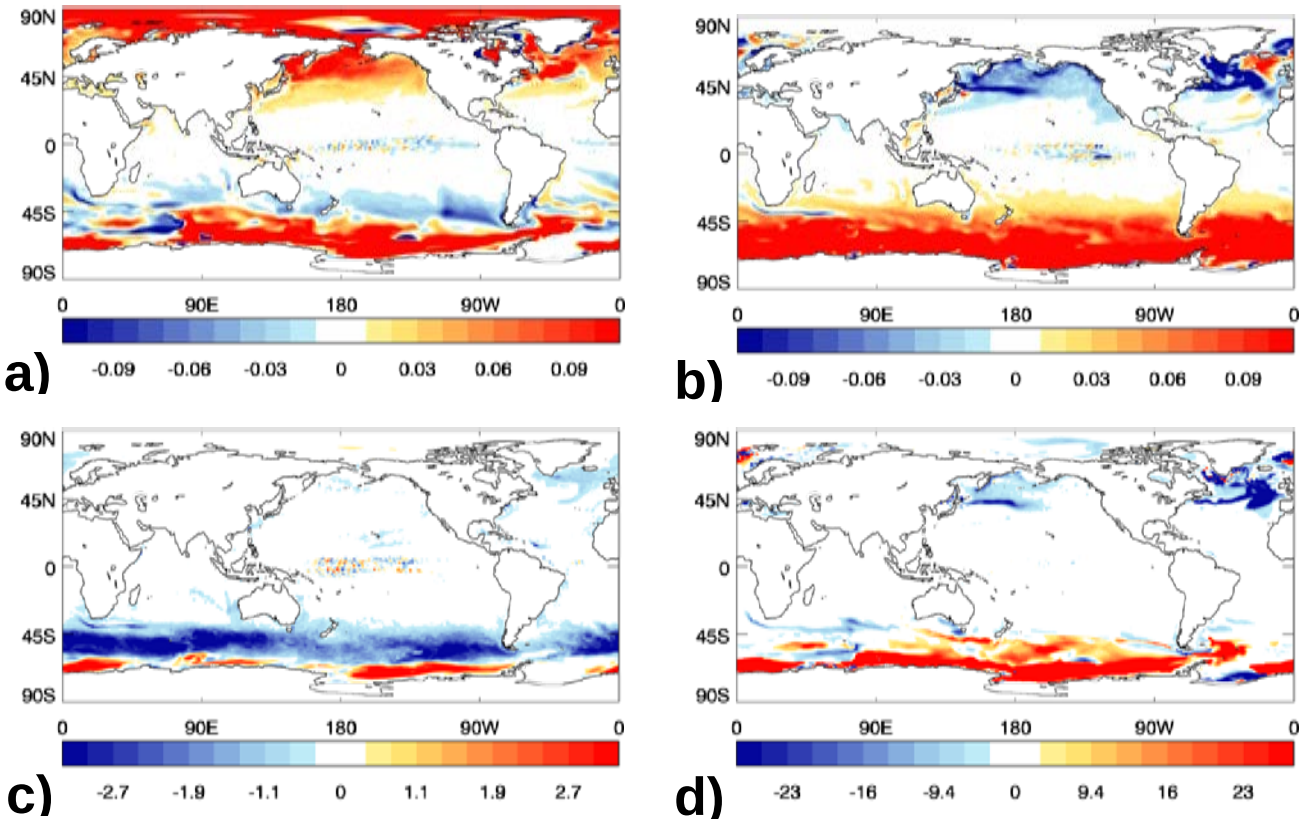

Figure 4.3: Difference in: (a) JJA SST, (b) DJF SST, (c) mean annual minimum MLD and (d) mean annual maximum MLD for the experiment with I_{const} minus the reference configuration with $I_{Charnock}$.

breaking boundary condition is therefore unlikely to result in a significant alleviation of the biases related to insufficient summer mixing, but nevertheless minor improvements are still to be found.

The importance of the stipulation of a realistic surface length scale is also considered here. Figure 4.3 shows the impact on model SSTs and MLDs when the Charnock length scale ($l_{Charnock}$) is replaced with a constant numerical minimum (l_{const}). Compared with the impact of increasing α (figure 4.1) the spatial distribution of the changes in temperature and MLD are very similar. From (2.15) it can be seen that as for the surface TKE SBC in (2.12), $l_{Charnock}$ has a dependence on the surface wind stress and that for typical wind stress magnitudes this will usually equate to an increase in surface mixing length relative to the value of 0.4m used by l_{const}. As the eddy diffusivity approximation (2.2) is a product of the TKE and a mixing length it is therefore not surprising to find that an increase in α and the use of $l_{Charnock}$ have spatially similar impacts, as both result in an increase in the

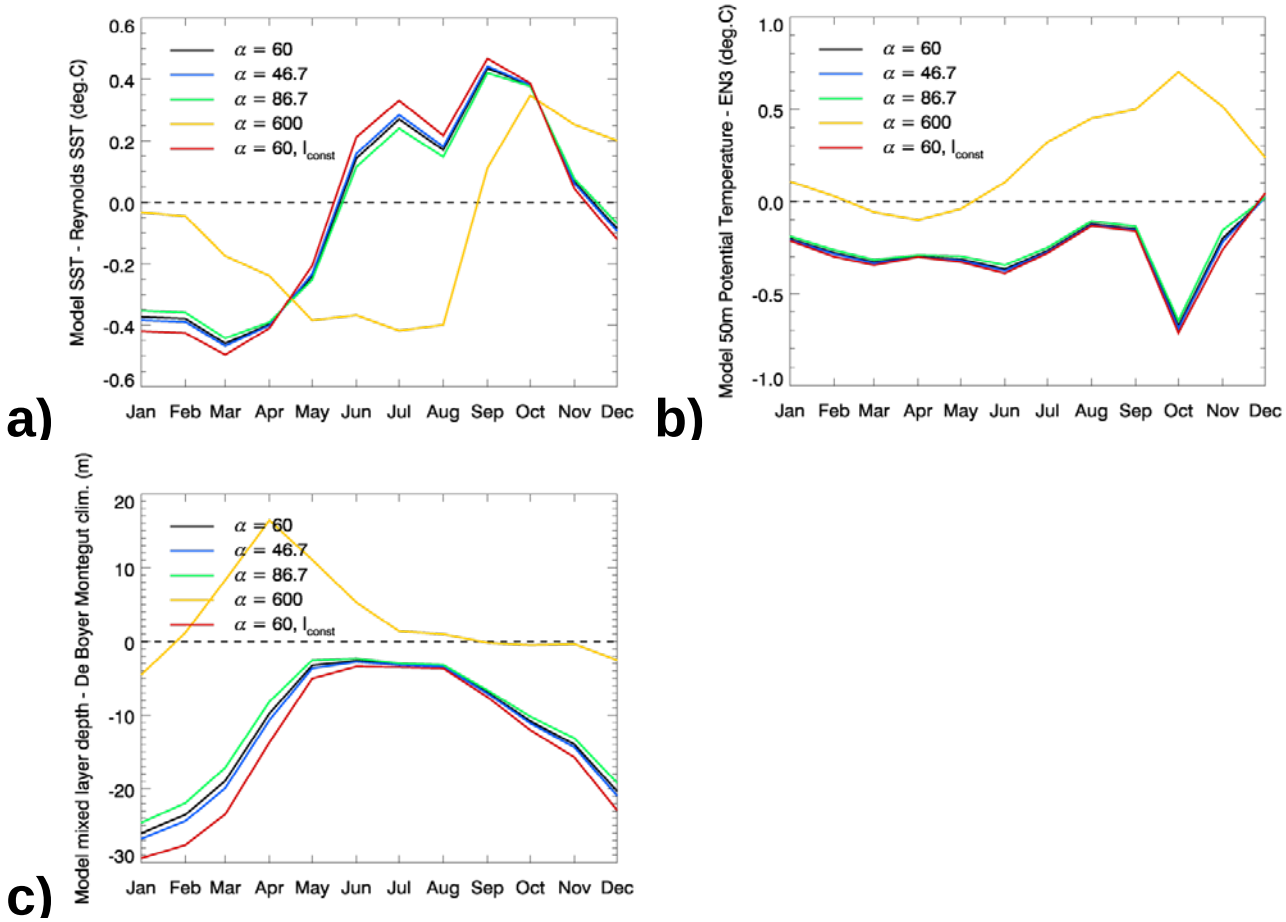

Figure 4.4: Mean annual cycles for 1982-1985 of biases in: (a) SST, (b) 50m potential temperature and (c) MLD averaged over the North Pacific (40-60N, 120-180W) for various values of α and for the experiment with l_{const}. The solid black line is the reference configuration.

near-surface eddy diffusivity that is proportional to the surface wind stress.

The use of l_{const} clearly results in a significantly detrimental impact on SST and MLD biases, increasing the summer hemisphere SST bias by O(0.1°) in places. If the range of α used in figure 4.1 is expanded to encompass the full range given by MB04 in section 2, then the magnitude of the SST and MLD change (not shown) is only slightly less than that seen in figure 4.3. This suggests that the choice of α over a realistic range of values is of comparable importance to the stipulation of a realistic surface mixing length in addressing the shallow summer mixing biases via the turbulence surface boundary condition.

Several of the experiments discussed above are compared in figures 4.4 and 4.5, which show biases in the mean seasonal cycles of SST, 50m temperature and MLD in the North Pacific and Southern Ocean. As previously noted, there is generally a small positive impact on upper ocean temperature biases as α increases. In the North Pacific

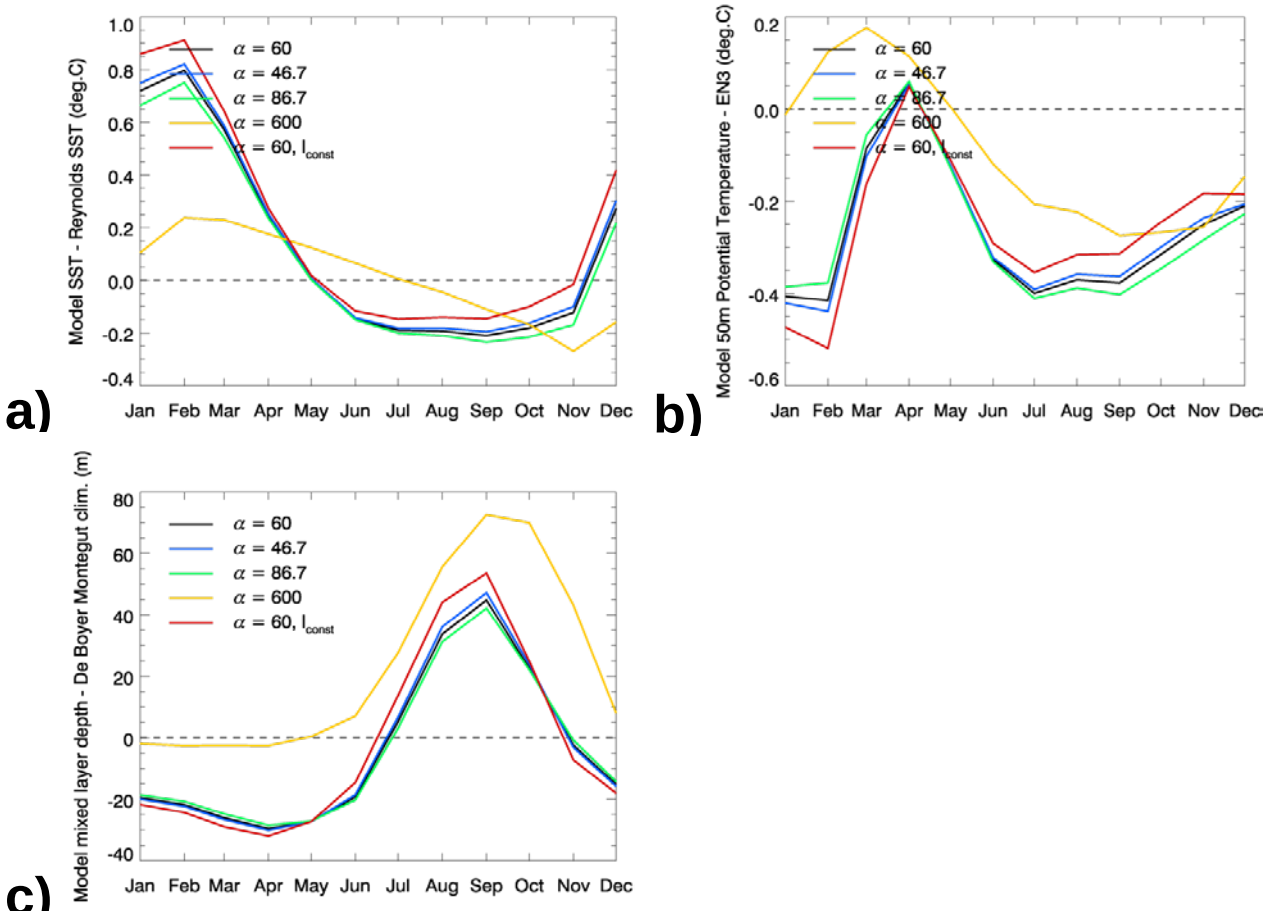

Figure 4.5: Mean annual cycles for 1982-1985 of biases in: (a) SST, (b) 50m potential temperature and (c) MLD averaged over the Southern Ocean (45-60S) for various values of α and for the experiment with l_{const}. The solid black line is the reference configuration.

the increase in transfer of heat below the summer mixed layer improves summer and winter upper ocean temperatures and MLDs, while in the Southern Ocean summer biases are similarly improved but cold winter temperature biases deteriorate. Winter MLD biases here also appear to improve; the Southern Ocean is dominated by excessively deep winter MLDs along the Antarctic Circumpolar Current which are alleviated somewhat by the reduction in MLD in the Pacific observed in figure 4.1d. However these deep biases are greatly reduced in the coupled model (figure 1.2b) and the MLD reduction appears to be attributable to increased melt water from the sea ice. Away from ice-covered areas the winter response is a slight warming and deepening of the MLD as for the North Pacific, which in general improves biases.

The use of the $l_{Charnock}$ mixing length is again shown to be of comparable importance to the specification of α here; similar improvements in biases are seen relative to l_{const} as for an increase in α between its bracketing values of 46.7 to 86.7. The experiment using $l_{Charnock}$ and α = 86.7 has improved summer SSTs of ~0.1°C in the North Pacific and ~0.2°C in the Southern Ocean relative to the experiment using l_{const} and α = 60, which exhibits the largest summer biases. However most of this improvement comes from the $l_{Charnock}$ mixing length, and while this helps to justify the use of $l_{Charnock}$ over l_{const} it also reaffirms the earlier observation that a realistic increase in α is not expected to result in a significant impact on biases in the reference configuration. As for figures 4.2b and 4.2d it is evident that to alleviate summer MLD biases in general a very large value of α of around 600 is required. This again highlights the limitations of α as a tuneable

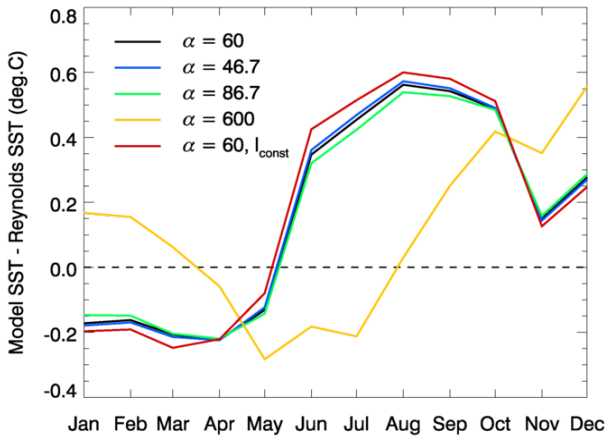

Figure 4.6: Mean annual cycles for 1982-1985 of biases in SST at OS PAPA (50N, 145W) for various values of α and for the experiment with l_{const}. The solid black line is the reference configuration.

parameter; within realistic limits it has only a minor impact on model biases and suggests that the deficiency in vertical mixing is unlikely to be significantly addressed by increasing the surface wave breaking TKE.

The response of ocean models to parameterizations of surface wave breaking remains an uncertain topic. Using a 1D column configuration of the Mellor and Yamada (1982) model at OS PAPA, MB04 observed a notable decrease in summer SSTs (~0.5°) when they increased the value of α_{CB} from 50 to 100 (α = 42.7 to 67.8). However, other studies (Klein and Coantic, 1981; D'Alessio et al., 1998; Burchard, 2001; Kantha and Clayson, 2004) have argued that the upper ocean can only be significantly influenced by surface wave breaking when the MLD is very shallow, as the mixing is confined to the near-surface within a depth scale comparable to the significant wave height.

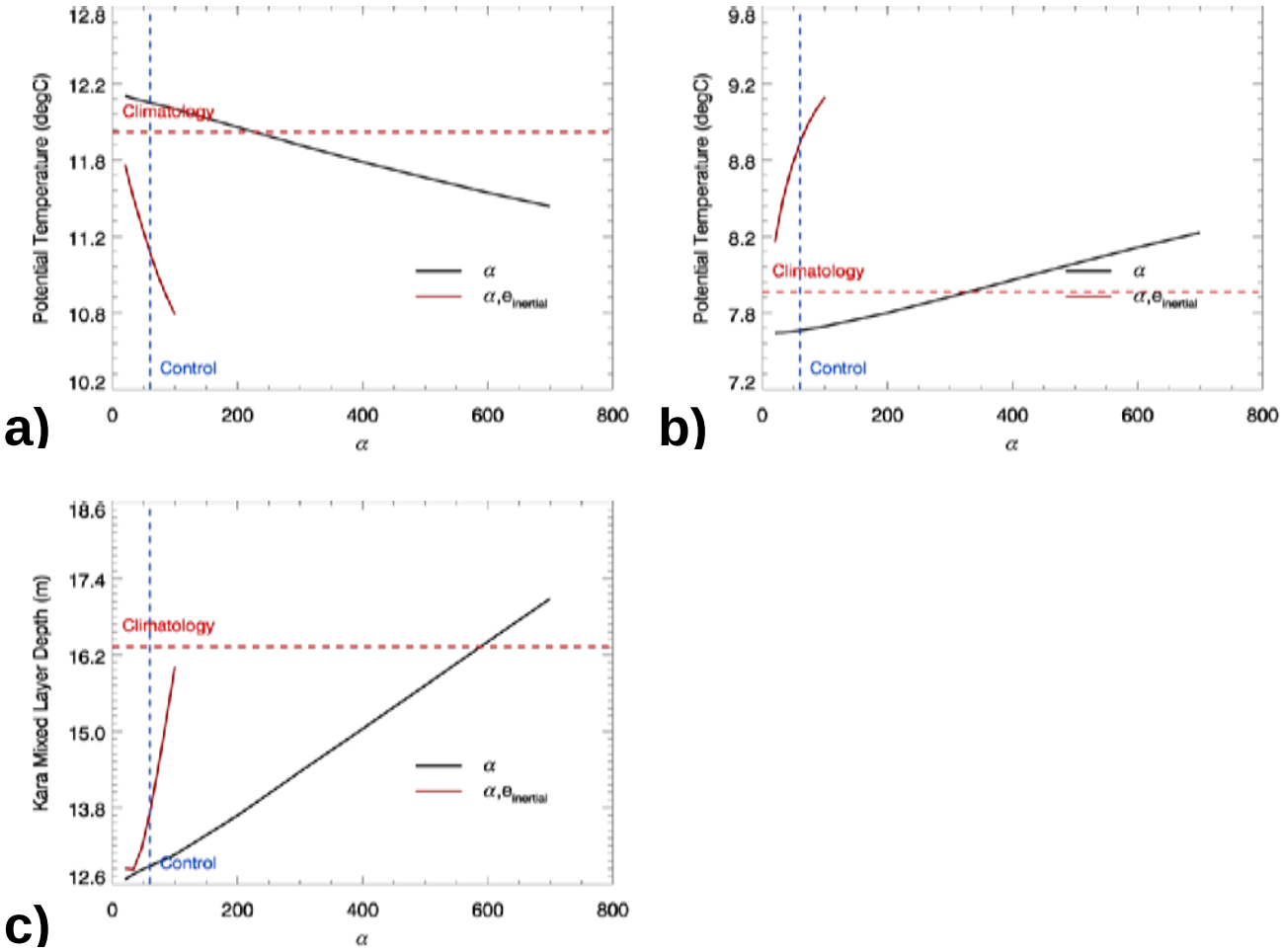

Figure 4.7: Mean JJA: (a) SST, (b) 50m potential temperature and (c) mean annual minimum MLD averaged over the North Pacific (40-60N, 120-180W), as a function of (black solid line) α and (red solid line) α including $e_{inertial}$ mixing (using the $\lambda_{5\text{-}40m}$ length scale). The blue dashed lines correspond to the reference configuration value of α, while the red dashed lines represent the climatological (a) Reynolds SST, (b) EN3 temperature and (c) de Boyer Montégut MLD.

Figure 4.6 shows a comparison of biases in the mean annual cycle of SST as for figure 4.4a, except for the grid point nearest to OS PAPA. The limited influence of α on the summer SSTs is again apparent here, and given the values of α used by MB04 it is evident that the present model does not replicate their observed sensitivity to α. Rather, the present findings agree with the 1D testing of Huang et al. (2011) who find little sensitivity at OS PAPA for a much larger perturbation to α using a similar model to MB04.

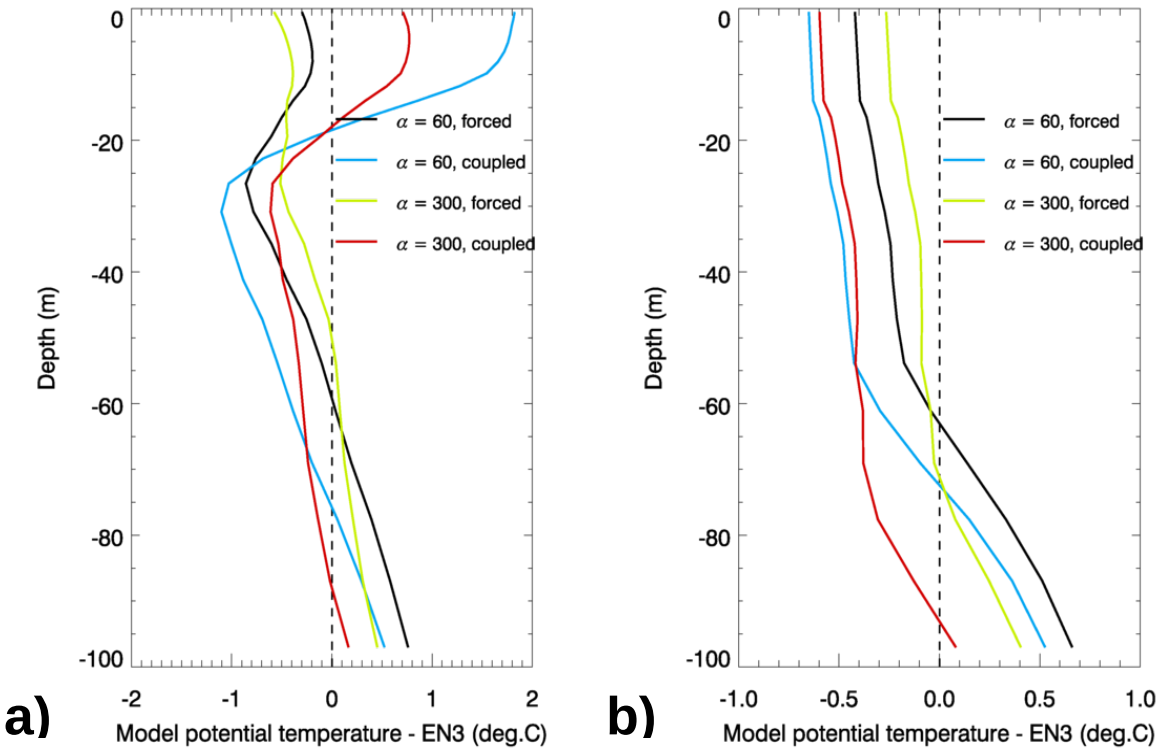

Figure 4.8: (a) JJA and (b) DJF average potential temperature bias profiles for the North Pacific (40-60N, 120-180W). 'Forced' refers to NEMO-CICE bulk-forced experiments while 'coupled' refers to HadGEM3 atmosphere-coupled experiments.

The impact of the wave breaking parameterization therefore appears to be inherently limited by the surface confinement of its contribution to the TKE budget (or from a modelling point of view its implementation as a surface boundary condition). This can be illustrated with the use of the $e_{inertial}$ parameterization. Since this parameterization is implemented as an arbitrary source profile of TKE based on the TKE surface boundary condition (equation 2.20), it can be considered from a practical point of view to be a depth-extension of the surface wave breaking parameterization (2.12).

Figure 4.7 shows the summer SST, 50m temperature and MLD for the North Pacific as a function of α, with and without the $e_{inertial}$ parameterization. Despite the narrow range of parameter values used for the former set of experiments it is clear that the use of $e_{inertial}$ greatly enhances the sensitivity to α and shows that the surface confinement of the wave breaking parameterization is a limiting factor in its impact on upper ocean mixing.

A further factor to consider is that the present experiments are not coupled to an atmosphere model. As the TKE surface boundary condition is dependant on the surface wind stress, the feedback of the ocean impacts of α onto the atmosphere should be considered in order to fully understand the parameter's sensitivity. A 10-year HadGEM3 atmosphere-coupled experiment was therefore performed to investigate the effect of coupling on the ocean model sensitivity to α.

Diagram 4.8 shows JJA and DJF average temperature bias profiles in the North Pacific from the bulk-forced and coupled configurations for two values of α. For both configurations there is a quantitatively similar impact on the summer subsurface temperatures from increasing α, showing a similar amount of warming at 20-60m. However the coupled configuration clearly exhibits a much greater cooling of the summer mixed layer and less warming of the winter mixed layer compared to the forced configuration. Given the similar impact on the subsurface temperatures across both configurations, this seems to indicate that the summertime surface response to α in the NEMO-CICE configuration is suppressed, possibly as a result of the bulk forcing algorithm.

The above results suggest that an increase in α will result in minor improvements to near-surface biases in NEMO-CICE, but there is evidence that a somewhat greater impact should be expected in coupled configurations where these biases are typically larger. The 'optimal' value of α_{CB} from testing by Craig and Banner (1994) and MB04 is given as 100 (α = 67.83), although ideally α should be a function of the wave age (and will therefore be most accurately portrayed with the coupling of a wave model). This value is however a justifiable increase to propose for the current fixed value of α and subsequently it is proposed that α be increased from 60 to 67.83 in the GO5.0 configuration.

4.2. Impact and sensitivity of the near-inertial wave breaking parameterization

Here the results of the experiments concerning the near-inertial wave breaking parameterization $e_{inertial}$ are discussed, where perturbations were made to the scaling parameter γ and to the choice of e-decay length scale λ (equations 2.20 and 2.21).

The behaviour of this parameterization in NEMO is not particularly well understood. It is thought to have been implemented to compensate for a lack of inertial current-related mixing in configurations with a daily coupling frequency, but both its theoretical basis and the testing underlying its formulation are unclear. There is therefore no real guidance as to what constitutes a realistic range of parameter values and no apparent justification for the standard settings given in section 2.2 (where γ = 0.05 and from equation 2.21, λ = $\lambda_{0.5\text{-}30m}$). There is therefore a risk that due to poorly-defined parameter constraints $e_{inertial}$ could be tuned to alleviate unrelated mixing biases. Additionally, the standard settings for this parameterization may no longer be appropriate for ocean models with wind forcing or coupling at sub-diurnal frequencies. The behaviour of the $e_{inertial}$

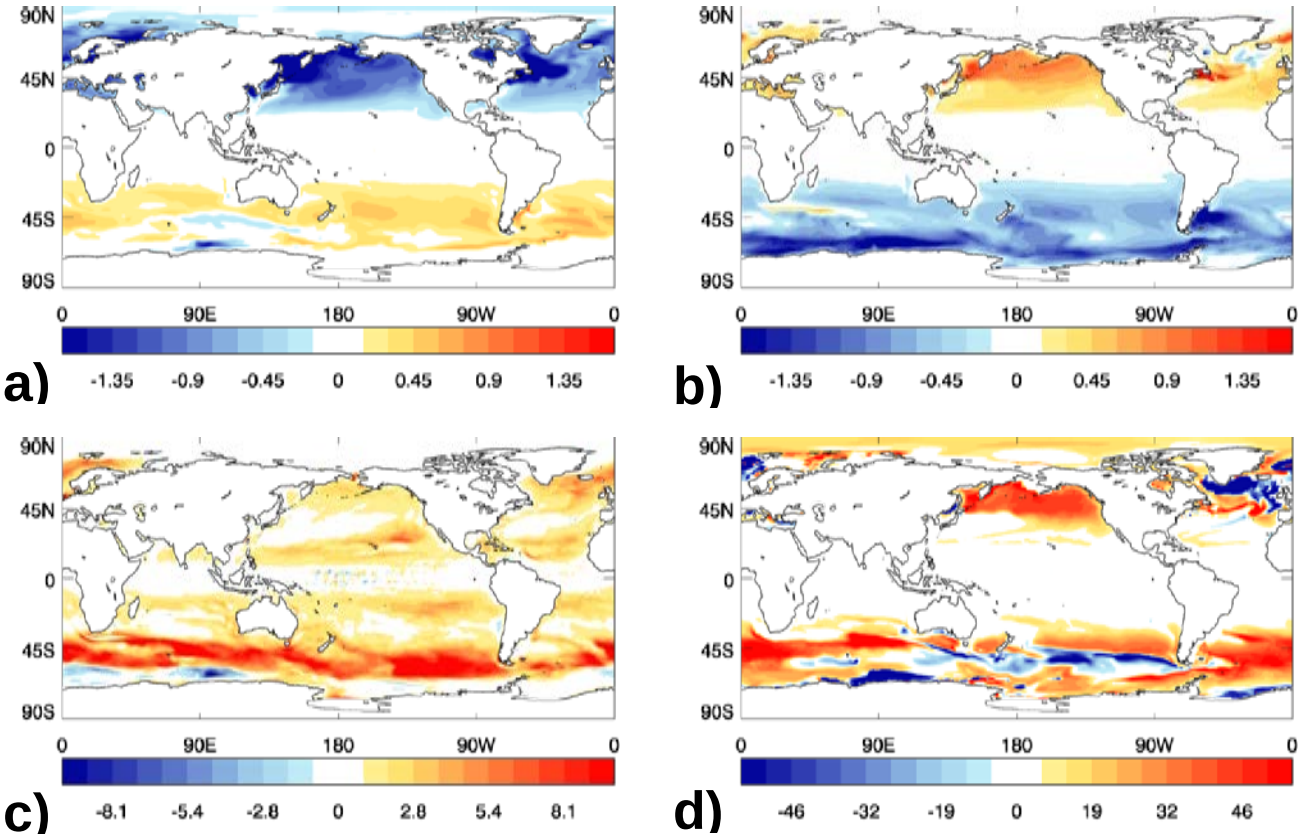

Figure 4.9: Difference in: (a) JJA SST, (b) DJF SST, (c) mean annual minimum MLD and (d) mean annual maximum MLD for the experiment with γ = 0.065 minus the experiment with γ = 0.05. The $\lambda_{0.5\text{-}30m}$ length scale profile is used for both experiments.

parameterization is therefore examined here by looking at the model sensitivity to γ and to the choice of profile for λ, so that the impacts from the use of this parameterization and the significance of its poorly-constrained parameter values are better understood.

Figure 4.9 illustrates the impact on the model SST and MLD of an increase in γ, using the standard length scale profile $\lambda_{0.5\text{-}30m}$. In the absence of an upper bound on γ an arbitrary increase of 30% has been used, so that γ has been increased here from 0.05 to 0.065.

As for an increase in the parameter α the largest impacts on the SST and MLD are observed in the extratropics; from a comparison of figures 4.1 and 4.9 there is a qualitative similarity in the spatial distribution of the observed changes. An increase in

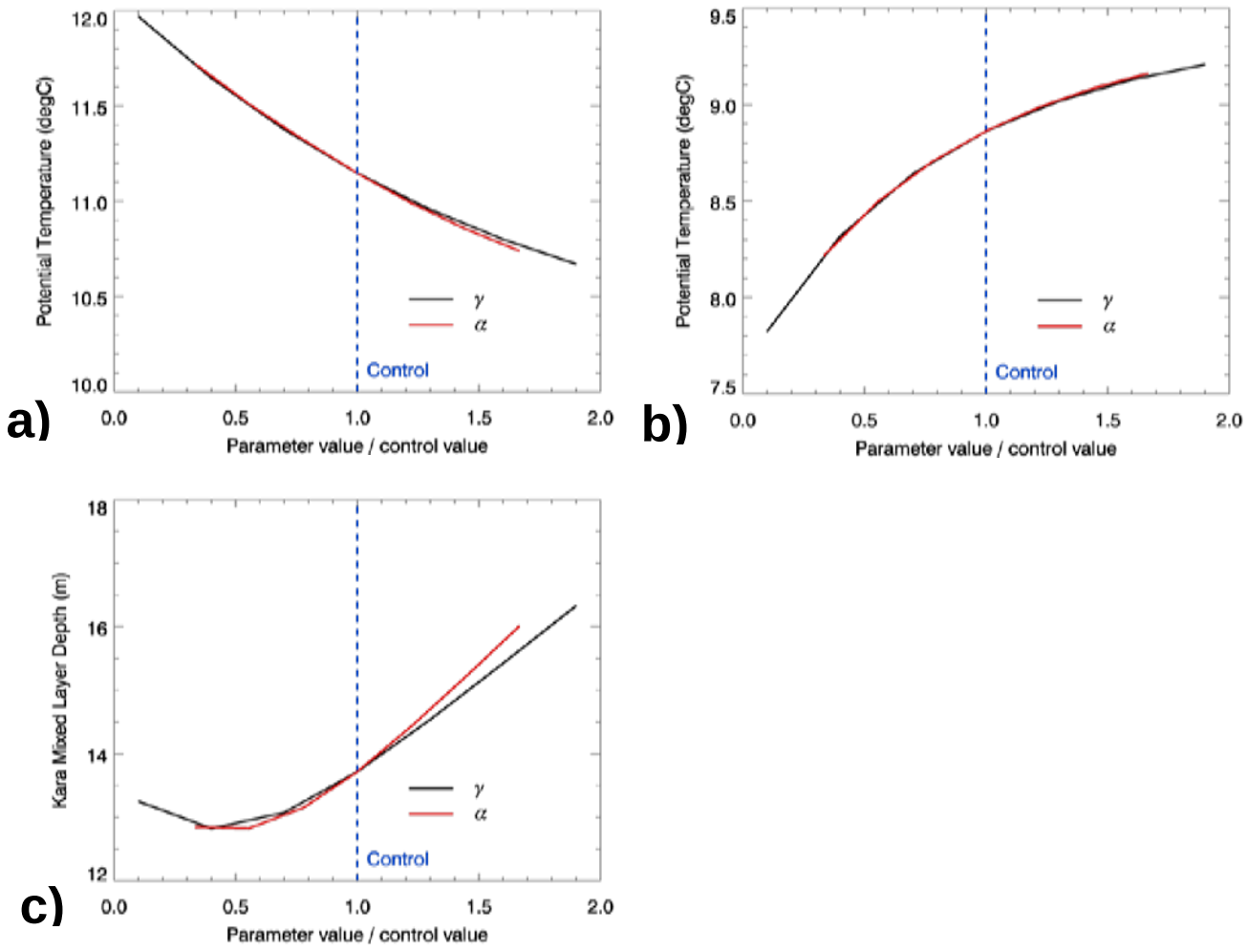

Figure 4.10: JJA mean (a) SST and (b) 50m potential temperature and (c) mean annual minimum MLD for the North Pacific (40-60N, 120-180W) as a function of γ and α divided by their control values, for experiments with $e_{inertial}$ mixing and using the length scale profile $\lambda_{5\text{-}40m}$. The blue dashed lines correspond to the control value of α and standard setting for γ.

vertical mixing in the summer mixed layer leads to a cooling of summer SSTs and a deepening of summer MLDs, with a similar warming and pattern of MLD deepening and shoaling being observed for the winter mixed layer as for an increase in α.

It is important to note the magnitude of the response resulting from this arbitrary increase in γ, which is much larger than seen for α in figure 4.1. Summer MLDs increase by 1-10m globally and summer SSTs decrease by O(1°) polewards of the subtropics in both hemispheres, which when compared to the typical magnitude of model biases in figures 1.1 and 1.2 represent significant impacts on the model. γ should therefore be considered a sensitive parameter when the standard length scale profile of $\lambda_{0.5\text{-}30m}$ is used, which given the lack of constraints on its value implies that there is considerable uncertainty associated with the magnitude of the impact of the $e_{inertial}$ parameterization.

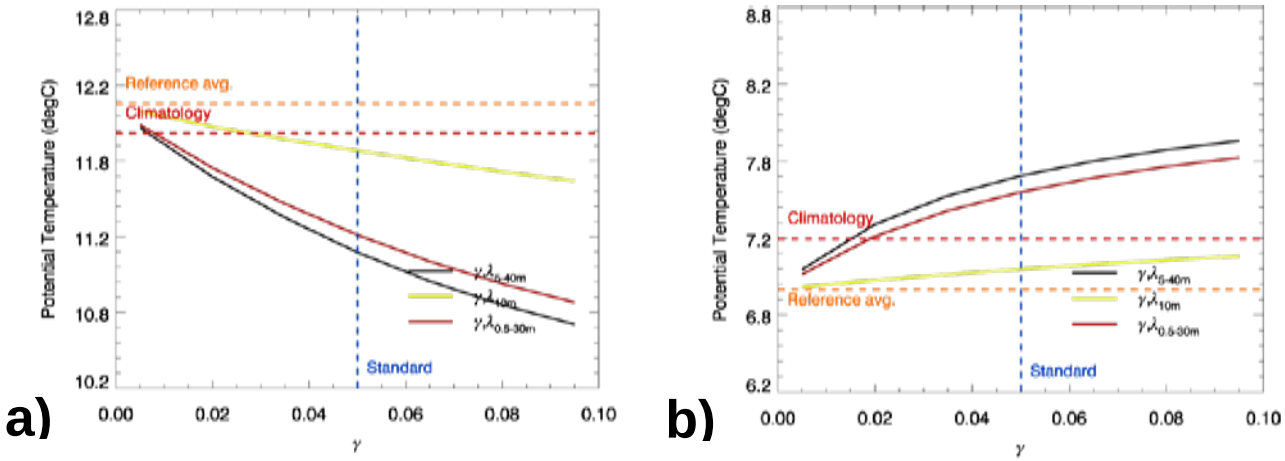

Figure 4.11: (a) JJA and (b) DJF SST averaged over the North Pacific (40-60N, 120-180W), as a function of γ for various profiles of λ. The red dashed lines show the climatological Reynolds SST, the blue dashed lines denote the standard setting for γ and the orange dashed lines show the SST in the reference configuration without $e_{inertial}$.

From (2.20) it can be seen that the TKE added by the $e_{inertial}$ parameterization is dependant on the TKE SBC and so the qualitative similarity of the impacts of γ and α can likely be explained by their mutual dependence on the surface wind stress. Furthermore this means that the $e_{inertial}$ parameterization is dependant on both parameters, and so it is useful to consider their respective contributions to the sensitivity of this parameterization.

Figure 4.10 compares the sensitivity of the North Pacific summer upper ocean temperature and MLD to γ and α when the $e_{inertial}$ parameterization is used. Expressed in terms of a fraction of their control values, the response to both parameters is clearly very

similar and begins to diverge only in their impact on the summer MLD for larger parameter values. This similarity is likely a consequence of the weak impact of α in the absence of $e_{inertial}$ as demonstrated in section 4.1, but also serves to illustrate the role that γ plays in scaling the amount of TKE available from the surface wave breaking.

It is also evident from (2.20) that the magnitude of the e-decay length scale λ will have an influence on the sensitivity to γ. To illustrate this, figure 4.11 shows the sensitivity of the North Pacific JJA and DJF average SSTs to γ for the three λ profiles given by (2.21). The magnitude of the response is clearly shown to be proportional to both γ and the value of λ in the extratropics (from (2.21) this is shown to have a latitudinal dependence). As γ approaches 0, the SSTs converge towards that of the reference configuration where $e_{inertial} = 0$. As γ increases there is an increase in the amount of heat mixed down from the surface in the summer, the mixed layer heat content and therefore the temperature of the winter mixed layer.

The magnitude of this response to γ is dependant on the size of λ, which is to be expected given that a larger value of λ allows the TKE added by $e_{inertial}$ to penetrate deeper and be larger at a given depth. The size of λ therefore modifies the depth penetration and overall ability of the $e_{inertial}$ parameterization to exchange heat between the surface and subsurface, while the γ parameter acts to scale the magnitude of the response. The greatest SST response in figure 4.11 is therefore observed for the two length scale profiles with the largest extratropical values of λ: $\lambda_{0.5\text{-}30m}$ and $\lambda_{5\text{-}40m}$. However, relative to the reference configuration ($\gamma = 0$) these two profiles also cause the greatest deterioration in seasonal SST biases for most of the γ parameter range studied.

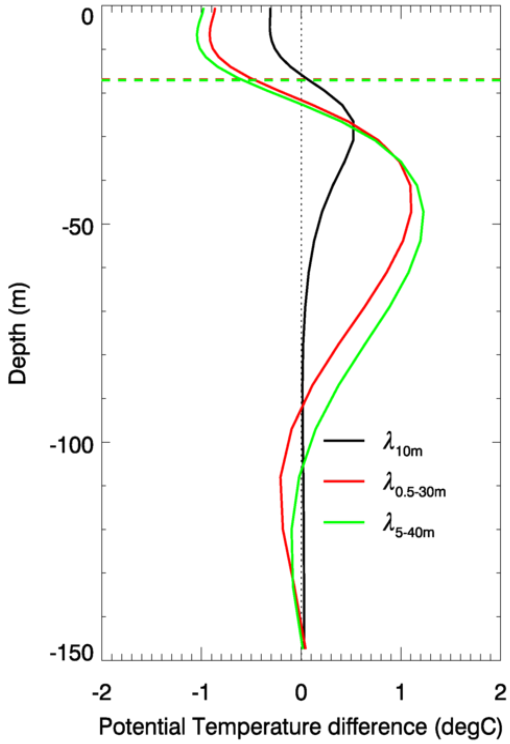

Figure 4.12: JJA potential temperature difference profiles for the various profiles of λ used in this study, relative to the reference configuration without this parameterization. The profiles are averages for the North Pacific (40-60N, 120-180W) and $\gamma = 0.05$. The dashed horizontal lines are the MLDs of the respective experiments.

To better differentiate between the behaviour of the λ profiles, figure 4.12 presents their impacts on the JJA average temperature profile in the North Pacific for $\gamma = 0.05$, relative to the reference configuration. Here it is again evident that an increase in the extratropical value of λ causes more heat to be mixed down from the surface layers. However the centre of the heat exchange dipole also moves downwards; for the smallest value of λ shown by the solid black line this is located at the base of the mixed layer. For larger values of λ the dipole centre becomes deeper and instead heat exchange occurs across the summer thermocline, giving $e_{inertial}$ a more strongly diffusive behaviour.

The behaviour of the heat exchange is likely to be related to how the size of λ compares to the summer MLD. The λ_{10m} length scale profile is likely to be smaller than or comparable to the extratropical summer MLD and so $e_{inertial}$ will have the effect of predominantly increasing TKE within the summer mixed layer, enhancing entrainment across the mixed layer base. By contrast the two other length scale profiles are likely to increase the TKE over a depth scale deeper than the summer MLD and will subsequently give rise to a broadly more diffusive upper ocean.

Figure 4.13 shows the impact of this differing heat exchange behaviour on the summer and winter MLDs in the North Pacific and Southern Ocean. For the summer MLD there is a nonlinear response with an increase in γ for the $\lambda_{0.5\text{-}30m}$ and $\lambda_{5\text{-}40m}$ length scale profiles, while for the λ_{10m} profile the response is more linear and monotonic. This is possibly a consequence of the diffusive behaviour of the former length scales: heat exchange centred at the base of the mixed layer will act to deepen the layer while maintaining its homogeneity, while heat exchange centred at a point below the MLD will act to diffuse the density profile in general and will therefore not necessarily deepen the MLD. This is particularly evident in the North Pacific (figure 4.13a) where the λ_{10m} length scale profile exhibits the largest MLD for $\gamma < 0.055$, while for the deeper summer MLD in the Southern Ocean this nonlinear behaviour is only apparent for the larger $\lambda_{5\text{-}40m}$ profile.

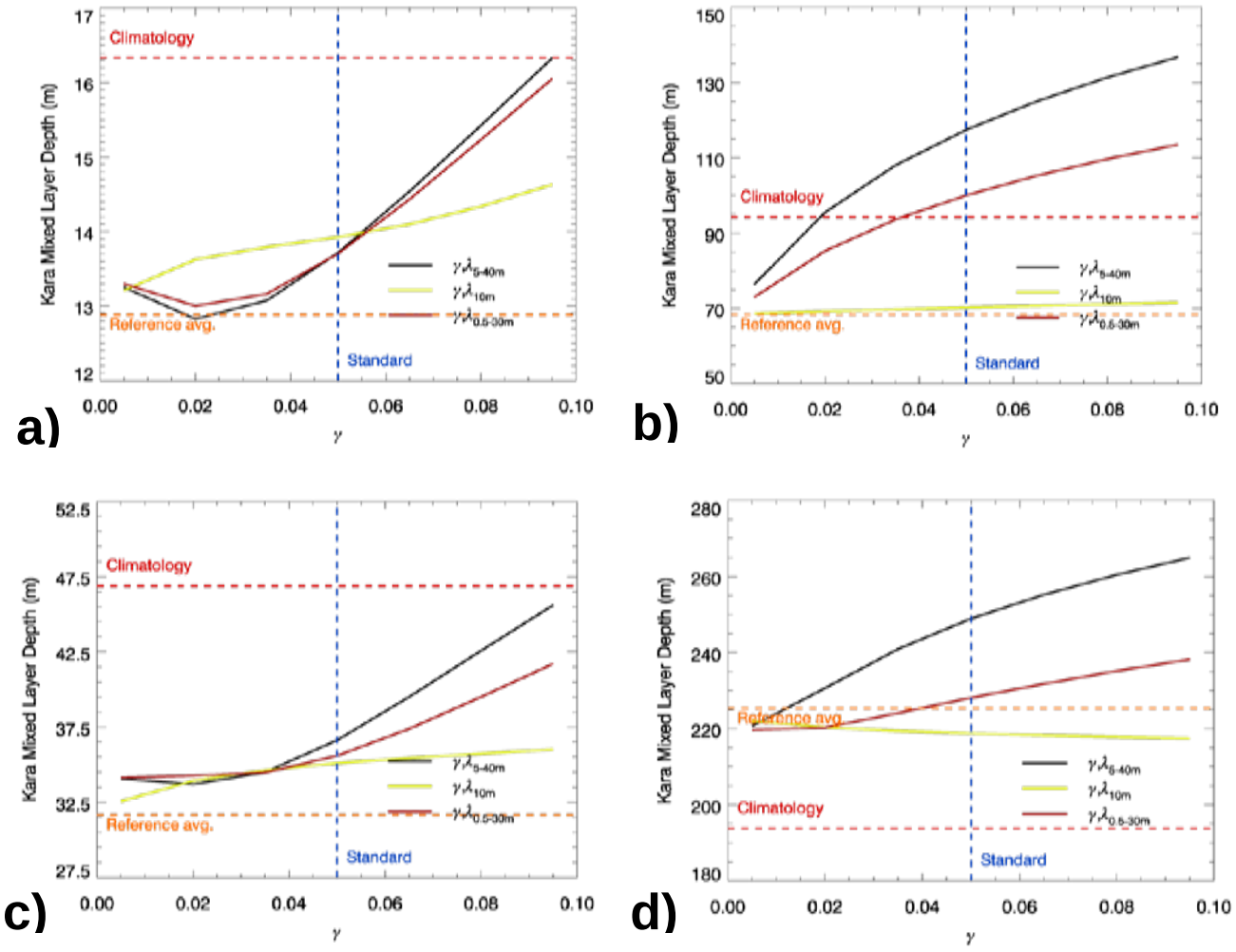

Figure 4.13: Annual mean (a,c) minimum and (b,d) maximum MLD averaged over (top row) the North Pacific (40-60N, 120-180W) and (bottom row) Southern Ocean (45-60S) as a function of γ for various profiles of λ. The red dashed lines show the climatological de Boyer Montégut MLD, the blue dashed lines denote the standard setting for γ and the orange dashed lines show the MLD in the reference configuration without $e_{inertial}$.

In the winter the MLD is generally much deeper than the scale of the added $e_{inertial}$ TKE, and so there is a general increase in the winter MLD with λ and γ for both the North Pacific and Southern Ocean. An exception to this is observed for the λ_{10m} length scale profile in the Southern Ocean which is dominated by the stratifying effects of increasing melt water, causing the winter MLD to decrease with γ.

In general for the standard value of $\gamma = 0.05$, $e_{inertial}$ is seen to improve summer MLDs and winter MLDs in the North Pacific but seems to cause the deep winter MLD biases in the Southern Ocean to deteriorate for the $\lambda_{0.5\text{-}30m}$ and $\lambda_{5\text{-}40m}$ length scale profiles. As previously mentioned however, these biases are much less severe in atmosphere-coupled configurations and so whether the winter MLD will deteriorate in these configurations is rather uncertain. In the absence of a theoretical basis for the $e_{inertial}$ parameterization it is particularly difficult to determine which of the two types of behaviour discussed above can be considered most representative of the given process. However some perspective may be gained here by looking at upper ocean temperature biases under the three profiles of λ.

Figure 4.14 illustrates this for global DJF and JJA SST biases. The summer cooling and winter warming behaviour demonstrated in figure 4.11 clearly increases in magnitude in both hemispheres with an increasing value of λ in the extratropics and has a mixed impact on biases in each hemisphere. In the northern hemisphere, the cold summer SST bias deteriorates and the cold winter SST biases are alleviated (with the exception of a deterioration of the warm winter SST bias in the north Pacific). In the southern hemisphere, the prominent warm summer SST bias is alleviated at the expense of a developing cold bias to the north of this and while the cold winter SST bias is somewhat alleviated, a warm bias begins to develop for the $\lambda_{5\text{-}40m}$ length scale profile.

From examination of figure 4.14, a balanced improvement over the reference configuration seems to be struck for summer SSTs with the use of the $e_{inertial}$ parameterization and the λ_{10m} length scale profile, while the profiles with larger extratropical values of λ appear to cause too much surface cooling. SST biases in the tropics do not exhibit much change between the three profiles of λ (which varies in value here from 0.5 to 10 m), suggesting that the value of λ in the extratropics is the most sensitive aspect of these latitudinal profiles.

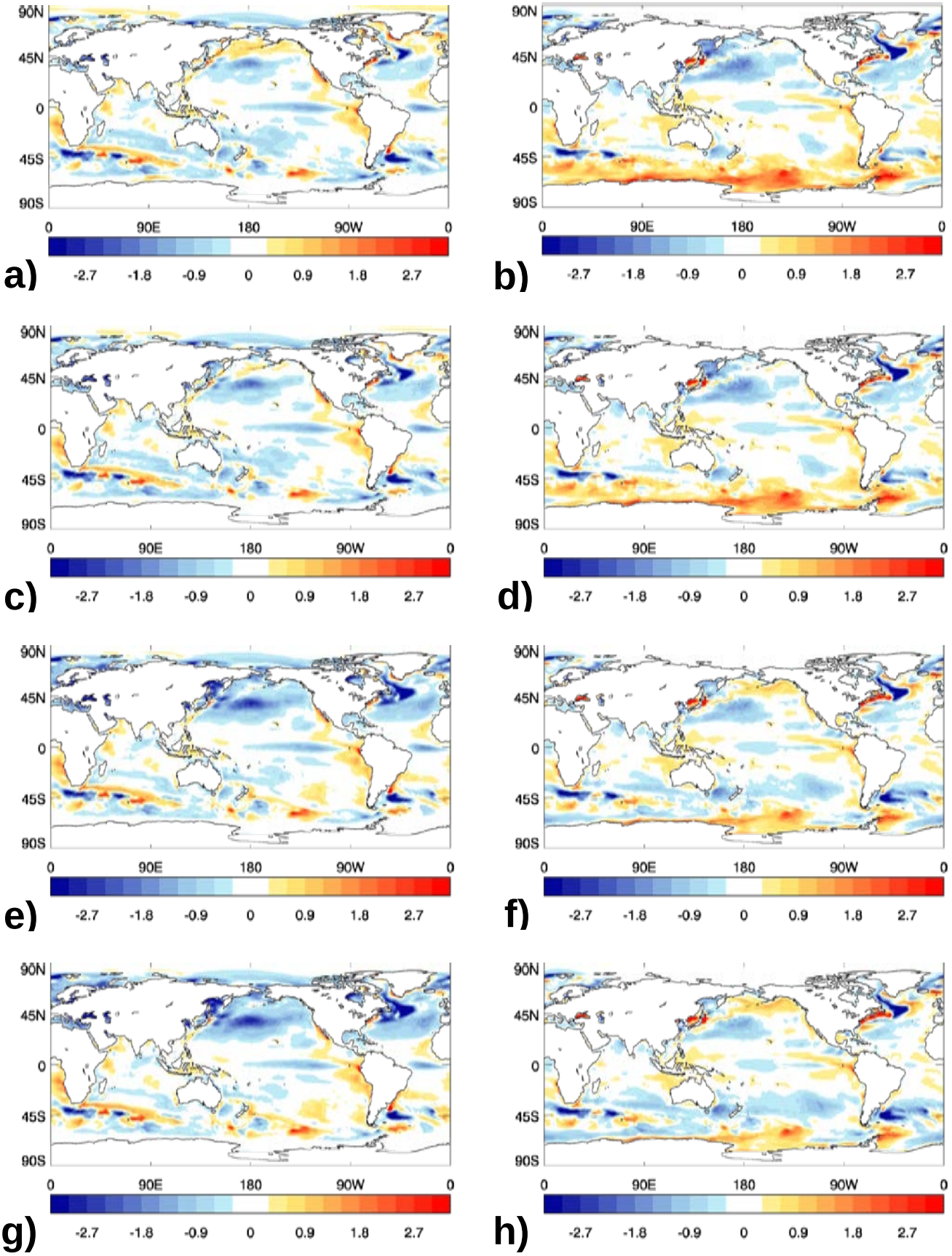

Figure 4.14: JJA (left hand side) and DJF (right hand side) mean SST biases for: (a,b) the reference configuration without $e_{inertial}$ and for experiments using the length scale profiles (c,d) λ_{10m}, (e,f) $\lambda_{0.5\text{-}30m}$ and (g,h) $\lambda_{5\text{-}40m}$, averaged from 1982-1985.

Figure 4.15 shows JJA temperature bias cross-sections in the North Pacific for the three length scale profiles and for the reference configuration without $e_{inertial}$. The reference configuration (figure 4.15d) exhibits a surface warm bias to the north of the basin and a subsurface cold bias beneath the mixed layer suggesting insufficient vertical mixing, while further south there is a cold bias throughout the top 100m which is largest just beneath the mixed layer.

When the standard $\lambda_{0.5\text{-}30m}$ length scale profile is used (figure 4.15b) the temperature profiles clearly become too diffusive; a surface cold bias develops throughout and below the mixed layer in the north of the basin and a warm bias develops at around 50m (although this is due in part to diffusion of the deeper warm bias at ~100m), while the cold bias to the south is now largest within the mixed layer. The increased extratropical value of λ in the $\lambda_{5\text{-}40m}$ profile further accentuates these diffusive biases.

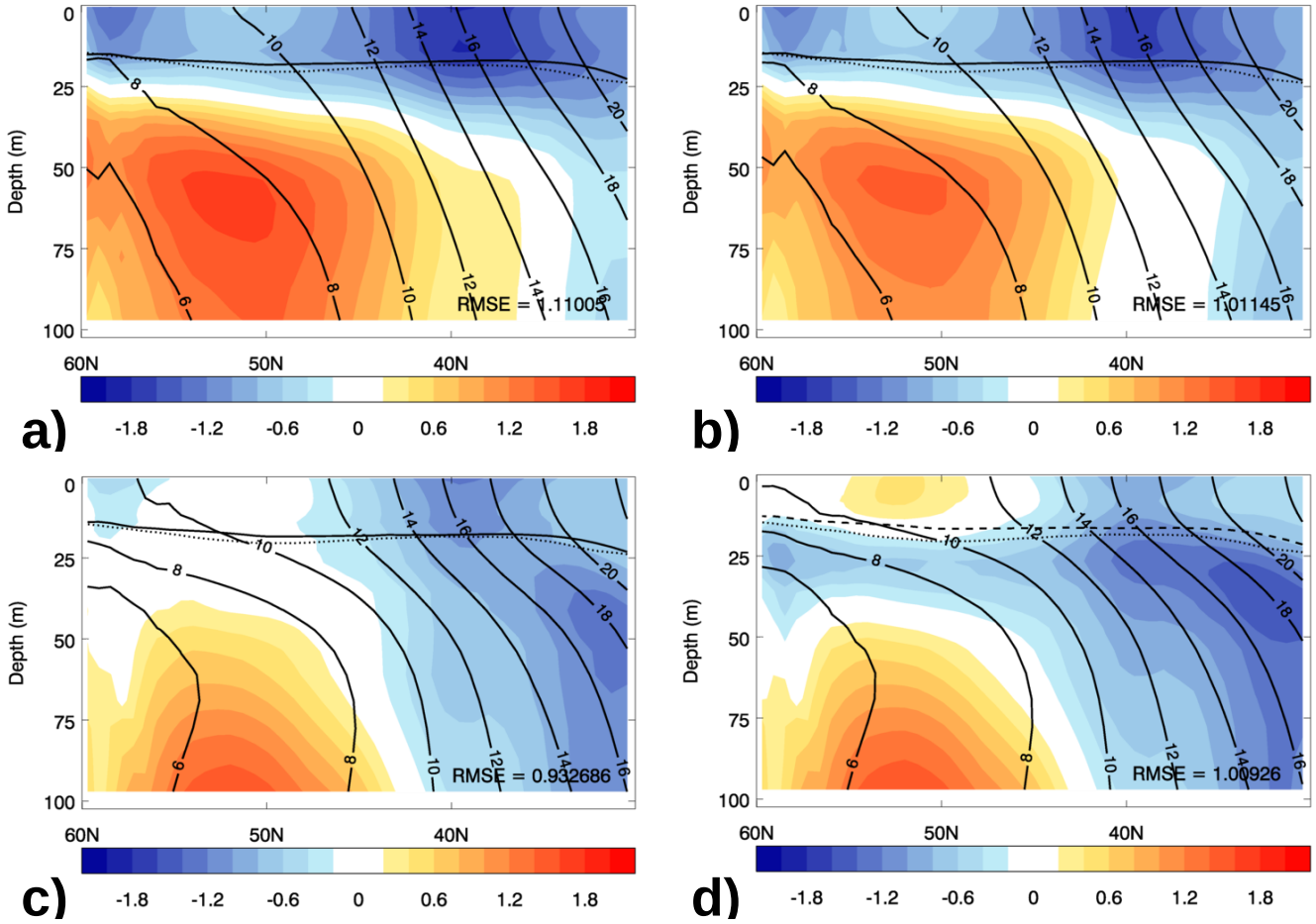

Figure 4.15: JJA potential temperature bias cross sections for the North Pacific (120-180W) relative to the EN3 climatology, for $\gamma = 0.05$ and λ profiles: (a) $\lambda_{5\text{-}40m}$, (b) $\lambda_{0.5\text{-}30m}$ and (c) λ_{10m}, and (d) for the reference configuration with no $e_{inertial}$ mixing. The overlaid black lines are JJA MLDs for the climatology (dotted), reference configuration (dashed) and respective experiments using $e_{inertial}$ (solid). The labelled solid lines are model isotherms.

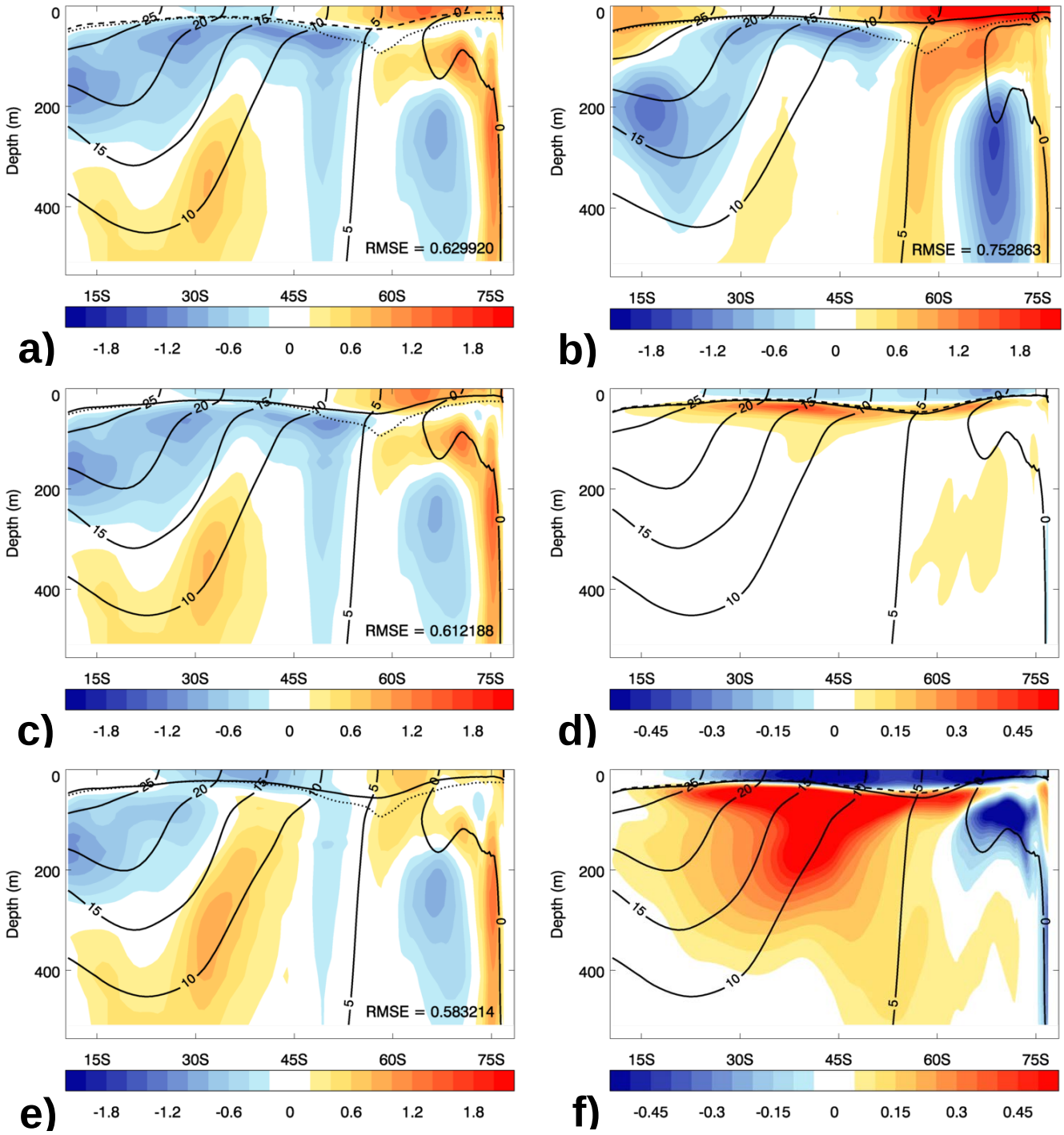

Figure 4.16: DJF potential temperature bias cross sections for the Southern Ocean Pacific sector (90-180W) relative to the EN3 climatology for: (a) the reference configuration with no $e_{inertial}$ mixing, (b) a NEMO v3.2 experiment with identical vertical mixing settings to (a), and for the experiments with $\gamma = 0.05$ and λ profiles: (c) λ_{10m} and (e) $\lambda_{0.5\text{-}30m}$. Also shown are the differences between these latter two experiments and the reference configuration (d and f respectively). The overlaid black lines are DJF MLDs for the climatology (dotted), reference configuration (dashed) and respective experiments using $e_{inertial}$ (solid). The labelled solid lines are model isotherms; in (d) and (f) these are the same isotherms as in (c) and (e) respectively.

When the λ_{10m} length scale profile is instead used (figure 4.15c), the temperature bias dipole observed in figure 4.15d is alleviated without any significantly detrimental impact

on subsurface temperatures. Although the depth of the maximum cold bias to the south again moves into the mixed layer, the RMSE for the region is lowest for this length scale choice.

A similar look at DJF biases in the Southern Ocean Pacific sector is presented in figure 4.16. While biases in the reference configuration (figure 4.16a) are more complex than seen for the North Pacific, NEMO-CICE experiments using a more recent version of NEMO (v3.2) and an identical vertical mixing scheme have been shown to exhibit a different bias structure in this region north of 60S and below 200m (figure 4.16b). Therefore the focus here is on two biases that persist between the NEMO v3.2 experiment and the reference configuration: the warm SST bias poleward of 55S and the cold bias just beneath the mixed layer from 30 to 60S.

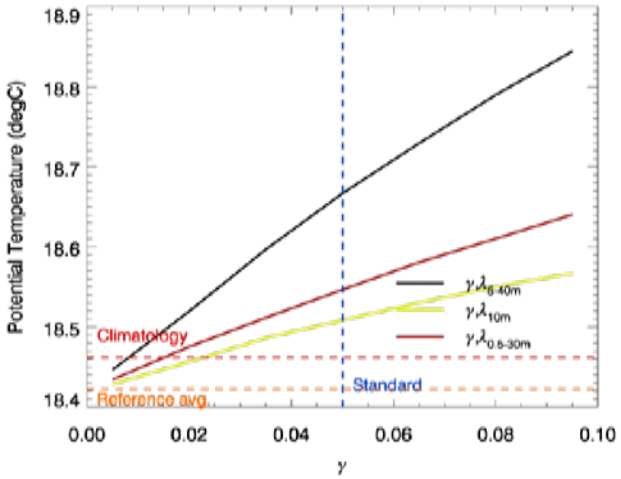

Figure 4.17: Annual average 150m potential temperature averaged over the Tropical Pacific (5N-5S, 140E-80W), as a function of γ for various profiles of λ. The red dashed line shows the climatological EN3 temperature, the blue dashed line denotes the standard setting for γ and the orange dashed line shows the temperature in the reference configuration without $e_{inertial}$.

From figure 4.16 both of these biases are seen to be better alleviated with the use of the $\lambda_{0.5\text{-}30m}$ length scale profile rather than the λ_{10m} profile. Additional improvements to other subsurface biases result in an improved RMSE for this region compared to the reference configuration and to the other length scale profiles. However it is also apparent that use of the $\lambda_{0.5\text{-}30m}$ length scale profile leads to deterioration of the surface cold bias and subsurface warm bias at around 40S, which is seen from figure 4.14 to be a widespread feature. Additional NEMO v3.2 experiments at a ¼° resolution suggest that north of 45S vertical mixing is the dominant process governing near-surface temperature trends in the model, while to the south lateral advection processes become important. The

deterioration of the subsurface warm bias at 40S (observed to a lesser degree in the separate NEMO v3.2 experiments) therefore suggests that use of the $\lambda_{0.5\text{-}30m}$ length scale profile results in an excessive amount of vertical mixing.

This is supported by the observation that for the λ_{10m} length scale profile (figure 4.16c) heat is mixed down over a much shallower depth than for the $\lambda_{0.5\text{-}30m}$ profile, which comparatively worsens the warm SST bias poleward of 55S but reduces the deterioration of the surface cold bias and subsurface warm bias at 40S. Furthermore, use of the $\lambda_{5\text{-}40m}$ profile leads to an increase in the RMSE for this region as the diffusive biases at 40S deteriorate further (figure 4.14h). As a result the λ_{10m} length scale profile seems to be a more appropriate choice than the $\lambda_{0.5\text{-}30m}$ profile despite resulting in reduced alleviation of the two biases of interest, although further improvements to these two biases (which also occur outside of the Pacific basin) could be achieved by increasing the γ parameter. However as previously mentioned there is considerable uncertainty associated with this in the absence of known bounds on the value of γ.

A further distinction between the behaviour of the λ_{10m} and $\lambda_{0.5\text{-}30m}$ length scale profiles is observed in the tropics. At the equator λ has values of 10m and 0.5m for the λ_{10m} and $\lambda_{0.5\text{-}30m}$ length scale profiles respectively and therefore the increase in vertical mixing from $e_{inertial}$ in the tropics is largest for the λ_{10m} profile. However from figure 4.17, which shows the impact of $e_{inertial}$ on 150m annual mean temperatures in the tropical Pacific, it is evident that the increase in heat with γ beneath the tropical thermocline is greatest for the $\lambda_{0.5\text{-}30m}$ and $\lambda_{5\text{-}40m}$ length scale profiles.

Figures 4.18a-d show global 150m and tropical Pacific cross-section diagrams of annual mean temperature changes for the λ_{10m} and $\lambda_{0.5\_30m}$ length scale profiles, relative to the reference configuration without $e_{inertial}$. The $\lambda_{0.5\text{-}30m}$ length scale profile (figures 4.18b,d) clearly has a relatively greater impact on subsurface temperatures outside the tropics compared to the λ_{10m} profile. This is a result of the diffusive behaviour of the length scale at these latitudes, which causes it to be particularly proficient at ventilating the extratropical and subtropical thermoclines and in turn leads to enhanced ventilation of the tropical thermocline via subtropical-tropical heat exchange (Harper, 2000). For the λ_{10m} length scale profile (figures 4.18a,c) the absence of this diffusive behaviour greatly reduces this ventilation and subsequently local heat diffusion across the tropical thermocline becomes more important in controlling tropical subsurface temperatures.

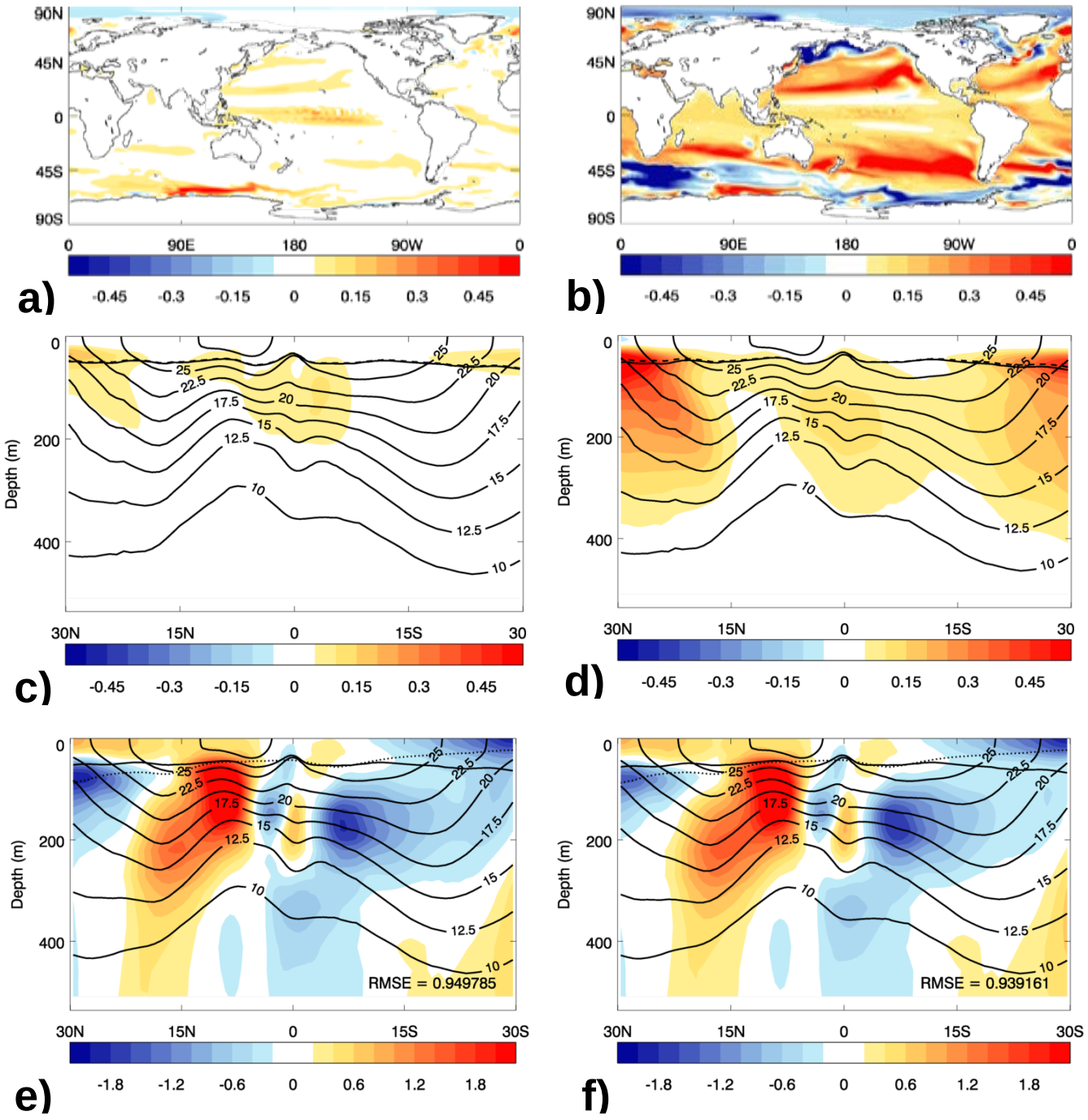

Figure 4.18: Annual mean potential temperature difference at 150m (top row) and for a cross section (middle row) of the Tropical Pacific (140E-80W) between the experiments using $e_{inertial}$ and λ profiles: (a,c) λ_{10m} and (b,d) $\lambda_{0.5\text{-}30m}$ and the reference configuration without $e_{inertial}$ mixing. Also shown are annual mean potential temperature bias cross sections relative to the EN3 climatology for the (e) λ_{10m} and (f) $\lambda_{0.5\text{-}30m}$ profiles. The overlaid black lines are annual mean MLDs for the climatology (dotted), reference configuration (dashed) and respective experiments using $e_{inertial}$ (solid). The labelled solid lines are model isotherms; in (c) and (d) these are the same isotherms as in (e) and (f) respectively.

Figures 4.18e,f show annual mean temperature bias cross-sections for the λ_{10m} and $\lambda_{0.5\text{-}30m}$ length scale profiles. Given that both profiles result in an increase in temperatures

beneath the tropical thermocline relative to the reference configuration, $e_{inertial}$ does not prove particularly beneficial to the tropical Pacific as a whole for either length scale. Rather, cold biases to the south which appear to be related to the cold winter mixed layer in the Southern Ocean improve at the cost of warm biases to the north. The increased ventilation from the $\lambda_{0.5\text{-}30m}$ length scale profile also improves deep cold biases beneath 300m, but as previously shown this is at the expense of an excessively diffuse thermocline at higher latitudes.

From the above results the tentative recommendation is made that the $e_{inertial}$ parameterization should be included in the GO5.0 configuration, but using the alternative λ_{10m} length scale profile instead of the standard $\lambda_{0.5\text{-}30m}$ profile. Using $e_{inertial}$ is expected to result in an increase in vertical mixing in the summer and winter hemispheres, and should subsequently result in notable improvements to the warm summer SST biases and minor improvements to the shallow summer MLD biases in both the NEMO-CICE and coupled configurations.

It is suggested that the standard length scale profile ($\lambda_{0.5\text{-}30m}$) is too large at extratropical and subtropical latitudes and that the use of the λ_{10m} profile largely avoids the development of biases associated with excessive vertical mixing. It is possible that the standard settings for $e_{inertial}$ have been tuned for a NEMO configuration with daily wind forcing; given the 6-hourly wind forcing in the present configuration this implies that the contribution of $e_{inertial}$ to the vertical mixing would be overestimated. It is important to note that the proposed λ_{10m} profile has been chosen from the few available profiles implemented within NEMO based on its impact on the model biases and is therefore by no means an optimal solution.

Furthermore the model SST has been shown to be particularly sensitive to the parameter γ, although it is expected that this sensitivity will be reduced with the proposed λ_{10m} length scale profile. Given the lack of constraints on the value of this parameter at present, efforts to tune this parameter will likely run the risk of compensating for other vertical mixing processes that may be poorly represented or absent in the model. An example of this has been illustrated for the Southern Ocean where the warm SST bias poleward of 55S can be improved by using the $\lambda_{0.5\text{-}30m}$ and $\lambda_{5\text{-}40m}$ profiles, but at the cost of deterioration in subsurface biases further north. As a result it is difficult to propose any change to the current standard setting of 0.05.

Therefore the proposed settings for $e_{inertial}$ (γ = 0.05 and $\lambda = \lambda_{10m}$) have an important caveat: the parameterization in general requires validation against a theoretical framework in order to arrive at an optimal definition of λ and a justifiable range of values for γ. Given the potential difficulty of this task, a preferable approach may instead be to implement an existing theoretically-justified parameterization such as that derived by Jochum et al. (2013).

4.3. Impact of the Langmuir turbulence parameterization

This section concerns the parameterization of Langmuir turbulence formulated by Axell (2002), who briefly examined its impact on salinity fields for a 1D configuration in the Baltic Sea. There has since been little subsequent examination of this parameterization however, particularly within 3D global configurations.

Despite having been implemented within the NEMO model for quite some time, to date HadGEM3 has not used this parameterization. Langmuir turbulence is increasingly being recognised as a fundamental turbulent process in the ocean mixed layer, one that is not represented by the TKE scheme or any turbulent closures of this type. Its absence from HadGEM3 may therefore be a potentially significant contribution to the ocean biases described in section 1. This section therefore examines the impact of the Axell (2002) Langmuir turbulence parameterization on the near-surface state of the model and briefly compares this impact to other empirical parameterizations that have been applied to turbulent closure models.

Figure 4.19 illustrates the impact of the parameterization on the model SST and MLD relative to the reference configuration, with c_{LC} = 0.15 as recommended by Axell (2002). The response of both the summer and winter MLD is comparable to that seen for an increase in surface wave breaking (α, figure 4.1) and inertial wave-breaking (γ, figure 4.9), exhibiting a widespread deepening of the MLD throughout the extratropics (and subtropics for the summer MLD). This leads to a cooling of the summer hemisphere SSTs and a warming of the winter mixed layer, a qualitatively similar response to that seen for α and $e_{inertial}$ in figures 4.1 and 4.9. This results in a similar impact on the biases illustrated in figures 1.1 and 1.2; the shallow summer MLD biases and accompanying warm SST biases (particularly those in the Southern Ocean) are generally improved, while the winter MLD and SST biases are a mixture of regional deterioration and

improvement (for example, cold winter SSTs in the Southern Ocean generally improve while deep winter MLDs in the Southern Ocean and North Atlantic generally deteriorate).

Quantitatively, the impacts are particularly significant when compared to the magnitude of the model biases. In the Southern Ocean for example, summer SSTs cool by up to ~0.2° and summer MLDs deepen by ~5m, which is a significant fraction of the biases exhibited here (up to 2° and 30m respectively). The similarity of this response to the surface wave breaking parameterization (figure 4.1) can again likely be explained by a dependence on the surface wind field via the Stokes drift in (2.17) and (2.18), resulting in increases to surface mixing predominantly in the storm track and trade wind regions.

These impacts are examined more closely in figures 4.20 and 4.21, which show biases in the mean seasonal cycles of SST, 50m temperature and MLD in the North Pacific and Southern Ocean. Compared to the impact of the surface wave breaking parameterization (figure 4.4), the impact of the Langmuir turbulence parameterization on the seasonal cycles in the North Pacific is qualitatively very similar. The MLD increases

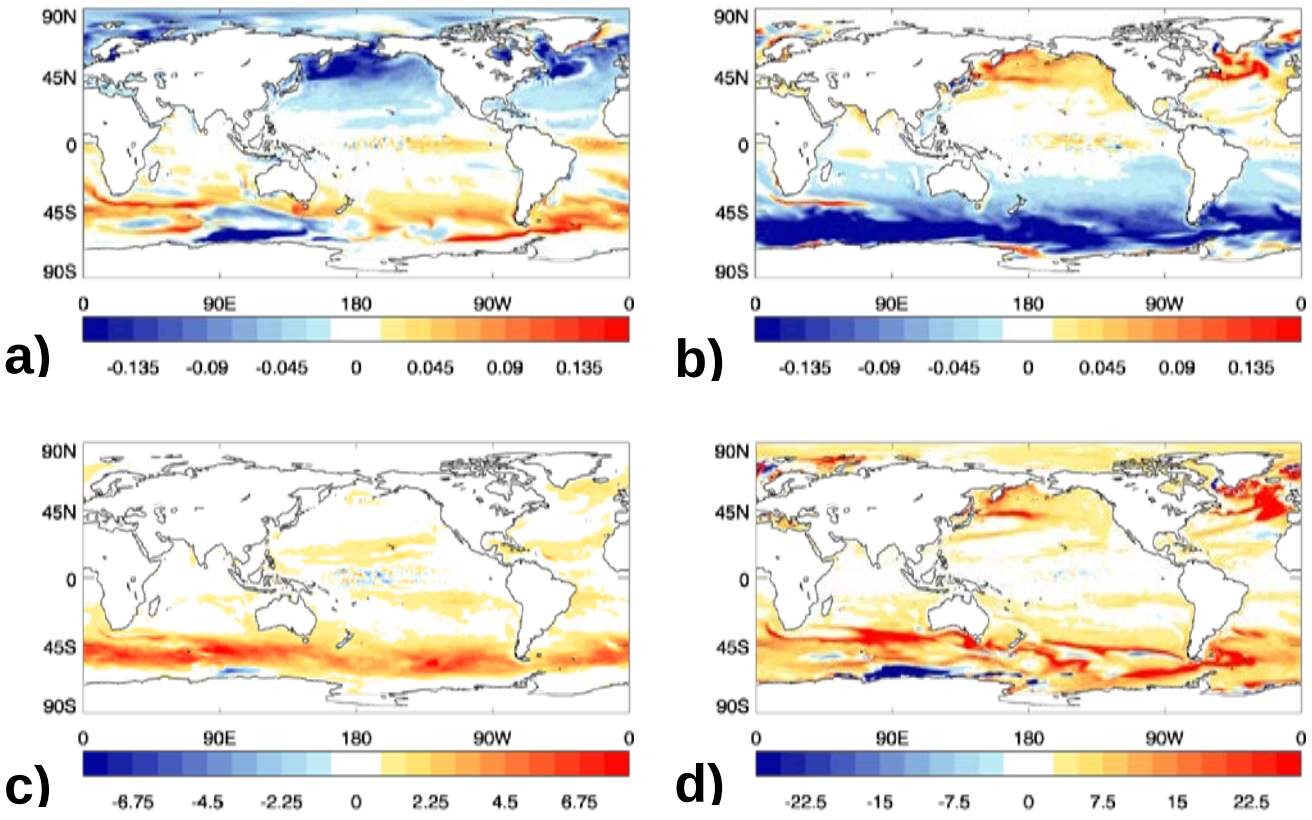

Figure 4.19: Difference in: (a) JJA SST, (b) DJF SST, (c) mean annual minimum MLD and (d) mean annual maximum MLD for the experiment with Langmuir turbulence and $c_{LC} = 0.15$ minus the reference configuration.

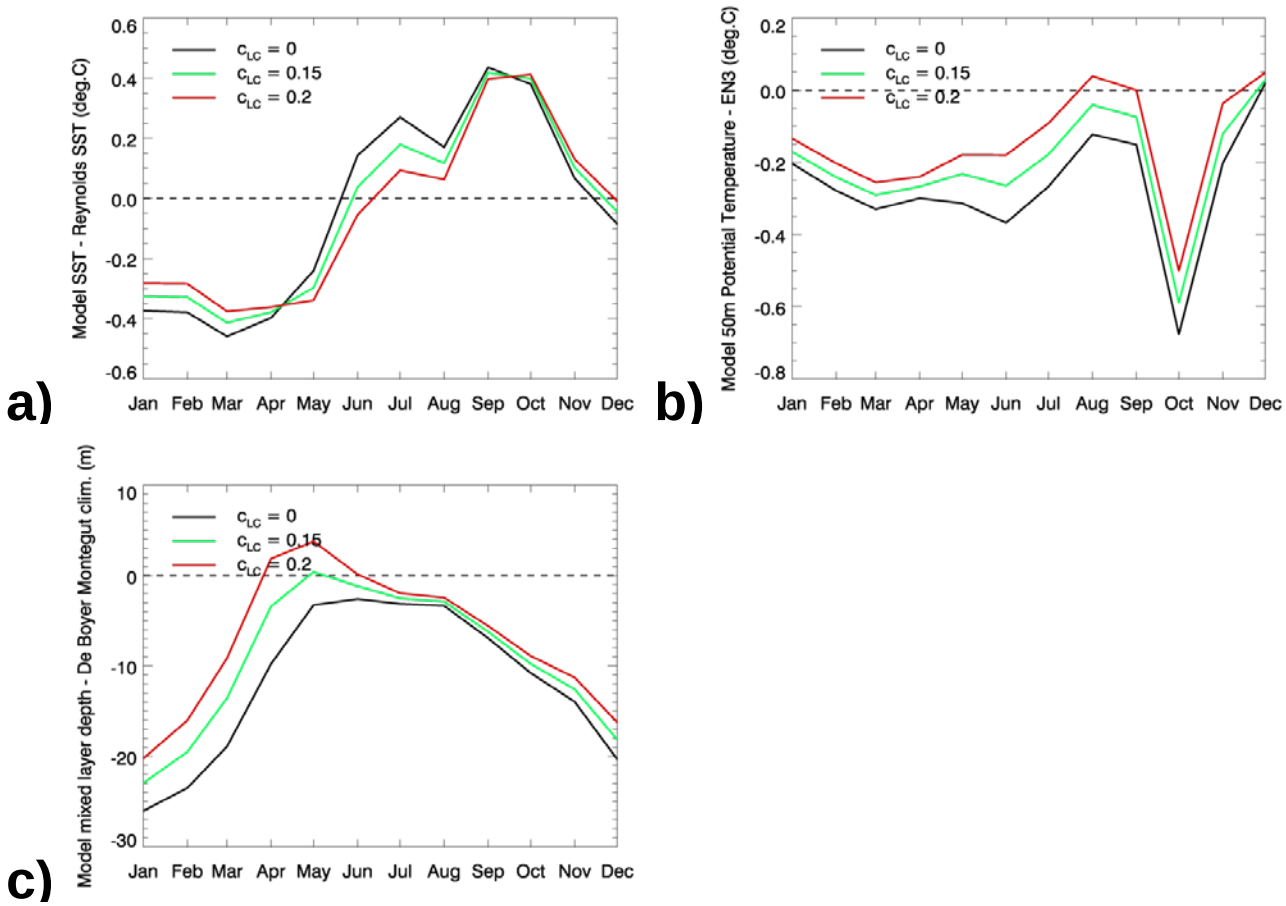

Figure 4.20: Mean annual cycles for 1982-1985 of biases in: (a) SST, (b) 50m potential temperature and (c) MLD averaged over the North Pacific (40-60N, 120-180W) for the range of values of c_{LC} given by Axell (2002) and for the reference configuration without Langmuir turbulence (c_{LC} = 0).

throughout the year resulting in improvements to the generally shallow MLD, with particularly significant impacts during the winter and during the spring heating period.

The cold subsurface temperatures found throughout the year here are also alleviated while SSTs are cooled during the summer and warmed during the winter. The seasonality of this warming and cooling of the SSTs does not match the seasonality of the biases however and as a result while warm summer and cold winter biases are improved, warm autumn and cold spring biases deteriorate. The value of c_{LC} clearly scales the magnitude of the response and so further improvement/deterioration of these biases are possible by an increase of c_{LC} to its upper bounding value of 0.2, although figure 4.20c indicates that this may begin to make the mixed layer too deep during the spring.

The response in the Southern Ocean (figure 4.21) is slightly different to that seen for the surface wave breaking parameterization (figure 4.5). There is warming during the winter

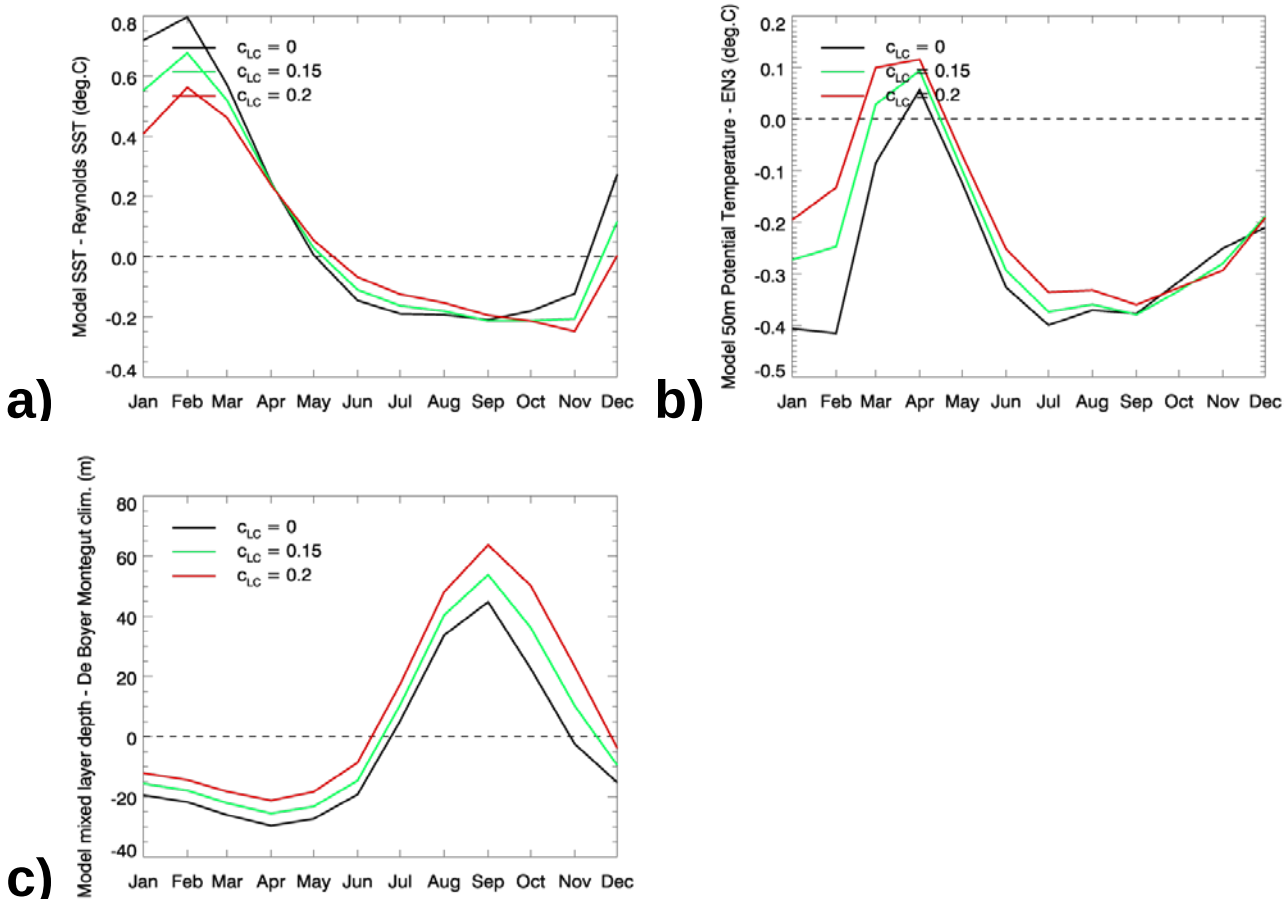

Figure 4.21: Mean annual cycles for 1982-1985 of biases in: (a) SST, (b) 50m potential temperature and (c) MLD averaged over the Southern Ocean (45-60S) for the range of values of c_{LC} given by Axell (2002) and for the reference configuration without Langmuir turbulence (c_{LC} = 0).

rather than the cooling seen for an increase in α, which results in an improvement of the cold winter temperature biases instead of a deterioration. Similarly, deep winter MLD biases further deteriorate while in figure 4.5 they are shown to slightly improve. It is therefore likely that the increased mixing from Langmuir turbulence is able to overcome the stratifying effects of increased Antarctic melt water, resulting in a warming and deepening of the winter mixed layer, while the weak impact of the surface wave breaking is not able to do this (compare also figures 4.1d and 4.19d). The remainder of the seasonal cycle behaves similarly to the surface wave breaking; the summer and autumn MLDs deepen resulting in surface cooling and subsurface warming, which improves summer and autumn SST and MLD biases but seems to make autumn subsurface biases too warm.

Comparing the upper range of α in figures 4.4 and 4.5 (α = 86.7) to that of c_{LC} in figures 4.20 and 4.21 (c_{LC} = 0.2), it is evident that within realistic parameter bounds, the introduction of the Langmuir turbulence parameterization has a much greater impact on

biases in the reference configuration than an adjustment to the surface wave breaking coefficient. Relative to the reference configuration, summer SST biases improve by ~0.05° in the Southern Ocean when α is increased to its upper bound, but improve by ~0.15° under Langmuir turbulence when c_{LC} = 0.15 and ~0.3° when c_{LC} = 0.2. A greater magnitude of surface heat exchange is also evident in the North Pacific, particularly when comparing the 50m temperatures in figures 4.4b and 4.20b. The MLD also exhibits a larger response (particularly during the spring) which results in a much greater alleviation of the shallow summer MLD biases; in the Southern Ocean and North Pacific these are potentially halved when c_{LC} = 0.2.

Although these experiments do not allow the respective impacts of surface wave breaking and Langmuir turbulence to be quantified (the experiments with c_{LC} > 0 use α = 60), this observation that Langmuir turbulence results in a much larger impact than that of surface wave breaking is consistent with the findings of Kantha and Clayson (2004), who attribute this behaviour to the greater depth penetration of TKE in their Langmuir turbulence parameterization. This is likely also the case for the Axell (2002) parameterization; from (2.17) it is shown to increase the TKE over a depth scale and it has been demonstrated in section 4.1 that the surface confinement of the surface wave breaking parameterization inherently limits its impact on the model.

Both D'Alessio et al. (1998) and Kantha and Clayson (2004) developed alternative parameterizations of Langmuir turbulence for one and two-equation turbulence closure models respectively. These are rather different to the Axell (2002) parameterization as both include Langmuir turbulence as a modification by the Stokes drift of the shear production term in (2.5), while Kantha and Clayson (2002) additionally include Stokes drift contributions to the horizontal momentum equations and to the prognostic equation for the turbulent length scale.

Figure 4.22 shows biases in the mean seasonal cycles of SST and MLD at OS PAPA, where both studies verify their parameterizations by performing 1D simulations for the year 1961. Despite differing definitions of the MLD both studies report that the MLD generally deepens, although D'Alessio et al (1998) shows that this happens predominantly during the Autumn and Winter while Kantha and Clayson (2002) show that the largest response occurs during the spring heating cycle. The Axell (2002) parameterization exhibits a compromise between this seasonality in figure 4.22b, but in agreement with Kantha and Clayson (2002) is most responsive during the spring.

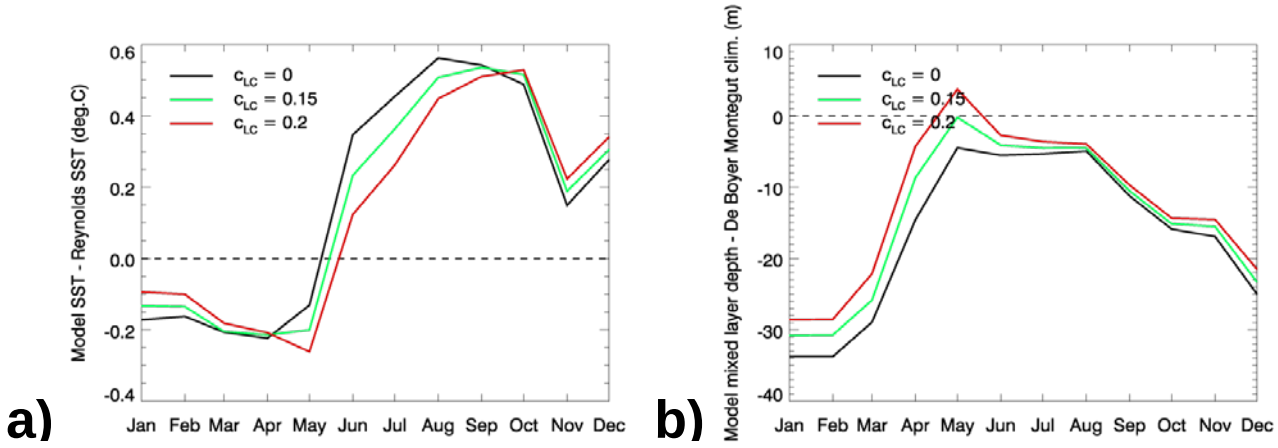

Figure 4.22: Mean annual cycles for 1982-1985 of biases in: (a) SST and (b) MLD at OS PAPA (50N, 145W) for the range of values of c_{LC} given by Axell (2002) and for the reference configuration without Langmuir turbulence (c_{LC} = 0).

The seasonality of peak impact on the SST in figure 4.22a also agrees with the findings of Kantha and Clayson (2002), occurring during late spring/early summer. However they do not observe the warming of the winter SST found in the present model and instead observe cooling. Additionally Kantha and Clayson (2002) generally observe a much larger SST cooling (up to 0.5°), but there are of course several differences to the present model configuration; in particular that a 3D configuration and one-equation turbulence closure are used and for a later and longer time period.

In spite of these caveats, it is reassuring that the impacts of the Axell (2002) parameterization exhibit a similar seasonality to alternative empirical formulations and also agree with the findings of the LES study by Noh et al. (2011). Furthermore, the spatial distribution of the resulting increase in turbulence is found to compare favourably with calculations of the Langmuir number performed by Belcher et al. (2012) for global reanalysis data. Regions of increased depth-integrated TKE in the model correspond well to regions in the subtropics and summer extratropics where Langmuir turbulence is expected to be important.

The Axell (2002) parameterization, as well as other parameterizations of this type (D'Alessio et al., 1998; Kantha and Clayson, 2002) is known to have a significant deficiency in that it fails to represent the effects of the downwelling jets of Langmuir circulations. LES studies have highlighted the importance of Langmuir circulations in enhancing entrainment of the mixed layer (Skyllingstad and Denbo, 1995; McWilliams et al., 2000) and have specifically highlighted the roles of these jets in this process (Polton

and Belcher, 2007; Grant and Belcher, 2009). The Axell (2002) parameterization specifically addresses the turbulence produced by Langmuir vortices (which have a depth scale of the order of the Stokes depth scale) but does not represent the TKE transported by these downwelling jets (which have a depth scale of the order of the Eckman depth). The parameterization is therefore missing a key process that may significantly enhance its impact on mixed layer deepening.

Additionally, the Axell (2002) parameterization makes the assumption of a fully developed sea so that the Stokes drift and surface wind speed may be algebraically related (see section 2.2). In practice however wavefields can be remotely formed and will likely not be in equilibrium with the local wind conditions (Hanley et al., 2010). Furthermore, the strength of Langmuir turbulence will depend on the angle between the Stokes drift and wind stress vectors though it is almost always present to some degree (Sullivan et al., 2008; Van Roekel et al., 2012). Langmuir turbulence is therefore not necessarily directly related to the surface wind field and consequently knowledge of the wave field is important in diagnosing the occurrence of Langmuir turbulence. Preliminary work by Webb and Fox-Kemper (2008) demonstrated significant improvements to shallow summer MLD biases in the NCAR CCSM 3.5 model when using a Langmuir turbulence parameterization dependant on wave model information instead of one dependant on the local surface wind field.

The above results suggest that even a basic implementation of Langmuir turbulence via the Axell (2002) parameterization will result in significant improvements to the summer mixed layer. In the Southern Ocean summer SSTs cool by ~0.15° and summer MLDs deepen by ~5m, a significant reduction of the biases exhibited by the NEMO-CICE model. It is therefore suggested that the Axell (2002) parameterization is used in GO5.0 with the standard coefficient of c_{LC} = 0.15. Other important attributes of Langmuir turbulence will need to be represented in the future and will in theory result in further enhancement to the capabilities of Langmuir turbulence parameterizations in deepening the wind-driven mixed layer.

4.4. Sensitivity of the turbulence closure stability functions

This section concerns the stability functions c_k and c_ε in (2.2a) and (2.6). In the present turbulence closure model, constraints on the values of these parameters are not well

known. The value of c_k is derived with respect to c_ε and the stationary Richardson number via (2.11), but the value of c_ε itself is determined from several unspecified experimental atmospheric dissipation profiles (Bougeault and Lacarrére, 1989) and as a result there is considerable uncertainty regarding the value of c_ε. Parameter tuning here becomes a difficult task, particularly for parameters that essentially govern the behaviour of the turbulence closure model and as such may prove to be particularly sensitive. The sensitivity of the model to variations in c_k and c_ε is therefore briefly addressed below and the implications for future work in developing this area of the model are discussed afterwards.

As mentioned above, (2.11) constrains the value of c_k with respect to c_ε and the value of the stationary Richardson number Ri_{st}. Given $c_\varepsilon = 0.7$ and an observational range of $0.2 \leq Ri_{st} \leq 0.25$ (see Umlauf and Burchard, 2005 and references within), a constrained range of values for c_k can be given as $0.088 \leq c_k \leq 0.117$. Figure 4.23 illustrates the impact on the model SST and MLD of increasing c_k from its control value of 0.1 to the upper bound of 0.12.

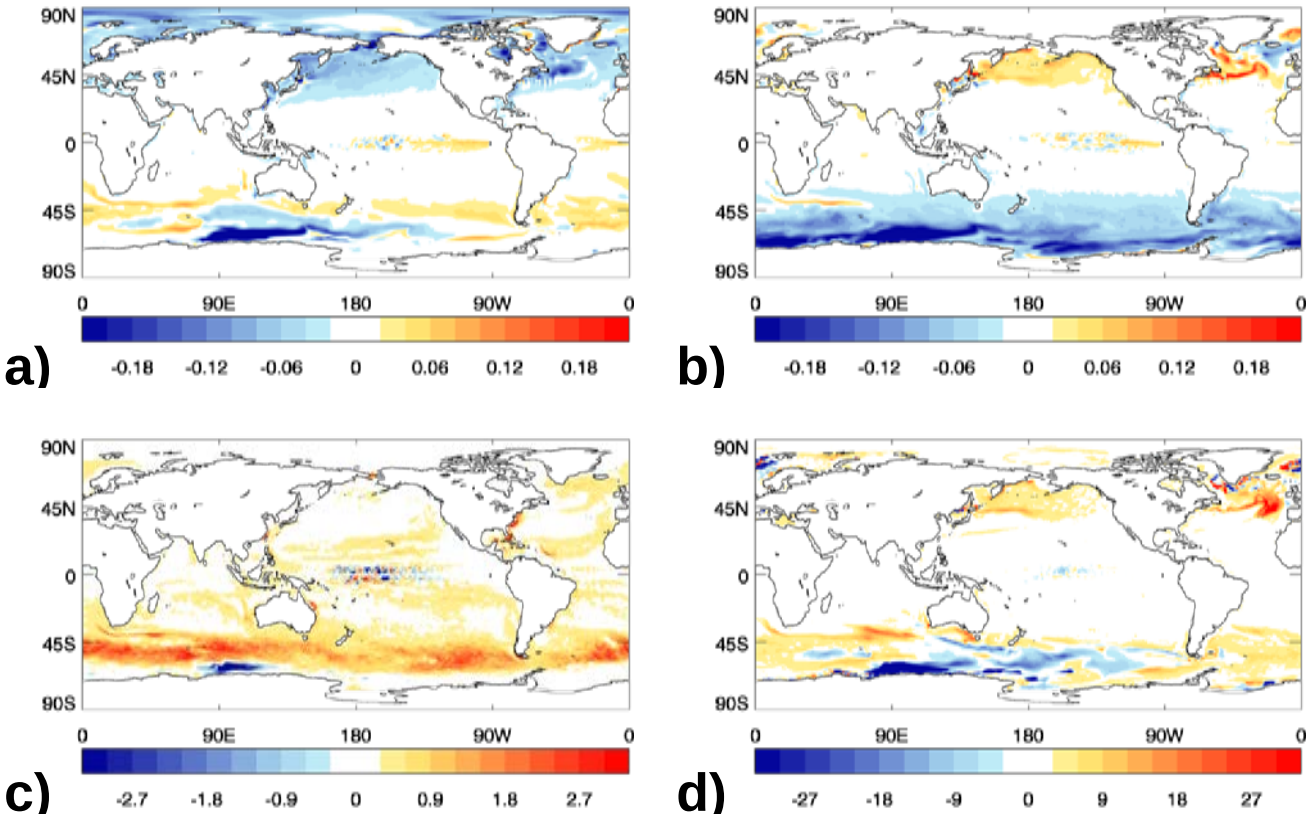

Figure 4.23: Difference in: (a) JJA SST, (b) DJF SST, (c) mean annual minimum MLD and (d) mean annual maximum MLD for the experiment with $c_k = 0.12$ minus the reference configuration with $c_k = 0.1$.

From comparison with the impact of the surface wave breaking parameterization (figure 4.1), it is evident that the response to this increase in c_k is qualitatively very similar to that of an increase in α. This can be explained by the proportionality of K_m and K_ρ to the TKE in (2.2) which implies that the increase in diffusivity will be largest where the TKE is largest; near the surface and in wind-driven regions where the surface wave-breaking parameterization is shown to have the biggest impact. Note that the adjustment of c_k will not directly influence convection; the diffusivity here is given an arbitrarily large fixed value to account for the fact that the TKE scheme does not adequately represent this process (see section 2.2).

The overall impact of this increase in c_k is larger than that seen for the increase in α (figure 4.1) however: summer MLDs in the Southern ocean deepen by ~1-3m and SSTs decrease in the summer extratropics by ~0.05-0.1°. A broader increase in the summer MLD is seen here too, with a relatively larger response seen in the subtropics compared to that of the Southern Ocean. Given that this parameter increase represents less than half of the range of c_k derived above, the magnitude of the impact for the full range of c_k will likely be at least twice as large. Therefore the stability function c_k is able to have a significant impact on the model SST and MLD within the above constraint on its range of values.

As discussed above, constraining the value of c_ε is a difficult task without knowing the details of the atmospheric dissipation profiles that it has been calibrated against and as a result an arbitrary range of c_ε is considered here. The Ri_{st} constraint (2.11) is applied such that c_k is varied in proportion to c_ε with Ri_{st} kept equal to 2/9. These settings are given in table 3 for the results that follow.

Figure 4.24 shows the global impact on the DJF model SST and summer MLD when c_ε and c_k are increased from their control values to 2.1 and 0.3 respectively, as well as the regional impact in the Southern Ocean for the settings given in table 3. The focus here is on the summer impacts as the winter impacts are shown to be qualitatively similar to those seen for an increase in c_k in figure 4.23.

c_k	0.1	0.2	0.3	0.4	0.5	0.6
c_ε	0.7	1.4	2.1	2.8	3.5	4.2

Table 3: Parameter settings of c_k and c_ε for the experiments where c_k and c_ε were varied in proportion to each other. The control values are underlined.

A key difference to the variation of c_k alone is that here the dissipation term in the TKE equation is also being increased via c_ε (2.6). Figures 4.24c and 4.24d show this proportional increase of c_k and c_ε to result in an overall increase in the vertical mixing, resulting in a linear cooling of the summer SST and deepening of the summer MLD. Globally, the impact on the summer MLD is much more widespread than when c_k is increased in isolation (figure 4.23c), with most of the global ocean exhibiting a MLD deepening of at least 1m and up to 3m in the Southern Ocean. The SST response is also broader in scale, with cooling of up to ~0.1° outside the ice-covered regions of the Southern Ocean and a qualitatively similar impact to that of increasing c_k in isolation (figure 4.23b) but with a larger response in the subtropical regions.

For the chosen arbitrary range of parameter values the response to this combined increase of c_k and c_ε has only a minor impact on biases in the Southern Ocean, but with no apparent constraint on the value of c_ε (and therefore on c_k) these results demonstrate that this uncertainty may potentially constitute a significant contribution to model biases.

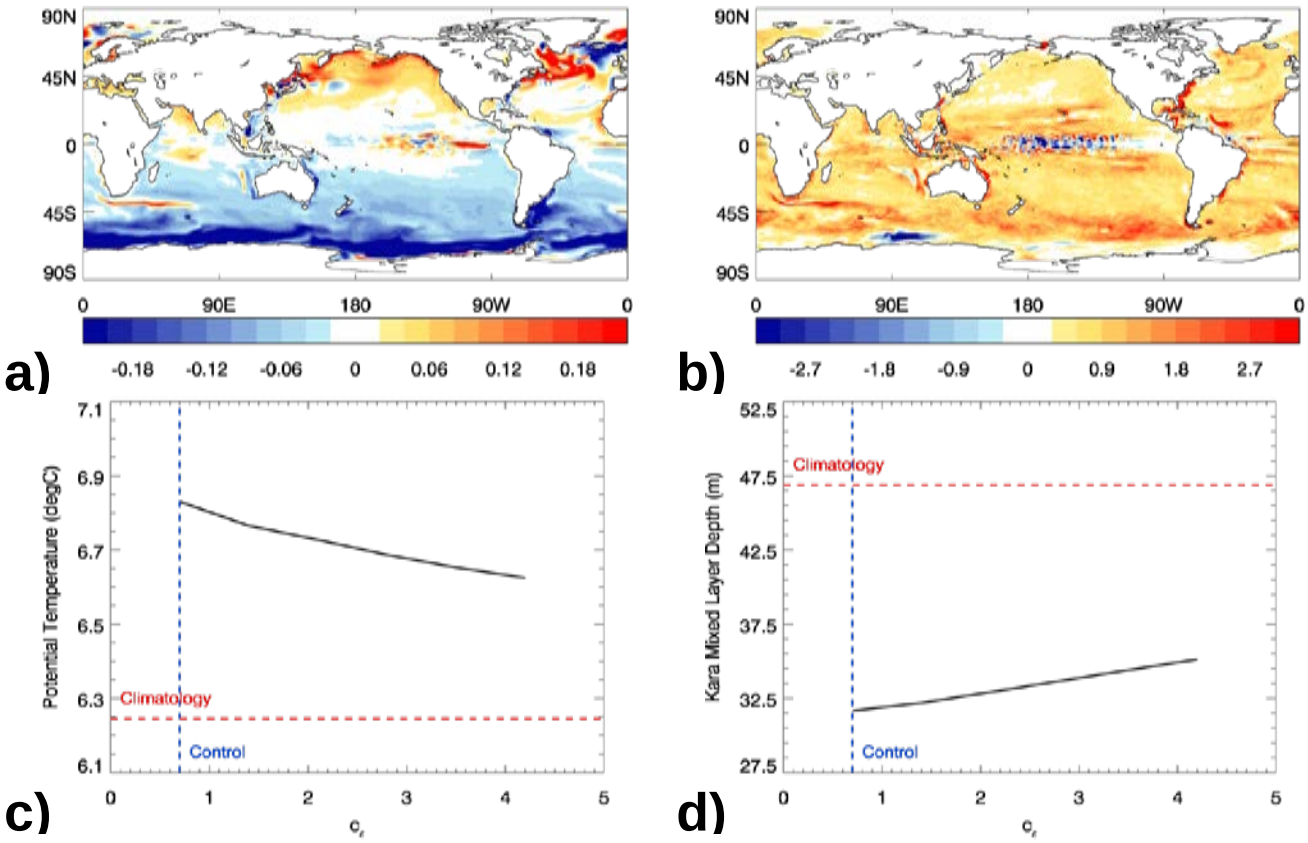

Figure 4.24: Difference in: (a) DJF SST and (b) mean annual minimum MLD for the experiment with c_k = 0.3 and c_ε = 2.1 minus the reference configuration with c_k = 0.1 and c_ε = 0.7. Also shown is the variation in: (c) DJF SST and (d) mean annual minimum MLD for the Southern Ocean (45-60S) for the parameter settings given in table 3. The blue dashed lines correspond to the reference configuration value of c_k, while the red dashed lines represent the climatological (c) Reynolds SST and (d) de Boyer Montégut MLD.

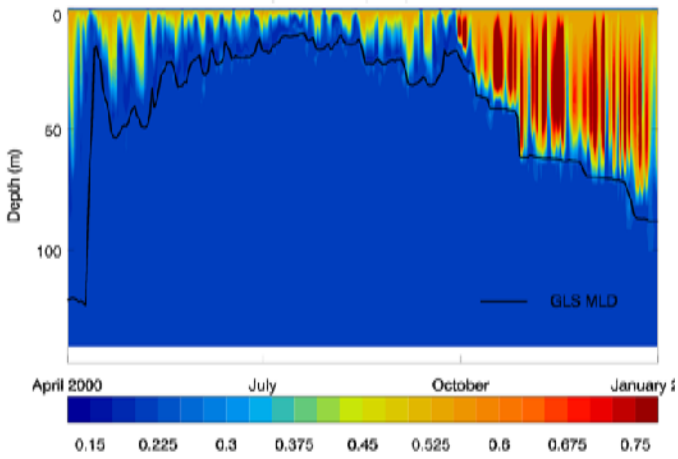

Figure 4.25: Hovmuller diagram of the stability function for heat in the North Pacific (40-60N, 120-180W), from the two-equation GLS scheme (k-ε closure) implemented in NEMO. The overlaid black line is the model MLD.

The focus of this report has so far been on the impact of parameter changes in NEMO-CICE relative to a set of reference parameter settings used by HadGEM3, placing emphasis on improvements that could be made to model biases through reasonable adjustments to these settings. However the above results are intended to demonstrate the sensitivity of the stability functions to variation, rather than identify prospective improvements to model biases they could be adjusted to produce. Therefore the key result here is that within the given constraint of (2.11) the variation of c_k and c_ε is able to have significant impacts on the model SST and MLD. This highlights an important weakness of these stability functions in that their inherent uncertainty may contribute significantly to the model biases discussed in section 1. Work is therefore required to implement a better-constrained and traceable set of stability functions within the TKE scheme.

One possible way that this could be achieved would be to derive a revised value of c_ε by calibrating (2.6) against independent observations of dissipation in the ocean, which would also allow for the determination of an associated uncertainty. However there has also been a considerable amount of research into physically more accurate and complex sets of stability functions (see for example Burchard and Bolding, 2001). These stability functions are dependant on the time-varying shear, buoyancy and turbulence and as a result exhibit a rich structure over the seasonal cycle and throughout the depth of the mixed layer, as illustrated in figure 4.25. Used in place of the existing constant value this time-varying structure may have a significant impact on the behaviour of the vertical mixing scheme, but for one-equation models like the TKE scheme the impacts of this

type of stability function are not well understood. In addition, the implementation of such stability functions would require a revision of the form of the master length scales in (2.9).

Alternatively a two-equation 'Algebraic Stress Model' could be used (Umlauf and Burchard, 2005) which is formally equivalent to the TKE scheme, except a prognostic equation for the turbulent length scale is used and expressions for the aforementioned complex stability functions are naturally arrived at via derivation from the Reynolds-averaged Navier-Stokes equations. Additionally, this prognostic length scale is valid for convective situations and as a result the arbitrary increase in diffusivity required to represent convection in the TKE scheme is arguably not needed in two-equation models.

A framework for four two-equation models known as the GLS scheme (Umlauf and Burchard, 2003) is implemented in the current version of NEMO (v3.4 at the time of writing). Experiments using this scheme have shown that despite the solution of an additional prognostic equation, a two-equation model results in only a small increase in computational cost relative to the TKE scheme (an observation also noted by Meier, 2001 for his one-equation model).

Therefore given the sensitivity of the fixed-value stability functions in the TKE scheme and the limited known constraints on their values, it is suggested that future work seeking to improve this aspect of the vertical mixing scheme in NEMO should focus on systematic comparisons of the implemented TKE and GLS schemes. Given that with modern parallelized computing resources there is no longer any significant computational benefit in using a simpler one-equation model like the TKE scheme over two-equation models like the GLS scheme, revising the current fixed value of the stability function may not prove to be particularly beneficial. Instead, the focus should be on investigating the improvements that may result from use of the physically more accurate stability functions and mixing length formulations within the GLS scheme.

4.5. Impact and sensitivity of the minimum TKE and length scale thresholds

This section concerns the parameters e_{min0} and e_{min}, controlling the minimum surface and subsurface TKE thresholds and the parameters l_{min0} and l_{min}, controlling the minimum surface and subsurface turbulent length scale thresholds.

The function of these parameters in a turbulent closure depends on how background mixing is parameterized. For example Gaspar et al. (1990) indirectly specify the background diffusivity in their model via the e_{min} parameter, but in the present model the background mixing is directly controlled by the parameters $K_{\rho 0}$ and K_{m0} and their profiles over latitude and depth (see section 2.2). As a result the function of the e_{min0}, e_{min}, l_{min0} and l_{min} parameters in the TKE scheme should purely be to recover certain numerical properties of the model and therefore should not have any notable impact on background mixing processes or the model result. This section discusses the sensitivity of the model to these four parameters in this context and comments on the suitability of their current values.

Figure 4.26 shows the impact of increasing e_{min0} on the DJF SST and the mean annual minimum MLD, 1m eddy diffusivity and surface TKE in the Southern Ocean, where the model was shown to be most sensitive to the TKE surface boundary condition in the summer (section 4.1).

The response of the surface TKE exhibits a similar behaviour globally, whereby the sensitivity increases with the value of e_{min0} until eventually a quasi-linear relationship occurs between e_{min0}, the surface TKE and the near-surface vertical mixing (figures 4.26 c,d). This behaviour has a simple explanation: the surface TKE is calculated solely from (2.13) and can therefore be related to a minimum wind speed threshold (~1ms^{-1} for α_{CB} = 60) below which the surface TKE will be set to e_{min0}. Increasing e_{min0} will raise this threshold and will therefore increase both the global area where winds are beneath this threshold and the value of e_{min0} the surface TKE is subsequently set to within this area. Given a large enough increase, the surface TKE field will be mainly determined by the value of e_{min0} and will result in a linear relationship between the two. This scenario places a rough limit on the value of e_{min0}, as at this point it will be more important than (2.13) in determining the TKE surface boundary condition.

For figures 4.26c,d this roughly occurs for $e_{min0} > 2\text{x}10^{-3}$ m^{2}s^{-2}, suggesting that the current value of 10^{-4} m^{2}s^{-2} is sufficiently small not to have a significant impact on the TKE surface boundary condition and near-surface mixing. However figures 4.26a,b show the response of the SST and MLD to e_{min0} to be very small, even for a value 80 times larger than the control value which suggests that the value of e_{min0} is of little consequence to the model result. This is likely to be related to the general insensitivity of the model to the

TKE surface boundary condition (see section 4.1) and supports the suggestion that the current value of e_{min0} is suitable.

Figure 4.27 shows the impact of increasing l_{min0} on the DJF SST and the mean annual minimum MLD and 1 m eddy diffusivity, again for the Southern Ocean. In contrast to e_{min0} (figure 4.26) the model is shown to be much more sensitive to the value of l_{min0}, resulting in a larger increase of the near-surface vertical mixing. This is partly due to the greater proportionality of the eddy viscosity and diffusivity to the turbulent mixing length than to the TKE (equation 2.2a), but is also related to the control value of l_{min0}. As discussed above, (2.13) can be used to associate e_{min0} with a minimum surface wind speed threshold and can also be done for (2.15) and the surface length scale. For e_{min0} = 10^{-4} m^2s^{-2} and l_{min0} = 0.4 m this gives corresponding wind speeds of ~1 ms^{-1} and ~5 ms^{-1}

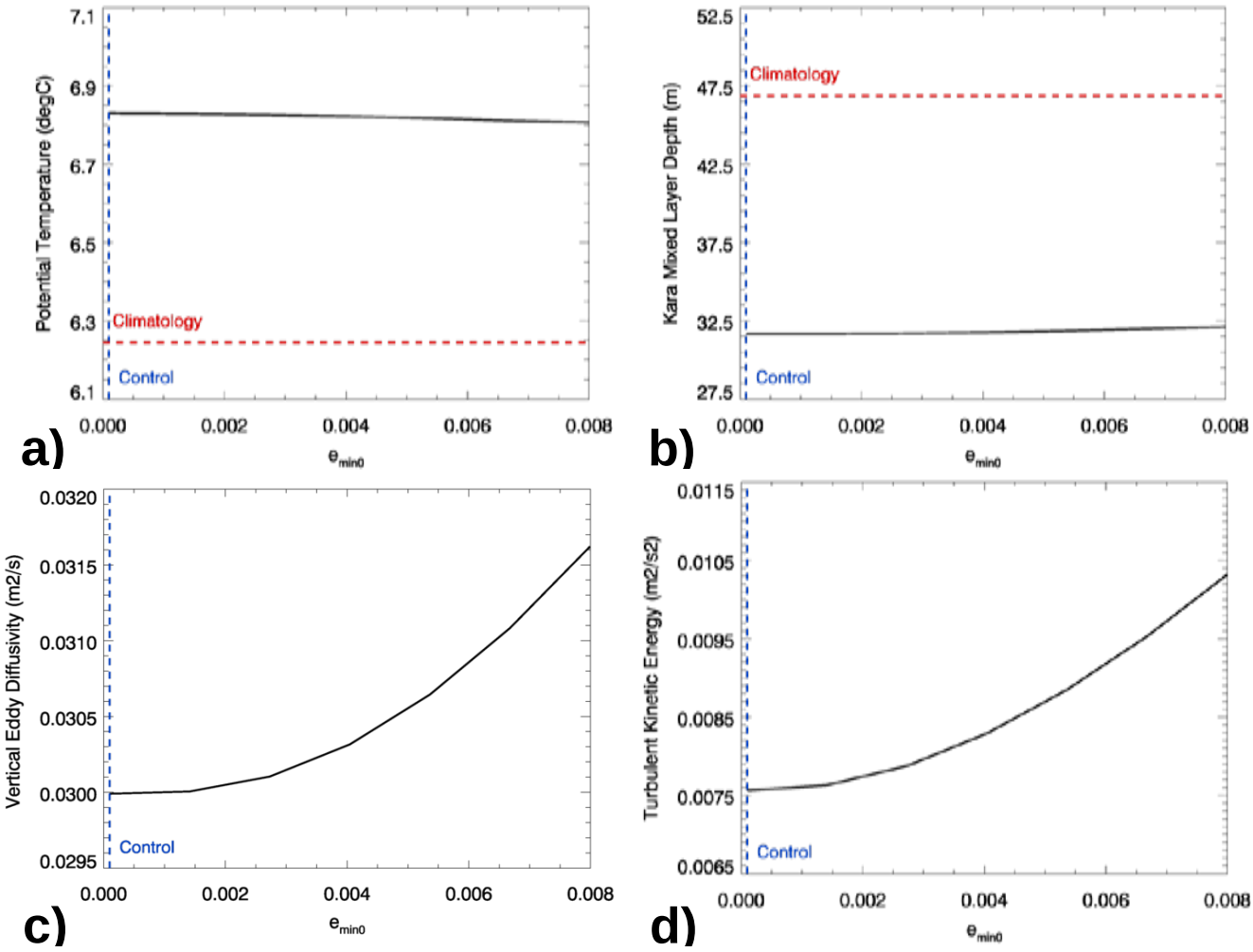

Figure 4.26: (a) DJF mean SST, (b) mean annual minimum MLD**,** (c) mean annual minimum eddy diffusivity at 1 m and (d) mean annual minimum surface TKE averaged over the Southern Ocean (45-60S), as a function of e_{min0}. The blue dashed lines correspond to the reference configuration value of e_{min0}, while the red dashed lines represent the climatological (a) Reynolds SST and (b) de Boyer Montégut MLD.

respectively, suggesting that an inconsistent level of vertical mixing is recovered by these parameters for the surface boundary condition. Following earlier arguments this implies that the current value of l_{min0} is globally more important than that of e_{min0} in controlling the near-surface vertical mixing and as a result the area-averaged eddy diffusivity is more sensitive to small increases in l_{min0}. Additionally, a quasi-linear relationship occurs between the eddy diffusivity and l_{min0} in figure 4.27c as observed for larger values of e_{min0} in figure 4.26c.

The above inconsistency suggests that the control value of l_{min0} does not equate to an appropriate scale for the surface roughness length ($z_0 \approx 1$ m, where from section 4.2 $l_{min0} = \kappa z_0$) and that this should be smaller. The current version of NEMO (v3.4) follows Craig and Banner (1994) where $z_0 = 0.1$ m, giving $l_{min0} = 0.04$ m and a corresponding wind speed threshold of ~1.7 ms^{-1}. This is much closer to the threshold of 1 ms^{-1} derived for

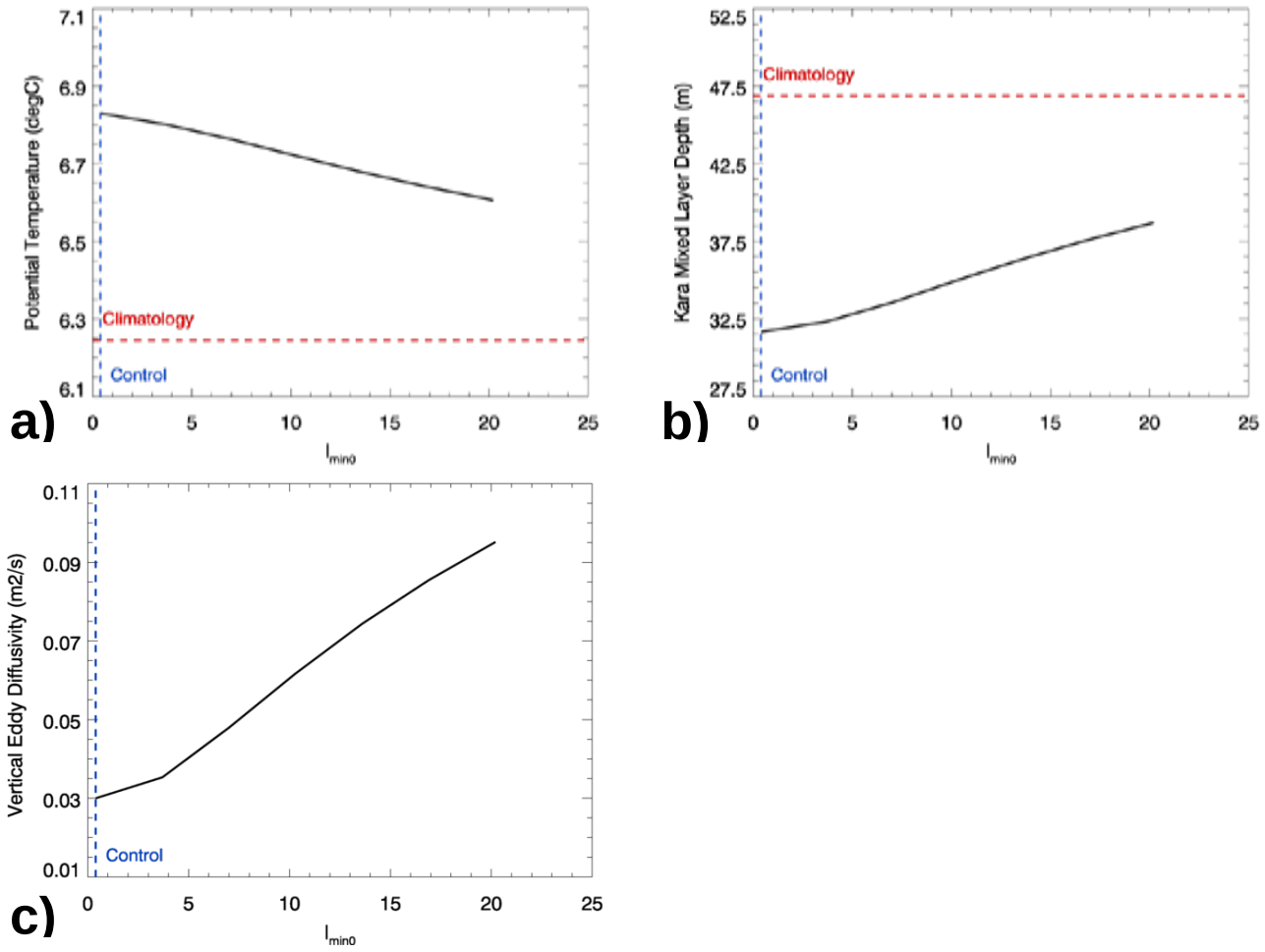

Figure 4.27: (a) DJF mean SST, (b) mean annual minimum MLD and (c) mean annual minimum eddy diffusivity at 1 m averaged over the Southern Ocean (45-60S), as a function of l_{min0}. The blue dashed lines correspond to the reference configuration value of e_{min0}, while the red dashed lines represent the climatological (a) Reynolds SST and (b) de Boyer Montégut MLD.

e_{min0} = 10^{-4} m^2s^{-2} and it is therefore suggested that l_{min0} be reduced from 0.4 m to 0.04 m.

Whilst the parameters l_{min} and e_{min} exist to ensure that the turbulent mixing length and TKE do not become too low in weakly turbulent regions, their role is purely numerical and as such should not interfere with background mixing processes which are represented by the parameters $K_{\rho 0}$ and K_{m0} and their global profiles. Equation (2.2a) can therefore be used to define a basic requirement for e_{min} and l_{min} where:

$$K_{m0} \geq c_k l_{min} \sqrt{e_{min}} \tag{4.1}$$

For K_{m0} = 1.2x10^{-4} m^2s, c_k = 0.1 and the control values of e_{min} and l_{min}, this gives upper limits of l_{min} = 1.2 m (for e_{min} = 10^{-6} m^2s^{-2}) and e_{min} = 9x10^{-6} m^2s^{-2} (for l_{min} = 0.4 m). This constraint is rather simplistic in the sense it only ensures that the minimum possible calculated value of the eddy viscosity K_m will not exceed its background value.

Figure 4.28 illustrates the impact of these derived limits for e_{min} and l_{min} on the temperature and eddy diffusivity in the North Pacific and there is a clear contrast in how the temperature profiles are affected by these two parameters. The increase in e_{min} results in an increase in the eddy diffusivity beneath the thermocline and causes diffusion of the large warm bias beneath 100m that is found throughout the year. The increase in l_{min} instead results in a small increase in the near-surface eddy diffusivity, which increases the amount of near-surface heat exchange and slightly deepens the summer and winter MLD.

Clearly the upper limits for l_{min} and e_{min} derived via (4.1) are too large; they have a notable impact on the solution of the eddy diffusivity and therefore supercede $K_{\rho 0}$ and K_{m0} in determining the level of background mixing in the model. This is simply because regions where l_k = l_{min} and where e = e_{min} do not necessarily coincide and because an increase in the TKE via e_{min} may also cause the surface mixing length to exceed l_{min} (equation 2.9). Equation (4.1) should therefore attempt to recover a much lower base state of turbulence, e.g. the molecular viscosity:

$$10^{-6} \geq c_k l_{min} \sqrt{e_{min}} \tag{4.2}$$

which requires the values of e_{min} and/or l_{min} to be lowered.

Initial sensitivity tests using a coarser-resolution configuration of NEMO with an ORCA2 grid and 31 vertical levels (5m surface grid box thickness) were performed prior to the present study to test very large perturbations to the TKE scheme parameters. One such experiment that used a setting of $e_{min} = 10^{-10}$ m^2s^{-2} showed that the TKE could indeed fall to this level beneath the thermocline. However this was found to have a minimal impact on eddy diffusivity profiles and consequently had very little impact on the model thermal structure, which suggests that the current value of $e_{min} = 10^{-6}$ m^2s^{-2} is sufficiently small enough to not impact the model result. In the present set of experiments, l_{min} was

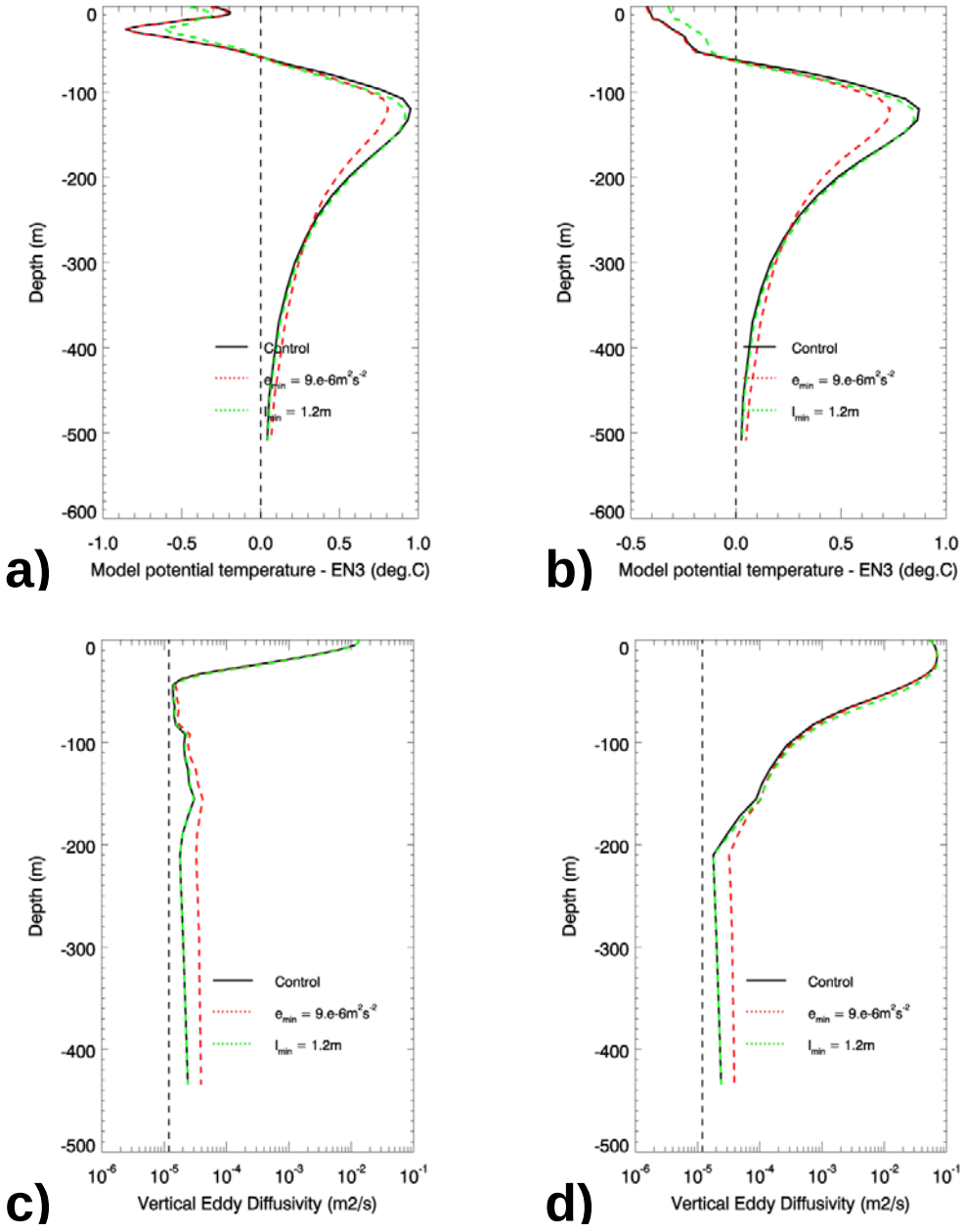

Figure 4.28: (top row) potential temperature bias profiles and (bottom row) eddy diffusivity profiles for the North Pacific (40-60N, 120-180W), averaged over (a,c) JJA and (b,d) DJF periods. Dashed black vertical lines correspond to (top row) zero bias and (bottom row) the background diffusivity.

decreased to 0.2 m and resulted in a small but globally-coherent decrease in the near-surface mixing relative to the reference configuration. This suggests that the current value of l_{min} = 0.4 m causes an increase in vertical mixing in the model and is consequently too large. Maintaining the current value of e_{min}, (4.2) therefore suggests that l_{min} = 0.01 m is a more appropriate value for this parameter.

The above discussion suggests that the parameters governing the surface and interior values of the minimum length scale thresholds (l_{min0} and l_{min}) are currently too large and so it is suggested that their values are revised from l_{min0} and l_{min} = 0.4 m to l_{min0} = 0.04 m and l_{min} = 0.01 m in the GO5.0 configuration. The parameters governing the surface and interior values of the minimum TKE thresholds (e_{min0} and e_{min}) do not require any change from their current values. While the suggested changes to l_{min} and l_{min0} are expected to result in a decrease in the near-surface vertical mixing, the likely magnitude of the impact is uncertain as the NEMO-CICE configuration analysed in this study was not run for parameter values this small. Further experiments are therefore required in order to quantify the impact of this proposed parameter change.

5. Summary and recommendations

The representation of vertical mixing has been a long-standing issue in global ocean modelling. Both atmosphere-coupled and bulk-forced OGCMs consistently suffer from a lack of vertical mixing during the summer, with shallow summer mixed layer depth (MLD) errors of up to 50% of climatological values being observed in the extratropics in the current version of the Met Office Hadley Centre coupled climate model (HadGEM3), accompanying large summer SST biases of up to ~4°C in the extratropical oceans.

While a significant proportion of this vertical mixing shortfall is likely to be due to poorly-represented or missing processes, errors will also be introduced by poorly-tuned parameters in the vertical mixing scheme. In defining the latest standard configuration (GO5.0) of the ocean component of HadGEM3 (the NEMO OGCM) revisions have been made to the settings of the vertical mixing scheme, a task which has to date been complicated by uncertainty in the parameterizations that comprise the scheme. To aid in this, sensitivity experiments were performed for the parameters of the NEMO vertical mixing scheme (the 'TKE scheme') in order to understand their behaviour and to investigate possible improvements to vertical mixing biases from reasonable adjustments to their settings. The aim of this technical report is to describe this work and to provide an overview of the revisions to the vertical mixing parameters that it has helped inform. The findings and recommendations are relevant to all Met Office model configurations that use NEMO (including HadGEM3, FOAM and GloSEA).

The sensitivity experiments used a 75 vertical level, ORCA1 (1° tripolar horizontal grid) configuration of NEMO coupled to the CICE ice model, which was started from rest and initialized with temperature and salinity from the EN3 2004-2008 climatology. The model was forced with the DFS4.1 surface forcing dataset (using the CORE bulk forcing algorithm) for 10 years (forcing years 1976-1985) and analysis was performed for years 7-10. The control experiment (or 'reference configuration') was based on the vertical mixing parameter settings used in the N96-ORCA1 development configuration of HadGEM3.

Table 4 summarises the revised vertical mixing parameters discussed by this report and their values in the reference and GO5.0 configurations.

Parameter	NEMO parameter	Description	Reference	GO5.0
α	rn_ebb	Surface wave breaking coefficient	60	67.83
γ	rn_efr	Near-inertial wave breaking TKE scaling	-	0.05
λ	nn_htau	Near-inertial wave breaking length scale	-	10 m
l_{min}	rn_lmin	Minimum interior length scale threshold	0.4 m	0.01 m
l_{min0}	rn_lmin0	Minimum surface length scale threshold	0.4 m	0.04 m
c_{LC}	rn_lc	Langmuir turbulence coefficient	-	0.15

Table 4: Revised parameter settings in the GO5.0 configuration as recommended by this report, compared to their settings in the reference configuration. Blank settings in the reference column refer to parameterizations that were not used in the configuration.

In general these changes are shown to improve biases attributable to insufficient vertical mixing in the reference configuration; warm SST biases and shallow MLD biases in the summer subtropics and extratropics are alleviated to varying degrees. The most significant changes are the introduction of the near-inertial wave breaking and Langmuir turbulence parameterizations, which in the forced configuration individually reduce the warm area-averaged SST bias in the Southern Ocean (45-60S) by ~0.15° (~25%) and reduce the shallow MLD bias by ~5 m (~25%). Caveats are associated with these particular parameterizations: there is considerable uncertainty associated with the parameters of the near-inertial wave breaking parameterization and the Langmuir turbulence parameterization is known to have several key shortcomings.

In addition to the revised parameter settings in table 4, several suggestions for the direction of future work are recommended by this report.

Firstly, a combined test of the above changes should be performed in a multidecadal simulation of HadGEM3, particularly as the results indicate that the sensitivity of some TKE scheme parameters increases significantly when coupled to an atmosphere model.

Secondly, work is required to better define or replace the near-inertial wave-breaking parameterization; the theoretical basis and testing underlying its rather arbitrary formulation are still unknown.

Thirdly, although the Langmuir turbulence parameterization has been shown to result in significant improvements to summer SST and MLD biases, there is evidence that the process is under-represented in many respects and that its ability to deepen the mixed layer should be even greater than shown for the present results. Future work should consider driving both this and the surface wave-breaking parameterization with realistic wave boundary conditions and further developing Langmuir turbulence parameterizations to include the effects of the characteristic downwelling jets of Langmuir circulations.

Finally and perhaps most importantly, work is required to compare and contrast the performance of the TKE scheme and the more complex GLS vertical mixing scheme in NEMO. The physically more accurate stability functions and prognostic length scale of the GLS scheme combined with its small increase in computational cost strongly motivate such a study. The GLS scheme has additionally received much more attention than the TKE scheme and subsequently its parameters will be better constrained, which would greatly simplify future parameter tuning in both NEMO and HadGEM3.

6. References

Arribas, A., et al., 2011: The GloSea4 Ensemble Prediction System for Seasonal Forecasting. *Mon. Wea. Rev.*, **139**, 1891-1910.

Axell, L. B., 2002: Wind-driven Internal Waves and Langmuir Circulations in a Numerical Ocean Model of the Southern Baltic Sea. *J. Geophys. Res.*, **107**, 3204, doi:10.1029/2001JC000922.

Belcher, S. E., et al., 2012: A Global Perspective on Langmuir Turbulence in the Ocean Surface Boundary Layer. *Geophys. Res. Lett.*, **39**, L18605, doi:10.1029/2012GL052932.

Blanke, B., and P. Delecluse, 1993: Variability of the Tropical Atlantic Ocean Simulated by a General Circulation Model with Two Different Mixed-Layer Physics. *J. Phys. Oceanogr.*, **23**, 1363-1388.

Bougeault, P., and J. C. André, 1986: On the Stability of the Third-Order Turbulence Closure for the Modelling of the Stratocumulus-topped Boundary Layer. *J. Atmos. Sci.*, **43**, 1574-1581.

Bougeault, P., and P. Lacarrère, 1989: Parameterization of Orography-Induced Turbulence in a Mesobeta-Scale Model. *Mon. Wea. Rev.*, **117**, 1872-1890.

Brodeau, L., B. Barnier, A.-M. Tréguier, T. Penduff, and S. Gulev, 2009: An ERA40-based Atmospheric Forcing for Global Ocean Circulation Models. *Ocean Modelling*, **31 (3-4)**, 88–104.

Bryan, K., and L. J. Lewis, 1979: A Water Mass Model of the World Ocean. *J. Geophys. Res.*, **84**, 2503-2517.

Burchard, H., 2001: Simulating the Wave-Enhanced Layer under Breaking Surface Waves with Two-Equation Turbulence Models. *J. Phys. Oceanogr.*, **31**, 3133–3145. doi: 10.1175/1520-0485(2001)031<3133:STWELU>2.0.CO;2

Burchard, H., and K. Bolding, 2001: Comparative Analysis of Four Second-Moment Turbulence Closure Models for the Oceanic Mixed Layer. *J. Phys. Oceanogr.*, **31**, 1943–1968. doi: 10.1175/1520-0485(2001)031<1943:CAOFSM>2.0.CO;2

Burchard, H., 2002: Energy-conserving Discretisation of Turbulent Shear and Buoyancy Production. *Ocean Modelling*, **4 (3-4)**, 347–361, doi : 10.1016/S1463-5003(02)00009-4

Burchard, H., et al., 2008: Observational and Numerical Modelling Methods for Quantifying Coastal Ocean Turbulence and Mixing. *Progress in Oceanography*, **76(4)**, 399-442.

Canuto, V. M., A. Howard, Y. Cheng, and M. S. Dubovikov, 2001: Ocean Turbulence. Part 1: One-Point Closure Model - Momentum and Heat Vertical Diffusivities. *J. Phys. Oceanogr.*, **31**, 1413-1426.

Craig, P. D., and M. L. Banner, 1994: Modelling Wave-Enhanced Turbulence in the Ocean Surface Layer. *J. Phys. Oceanogr.*, **24**, 2546-2559.

Craik, A. D. D., and S. Leibovich, 1976: A Rational Model for Langmuir Circulations. *J. Fluid Mech.*, **73**, 401-426.

d'Alessio, S. J. D., K. Abdella, and N. A. McFarlane, 1998: A New Second-order Turbulence Closure Scheme for Modelling the Oceanic Mixed Layer. *J. Phys. Oceanogr.*, **28(8)**, 1624-1641.

de Boyer Montégut, C., G. Madec, A. S. Fischer, A. Lazar, and D. Iudicone (2004), Mixed Layer Depth over the Global Ocean: an Examination of Profile Data and a Profile-based Climatology. *J. Geophys. Res.*, **109**, C12003. doi:10.1029/2004JC002378.

Ezer, T., 2000: On the Seasonal Mixed Layer Simulated by a Basin-scale Ocean Model and the Mellor-Yamada Turbulence Scheme. *J. Geophys. Res.*, **105(C7)**, 16,843–16,855, doi:10.1029/2000JC900088.

Gargett, A. E., 1984 : Vertical Eddy Diffusivity in the Ocean Interior. *J. Mar. Res.*, **42**, 359-393.

Gaspar, P., Y. Grégoris, and J.-M. Lefevre, 1990: A Simple Eddy Kinetic Energy Model for Simulations of the Oceanic Vertical Mixing: Tests at Station Papa and Long-Term Upper Ocean Study Site. *J. Geophys. Res.*, **95(C9)**, 16179–16193, doi:10.1029/JC095iC09p16179.

Grant, A. L. M., and S. E. Belcher, 2009: Characteristics of Langmuir Turbulence in the Ocean Mixed Layer. *J. Phys. Oceanogr.*, **39**, 1871–1887. doi: 10.1175/2009JPO4119.1

Gregg, M. C., T. B. Sanford, and D. P. Winkel, 2003: Reduced Mixing from the Breaking of Internal Waves in Equatorial Waters. *Nature*, **422**, 513-515.

Hanley, K. E., S. E. Belcher, and P. P. Sullivan, 2010: A Global Climatology of Wind–Wave Interaction. *J. Phys. Oceanogr.*, **40**, 1263–1282. doi: 10.1175/2010JPO4377.1

Harper, S. ,2000: Thermocline Ventilation and Pathways of Tropical–Subtropical Water Mass Exchange. *Tellus A*, **52(3)**, 330-345.

Hewitt, H. T., D. Copsey, I. D. Culverwell, C. M. Harris, R. S. R. Hill, A. B. Keen, A. J. McLaren, and E. C. Hunke, 2010: Design and Implementation of the Infrastructure of HadGEM3: the Next-generation Met Office Climate Modelling System. *Geosci. Model Dev. Discuss*, **3**, 1861-1937.

Huang, C. J., F. Qiao, Z. Song, and T. Ezer, 2011: Improving Simulations of the Upper Ocean by Inclusion of Surface Waves in the Mellor-Yamada Turbulence Scheme. *J. Geophys. Res.*, **116**, C01007, doi:10.1029/2010JC006320.

Huang, C. J., F. Qiao, Q. Shu, and Z. Song, 2012: Evaluating Austral Summer Mixed-layer Response to Surface Wave–induced Mixing in the Southern Ocean. *J. Geophys. Res.*, **117**, C00J18, doi:10.1029/2012JC007892.

Hunke, E. and W. Lipscomb, 2008: CICE : the Los Alamos Sea Ice Model Documentation and Software User's Manual, Version 4.0.

Ingleby, B., and M. Huddleston, 2007: Quality Control of Ocean Temperature and Salinity Profiles - Historical and Real-time Data. *Journal of Marine Systems*, **65**, 158-175 10.1016/j.jmarsys.2005.11.019

Jayne, S. R., 2009: The Impact of Abyssal Mixing Parameterizations in an Ocean General Circulation Model. *J. Phys. Oceanogr.*, **39**, 1756-1775.

Jochum, M., 2009: Impact of Latitudinal Variations in Vertical Diffusivity on Climate Simulations. *J. Geophys. Res.*, **114(C01010**), doi:10.1029/2008JC005030.

Jochum, M., B. P. Briegleb, G. Danabasoglu, W. G. Large, N. J. Norton, S. R. Jayne, M. H. Alford, and F. O. Bryan, 2013: The Impact of Oceanic Near-Inertial Waves on Climate. *J. Climate.*, **26**, 2833-2844.

Kantha, L. H., and C. A. Clayson, 2004: On the Effect of Surface Gravity Waves on Mixing in the Oceanic Mixed Layer. *Ocean Modelling*, **6(2)**, 101-124.

Klein, P., and M. Coantic, 1981: A Numerical Study of Turbulent Processes in the Marine Upper Layers. *J. Phys. Oceanogr.*, **11(6)**, 849-863.

Kolmogorov, A. N., 1942: The Equation of Turbulent Motion in an Incompressible Fluid. *Izv. Akad. Nauk SSSR, Ser. Fiz.*, **6**, 56-58.

Kraus, E. B., 1990: Diapycnal Mixing. In Schlesinger, M. E., 1990: Climate-ocean Interaction. Kluwer, Amsterdam, Netherlands, pp 269-293

Large, W. G., J. C. McWilliams, and S. C. Doney, 1994 : Oceanic Vertical Mixing - a Review and a Model with a Nonlocal Boundary Layer Parameterization. *Reviews of Geophysics*, **32**, 363–404, doi :10.1029/94RG01872.

Large, W. G. and S. Yeager, 2004: Diurnal to decadal global forcing for ocean and sea-ice models : the data sets and flux climatologies. NCAR Technical Note, NCAR/TN-460+STR, CGD Division of the National Center for Atmospheric Research.

Ledwell, J. R., A. J. Watson, and C. S. Law, 1993: Evidence for Slow Mixing Across the Pycnocline from an Open-Ocean Tracer-Release Experiment. *Nature*, **364**, 701-703, doi:10.1038/364701a0.

Leibovich, S., 1983: The Form and Dynamics of Langmuir Circulations. *Ann. Rev. Fluid Mech.*, **15**, 391-427.

Li, M., and C. Garrett, 1993: Cell Merging and the Jet/Downwelling Ratio in Langmuir Circulation. *J. Mar. Res.*, **51**, 737-769.

Madec, G., 2008: NEMO ocean engine. Note du Pole de modélisation, Institut Pierre-Simon Laplace (IPSL), France, No 27 ISSN No 1288-1619.

Martin, P. J., 1985: Simulation of the Mixed Layer at OWS November and Papa with Several Models. *J. Geophys. Res.*, **90(C1)**, 903–916, doi:10.1029/JC090iC01p00903.

McWilliams, J. C., and P. P. Sullivan, 2000: Vertical Mixing by Langmuir Circulations. *Spill Science & Technology Bulletin*, **6(3)**, 225-237.

Meier, H. E. M., 2001: On the Parameterization of Mixing in Three-Dimensional Baltic Sea Models. *J. Geophys. Res.*, **106 (C12)**, 30997-31016, doi:10.1029/2000JC000631

Mellor, G., and A. Blumberg, 2004: Wave Breaking and Ocean Surface Layer Thermal Response. *J. Phys. Oceanogr.*, **34**, 693–698, doi:10.1175/2517.1

Mellor, G. L., and T. Yamada, 1974: A Hierarchy of Turbulence Closure Models for Planetary Boundary Layers. *J. Atmos. Sci.*, **31**, 1791-1806.

Molines, J. M., B. Barnier, T. Penduff, L. Brodeau, A. M. Treguier, S. Theetten, and G. Madec, 2006: Definition of the Interannual Experiment ORCA025-G70, 1958–2004. Tech. Rep. LEGI-DRA-2-11-200, LEGI, available at http://www.ifremer.fr/lpo/drakkar.

Murray, R. J., 1996: Explicit Generation of Orthogonal Grids for Ocean Models. *J. Comput. Phys.*, **126 (2)**, 251–273.

Noh, Y., G. Goh, and S. Raasch, 2011: Influence of Langmuir Circulation on the Deepening of the Wind-mixed Layer. *J. Phys. Oceanogr.*, **41(3)**, 472-484.

Polton, J. A., and S. E. Belcher, 2007: Langmuir Turbulence and Deeply Penetrating Jets in an Unstratified Mixed Layer. *J. Geophys. Res.*, **112 (C09020)**, doi:10.1029/2007JC004205.

Skyllingstad, E. D., and D. W. Denbo, 1995: An Ocean Large-eddy Simulation of Langmuir Circulations and Convection in the Surface Mixed Layer. *J. Geophys. Res.*, **100(C5)**, 8501–8522, doi:10.1029/94JC03202.

Sullivan, P. P., J. B. Edson, T. Hristov, and J. C. McWilliams, 2008: Large-eddy Simulations and Observations of Atmospheric Marine Boundary Layers above Nonequilibrium Surface Waves. *J. atmos. Sci.*, **65(4)**, 1225-1245.

Stacey, M. W., 1999: Simulations of the Wind-Forced Near-Surface Circulation in Knight Inlet: A Parameterization of the Roughness Length. *J. Phys. Oceanogr.*, **29**, 1363-1367.

Storkey, D., E. W. Blockley, R. Furner, C. Guiavarc'h, D. Lea, M. J. Martin, R. M. Barciela, A. Hines, P. Hyder, and J. R. Siddorn, 2010: Forecasting the Ocean State using NEMO: The New FOAM System. *J. Oper. Ocean.*, **3(1)**, 3-15.

Terry, E. A., M. A. Donelan, Y. C. Agrawal, W. M. Drennan, K. K. Kahma, A. J. Williams, P. A. Hwang, and S. A. Kitaigorodski, 1996: Estimates of Kinetic Energy Dissipation under Breaking Waves. *J. Phys. Oceanogr.*, **26**, 792-807.

Therry, G., and P. Lacarrère, 1983: Improving the Eddy Kinetic Energy Model for Planetary Boundary Layer Description. *Bound. Layer. Meteor.*, **25**, 63-88.

Umlauf, L., and H. Burchard, 2003: A Generic Length-scale Equation for Geophysical Turbulence Models. *J. Mar. Sys.*, **61 (2)**, 235–265.

Umlauf, L., and H. Burchard, 2005 : Second-order Turbulence Closure Models for Geophysical Boundary Layers. a Review of Recent Work. *J. Mar. Sys.*, **25**, 795–827.

Van Roekel, L. P., B. Fox-Kemper, P. P. Sullivan, P. E. Hamlington, and S. R. Haney, 2012: The Form and Orientation of Langmuir Cells for Misaligned Winds and Waves. *J. Geophys. Res.*, **117(C05001)**, doi:10.1029/2011JC007516.

Webb, A., and B. Fox-Kemper, 2009: Global Model Sensitivity to Parameterizing Langmuir Circulation. In CIRES Rendezvous, Boulder, CO, Apr 2009.

Weijer, W., B. M. Sloyan, M. E. Maltrud, N. Jeffery, M. W. Hecht, C. A. Hartin, E. van Sebille, I. Wainer, and L. Landrum, 2012: The Southern Ocean and its Climate in CCSM4. *J. Climate*, **25(8)**, 2652-2675.

Met Office
FitzRoy Road, Exeter
Devon EX1 3PB
United Kingdom

Tel: 0870 900 0100
Fax: 0870 900 5050
enquiries@metoffice.gov.uk
www.metoffice.gov.uk